STRUCTURAL STUDIES OF SOME POLYNUCLEAR IRON PROTEINS

Thesis by

John Mark Webb

In Partial Fulfillment of the Requirements

For the Degree of

Doctor of Philosophy

California Institute of Technology

Pasadena, California

1972

(Submitted August 31, 1971)

ACKNOWLEDGMENTS

During these Caltech years I have been fortunate to work closely with two imaginative and stimulating scientists, Harry Gray and Paul Saltman. Both have greatly influenced the course of this research. I have received advice and assistance from many friends at Caltech and elsewhere. Particular contributions to the thesis are noted within the text.

Caltech has given me also the unbelievable world of Dabney House, the education that is the Caltech Y, and a daughter. For the last mentioned and many other good things besides, I thank my wife, Sandy.

Without the patience of Peggy Lockhart who prepared the drawings and of Sue Brittenham who typed away for so long, this thesis may never have existed.

I gratefully acknowledge the generous financial support of the Commonwealth Scientific and Industrial Research Organization, Australia.

ABSTRACT

The coordination structure and electronic configuration of iron(III) bound in a polynuclear fashion to a number of proteins have been investigated by a variety of physical methods. These have included the temperature dependence of the magnetic susceptibility, electron spin resonance spectroscopy, electronic absorption spectroscopy at low temperatures, vibrational spectroscopy, X-ray analysis, Mössbauer spectroscopy down to helium temperature, and electron spectroscopy for chemical analysis (ESCA). The proteins investigated included the iron transport protein transferrin, the phosphoglycoprotein phosvitin, the gastric juice glycoprotein gastroferrin, and the two iron storage proteins ferritin and hemosiderin. On the basis of the results obtained by these techniques the structural relationship of the iron to the protein and to other iron atoms present in the polynuclear complex was clarified. Structural models for these relationships were proposed for the proteins listed. The implications of these results for the biological role of iron have been considered.

TABLE OF CONTENTS

I. INTRODUCTION

The essential role of iron for the human organism was recognized in antiquity, whence legend records[1] that a glass of wine and rust was sufficient to cure sexual impotence and to benefit those who, unfortunately, could not "cohabit properly." A complete understanding of these remarkable phenomena still escapes contemporary biochemistry, yet, of all the essential trace metals, iron and its biological functions are probably the best understood. Many of these functions depend on the aqueous chemistry of iron(III), and this chemistry is now known to be dominated by hydrolysis and polymerization, with the formation of polynuclear iron(III) species, i.e., species that contain at least two iron atoms interacting through some bonding arrangement. This research reports the results of structural studies, using a variety of physical methods, on a number of proteins that bind iron(III) in a polynuclear fashion, and on several model compounds that are structural analogs of the polynuclear iron in these iron-protein complexes. One of the proteins studied, transferrin, binds only two iron atoms. The other protein systems investigated, phosvitin - gastroferrin - ferritin - hemosiderin, all bind at least fifty iron atoms in polynuclear clusters.

The thesis is organized in the following way. First, the presently available information on the chemistry and biology of polynuclear iron is summarized and the systems studied in this work are introduced. A substantial debt of gratitude to the authors of a recent review[1] on this

subject is acknowledged. Second, the strengths and weaknesses of the various techniques used in this and other studies are discussed. Third, the results for each protein system and its structural analogs are presented and discussed. Fourth, the implications of these results for biologically active iron(III) are considered. A description of the experimental procedures used is included in a final section.

A. Hydrolytic Polymerization of Iron(III)

The hydrolysis of iron(III) has been the object of a series of careful potentiometric and other studies by a number of investigators.[2-5] Their results implicated a dinuclear complex, $Fe_2(OH)_2^{4+}$, as the predominant hydrolysis product in the solution even at low pH (< 2). The solution is metastable to the eventual precipitation of the polymerization product, iron(III) hydroxide. This familiar brown colloid was usually assumed to be amorphous and ill-defined, its presence being sufficient reason to discard the solution. Recently Towe and Bradley[6] and, separately, van der Geissen,[7] have reported the isolation of hydrolyzates of iron(III) that are of small particle size (< 100 Å diameter) yet of sufficient crystallinity to give X-ray powder patterns.

Use of the standard biochemical techniques of gel filtration and ultrafiltration on an iron(III) nitrate solution to which two moles of OH^-/Fe had been added resulted in the isolation of a remarkable[8] homogeneous polymer. The polymer has a molecular weight of 150,000 incorporating about 1200 iron atoms, and appears spherical in the electron microscope with a diameter of 70 Å. The structural

characteristics of this polymer, proposed as a model for the core of the protein ferritin, have been a matter of some controversy.

There are, however, a number of very well defined phases in the iron(III) oxide and iron(III) oxyhydroxide systems. They are α, β, and γ-Fe_2O_3, Fe_3O_4, and α, β, γ, and δ-FeOOH. Some occur naturally, and synthesis and interconversions have been extensively studied.[9,10] Of the two crystallographic sites available for iron(III) in these structures, octahedral and tetrahedral, αFe_2O_3, α-, β-, and γ-FeOOH have iron atoms in octahedral sites exclusively The other phases distribute the iron atoms between octahedral and tetrahedral sites in various proportions. A major emphasis of this present research has been the development and application of reliable methods to distinguish iron(III) atoms in these two different coordination sites. A number of the above phases, with other relevant minerals (e.g., $Fe.OH.SO_4$[11] and $FePO_4$[12]) have therefore been incorporated into this study.

B. Effect of Chelates on Polymerization

The inclusion of a number of chelating agents in hydrolyzed iron(III) solutions produces dimeric complexes that are stable and readily investigated.[13] The dimeric unit of the chelate-free system, $Fe(OH)_2Fe$, has been reasonably well characterized only in the iron(III): picolinic acid system.[14] Almost all the dimers are analogous to that formed with HEDTA, whose crystal structure shows an almost linear

(165°) oxo-bridged Fe-O-Fe structural unit linking the two subunits of the molecule together.[15]

Polymers analogous to the iron(III) nitrate polymer mentioned above have been isolated from solutions containing the complexing agents citrate and fructose. The iron(III)-citrate polymer also appears spherical,[16] 70 Å in diameter, with a molecular weight of 2.1×10^5. Its formation from the low molecular weight complexes can be prevented by a large (×20) citrate:iron ratio.[17] Analogous behavior has been observed in the iron(III)-fructose system.[1] This polymer has a molecular weight[18] of 0.65×10^5. Various sugar complexes with polynuclear iron(III) are used in the intravenous and/or intramuscular application of iron(III). One of the most widely used preparations,[19,20] an iron-dextran complex of molecular weight in excess of 1.5×10^5, was used in the preparation of the iron storage compound, hemosiderin.

C. Biological Uptake of Iron

Every living cell depends on iron in a wide variety of biochemical reactions. Various mechanisms have been developed by living organisms to take up environmental iron which is present mostly in a polynuclear form as the highly insoluble iron(III) hydroxide that cannot be transported across the cell membrane. The solubility product constant of $Fe(OH)_3$ is estimated[1] at $10^{-38.7}$ M^4, (25°, 3M $NaClO_4$), while that of $Fe(OH)_2$ is $10^{-15.1}$ M^3 (25°, zero ionic strength).

Many bacteria and fungi elaborate powerful chelating agents to convert iron(III) hydroxide[21] into soluble small molecular weight complexes. Plants utilize organic acids to extract the iron from alkaline soils,[22] and chelating agents of the EDTA type are widely used in agriculture to present iron to crops. Although iron metabolism in man has been extensively studied throughout the history of medicine,[23] the importance of chelation and of polynuclear iron in the control of iron uptake has only recently been realized. In contrast to the metabolism of other trace metals, most of the iron in the body is continuously recycled, very little iron being excreted via the urine, feces, and sweat.[24] Control of the amount of iron present occurs by the regulation of uptake, not of excretion. It is here that chelation and the polynuclear nature of many iron compounds play decisive roles.

It should be noted at this point that most orally administered therapeutic applications of iron in the treatment of iron deficiency anemia contain iron(II), not iron(III), salts. This preference follows historically from the spectacular success achieved by iron(II) salts in the early nineteenth century in the treatment of chlorosis.[24] Iron uptake is maximal in the gastric lumen and in the lumen of the small intestine,[1] both highly aerobic regions where iron(II) is oxidized to iron(III) which can then polymerize. The iron(II) hydroxide present is much more soluble than the iron(III), by about 15 orders of magnitude, providing many more simple metal ions for transport across the mucosal membrane. The application of iron(II) salts to stimulate iron

uptake is very inefficient, but more efficient than that of iron(III). Prevention of the polymerization of iron(III) by the presence of suitable chelating agents permits iron(II) and iron(III) to be utilized with equal effectiveness.[25] The body transports only low molecular weight complexes across the membrane.[30] Hence, the binding of iron(III) by proteins that are present in the gut is expected to lower the availability of iron for absorption. Even less iron is available for absorption if the protein ligands bind a large number of iron atoms, presumably forming polynuclear clusters of iron(III). This competition between the low molecular weight chelates and macromolecular ligands, both of which inhibit the deposition of iron(III) hydroxide, is now recognized as the major determinent of the amount of iron available for absorption. Two proteins that have been implicated in the inhibition of iron absorption in the gut are phosvitin and gastroferrin. The results presented and discussed in the following pages show that both proteins bind a large number of iron(III) ions in a polynuclear fasion.

D. Introduction to the Protein Systems Studied

1. Gastroferrin

Gastroferrin is a glycoprotein that can be isolated from human gastric juice but is more readily obtained from pig gastric mucin.[26,27] Its composition is predominantly carbohydrate, 85%, with only 15% polypeptide and its molecular weight has been estimated by various methods to be 2.6×10^5 ($\pm$ 0.2). It has an iron binding capacity of up to 6% by weight. Gastroferrin is known to possess some

blood group activity as measured by inhibition of agglutination, and its absence has been proposed as the genetic marker in hemachromatosis, a disease characterized by pathologically excessive iron uptake and storage.

2. Phosvitin

Phosvitin is a phosphoglycoprotein of molecular weight 40,000 which can be isolated from hens' egg yolk.[28] It contains 6.5% carbohydrate and a remarkable number, about 120, of phosphoserine residues (side chain: $-CH_2OPO_3H_2$) arranged, at least in part, in linear sequences of up to eight residues uninterrupted by other amino acids.[29] A postulate[32] of the biological function of such a phosphate-rich protein is that phosvitin acts as a source of phosphate for the developing chick embryo, and phosphorylation is activated by oxidation of the serine phosphate residues. Recent nutritional studies suggested that eggs in the diet have inhibitory effects on iron absorption.[31] Most proteins are broken down in the acid gastric environment but phosvitin has been shown to be resistant to the action of the proteolytic enzymes present in that environment.[33] The results in the pages following demonstrate that phosvitin does bind polynuclear iron(III), in an uncommon stereochemistry that is a consequence of the unusual composition of the polypeptide chain of this protein.

3. Ferritin

The best known example of polynuclear iron(III) in biology is the iron storage protein ferritin,[34] whose gross morphology is that of a spherical core, 70 Å in diameter, of iron(III) oxyhydroxide with a little phosphate of approximate composition $[(FeOOH)_8 \cdot FeO \cdot PO_4H_2]$. This core is surrounded by at least twenty identical protein subunits that coat the micelle, giving a sphere of 120 Å diameter. The iron content of the core varies up to a maximum core molecular weight of ~400,000, and the complete protein coat, present in all ferritin molecules has a molecular weight of ~460,000. This morphology produces a high percentage composition of iron (~20%) and a high iron/protein ratio (~2), as expected for a storage compound. The phosphate and protein apparently serve to prevent the formation of an insoluble phase of iron(III) hydroxide. The protein can be easily crystallized and the isolated cores also produce an X-ray diffraction pattern. Ferritin is widely distributed in nature occurring in vertebrates, invertebrates,[38] plants,[36] and fungi.[37] Its universal role appears to be as an iron storehouse for the organism. The structure of the core of ferritin has been the object of intensive investigation and controversy. The nitrate polymer,[8] a derivative of δ-FeOOH[35] and the iron(III) oxyhydroxide gels of Towe and Bradley,[6] and of van der Geissen,[7] have been variously proposed as structural models for the ferritin core. The structures of these models and of the core have been investigated in this work. The suitability of these models will be critically evaluated below.

4. Hemosiderin

Hemosiderin is the second major storage form of iron in mammalian tissues and is most evident in iron storage pathologies.[39] Hemosiderin differs from ferritin in its positive histological reaction with Prussian blue, in its chemical composition (~26% iron and little protein) and, by definition, in its total insolubility in water. Hemosiderin, an iron storehouse also incorporates polynuclear iron(III). Although the compound is not well defined, its structure was also investigated in this work.

5. Transferrin

Other polynuclear iron proteins are the transferrins and the non-heme iron-sulphur proteins. This latter group is excluded from this work. Transferrin[41] is a γ-globulin of molecular weight 80,000 that binds two iron(III) atoms and acts in iron transport. It has been found in various bodily fluids from many vertebrate species. It can be considered a polynuclear iron(III) protein in that it binds two iron atoms. In contrast to the several cases referred to above, these iron atoms are not in close proximity and do not interact.[40]

II. TECHNIQUES OF INVESTIGATION

The most useful techniques for identifying clusters of polynuclear iron(III) are those that are sensitive to the particular feature of the polynuclear cluster--the interaction between the sets of d electrons on different iron atoms. The magnetic behavior is primarily determined by the electron configuration of these d electrons. This in turn varies with the number and nature of the ligand atoms bound to the iron and with the different kinds of interaction between that and other iron atoms. The magnetic susceptibility, its behavior as a function of temperature, and the electron spin resonance spectrum are particularly important probes of the effect on the electronic configuration of polynuclear interaction. The importance of magnetic susceptibility measurements has prompted a somewhat detailed discussion of the theory behind the analysis of these measurements. As will be shown later, the e.s.r. spectrum is a less versatile probe for identifying iron-iron interactions. The discussion of this technique is correspondingly brief.

A number of other techniques has been used to elucidate structural details of the bonding between iron atoms in the polynuclear cluster and between the cluster and the protein. By far the most important one has been absorption spectroscopy of the electronic transitions occurring within the set of d electrons of the iron(III). An extensive discussion of the principles underlying this spectroscopy will be presented. Supplementary structural information has been obtained

from Mössbauer and vibrational spectroscopy, X-ray studies, and E. S. C. A., electron spectroscopy for chemical analysis. This section contains a brief discussion of each of these techniques.

A. Magnetic Behavior

1. Ground State

The distribution[42] of the five d electrons of iron(III) within the set of five d orbitals depends on the relative energies of those orbitals. The familiar splittings of the d orbitals by the ligand field created by octahedral, tetrahedral, and tetragonal arrays of ligands atoms around the iron are shown in Figure 1. The figure also shows the possible spin configurations for the various symmetries. In both octahedral (O_h) and tetrahedral (T_d) symmetries the high spin case corresponds to five unpaired electrons and the low spin case to one. With an electron spin quantum number, s of 1/2 the total spin number (S) in the two cases is 5/2 and 1/2. The three unpaired electrons situation S = 3/2 of the tetragonal symmetry has been characterized in only a few cases, e. g. in a series of monohalogen bis (N, N-dimethyldithiocarbamato) iron(III) complexes[43] of general formula [Fe(III) X. $(S_2CNR_2)_2$]. The S = 3/2 ground state is not attainable in O_h or T_d symmetries.

The choice between the 5/2 and 1/2 spin states in these symmetries is determined by the balance between the strength of the ligand field (10 Dq) that determines the splitting of the two sets of d orbitals, and the magnitude of the Coulomb and exchange energy for the d electrons.

Figure 1

Possible high-spin and low-spin electronic configurations possible for a d^5 ion in ligand fields of tetrahedral, octahedral, and tetragonal symmetry. 10 Dq is the splitting induced by the ligand field and is a measure of the strength of that field.

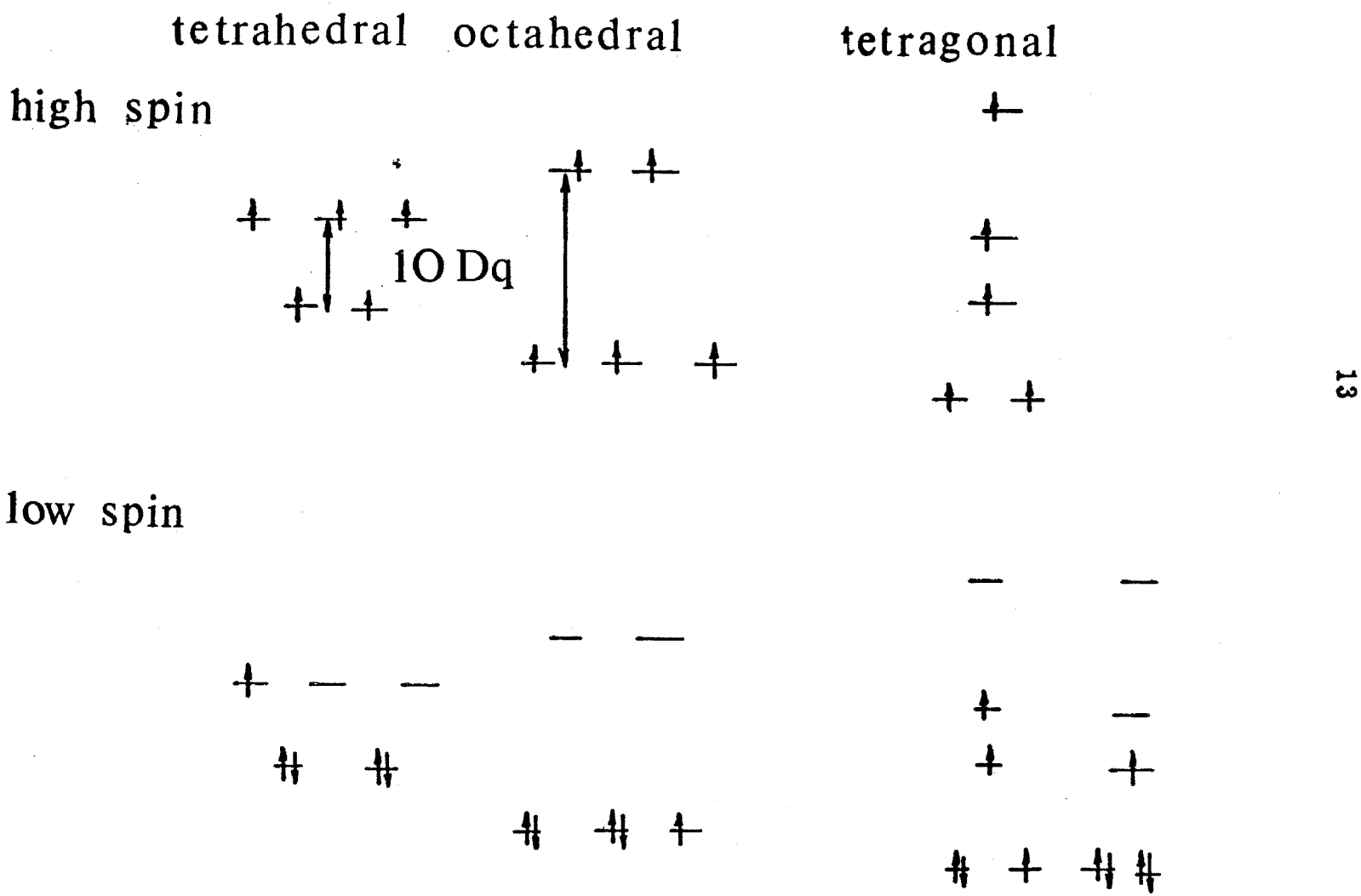
tetrahedral
octahedral
tetragonal
high spin
10 Dq
low spin

A quite strong ligand field of $\sim 30,000\ cm^{-1}$ is required to go from the 5/2 to the 1/2 ground state. Cyanide, dipyridine, and o-phenanthroline are examples of strong field ligands. An intermediate situation of a ligand field near the crossover point is possible. Specific examples of all these situations are presented in the following discussion of the magnetic characteristics of iron(III).

2. Spin-Only Magnetic Moment

The magnetic moment μ_s of a single electron is simply related to the electron spin quantum numbers. For an ion of total spin quantum number S describing the spin angular momentum, the analogous relation shown below gives the magnetic moment μ for the ion in Bohr Magnetons (B. M.)

$$\mu = g\sqrt{S(S+1}$$ g: the gyromagnetic ratio
= 2.00023 for free electron

For the single electron case, S = s and μ is 1.73 B. M. For S = 5/2, μ = 5.92 B. M., and for S = 3/2 μ is 3.87 B. M. These are the values of the "spin-only" magnetic moments, since no account is made of the contribution to the moment from the orbital angular momentum (of quantum number L). This contribution occurs through coupling to the spin angular momentum--i. e., spin-orbit coupling. For the S = 5/2 case, the ground state of the complex is $^6A_1$ derived from the ^6S ground state of the free ion. For such a ground state L = 0 and no orbital contribution to the moment is possible. $Na_3[FeF_6]$ has a magnetic moment per iron of 5.85 B. M. [42] For any other value of L

spin-orbit coupling is possible, and its extent can be determined from an experimental study of the magnetic behavior. The moment for $K_3Fe(CN)_6$ of 2.25 B.M.[42] is increased from the spin-only value of 1.73 B.M. by an orbital contribution allowed in the $^2T_2$ ground state.

3. Magnetic Susceptibility

Magnetic moments can lead to important chemical information, but they are not determined directly. They are derived from the measured magnetic susceptibility (χ) of the sample in a magnetic field. The magnetic moment is calculated from the gram susceptibility χ_g by applying a diamagnetic correction to the molar susceptibility χ_M (= χ_g × Mol. Wt.), giving χ_M^{corr} which is used in the following equation:

$$\mu = 2.828 \sqrt{\chi_M^{corr} \cdot T}$$

The temperature dependence of the magnetic susceptibility χ follows either Curie ($\chi \alpha 1/T$) or Curie-Weiss law ($\chi \alpha 1/(T - \theta)$. θ, the intercept on the T axis of a plot of χ^{-1} against T, is the Weiss constant. It has often been taken as a measure of the degree of intermolecular interactions, yet a finite θ can result from other causes, e.g., spin-orbit coupling on the $^3T_{1g}$ ground state of the monomeric $K_3[Mn(CN)_6]$.[42]

The diamagnetic correction accounts for the contribution to the susceptibility from the closed shell electrons in the metal and ligand. Although the contribution from the organic component of a metal

complex is small, $\sim -0.5 \times 10^{-6}$ cgs units per gram, a molar contribution from a protein of 50,000 molecular weight is $\sim -2.5 \times 10^{-2}$ cgs units. This is comparable to the paramagnetic molar susceptibility of $Fe(NO_3)_3 \cdot 9H_2O$ at 293°K of $+1.52 \times 10^{-2}$ cgs units.[44] Since diamagnetic and paramagnetic contributions to the observed susceptibility of a protein that binds only one or a few metal ions can be of the same order of magnitude yet of opposite sign, the net susceptibility is small and measurements of the paramagnetic component are subject to significant errors ($> 10\%$).

A situation intermediate to the high and low spin cases occurs when the ligand field strength is close to that required for the transition from the high to the low spin configuration. If the energy difference between these two configurations is comparable to kT (at 300°K, kT = 208 cm^{-1}), there is an equilibrium mixture of high spin and low spin states, giving a moment which is a weighted average of the two components, and extremely temperature sensitive. One of the few established examples of this equilibrium situation with iron(III) occurs in the compound Fe(III)(diethyldithiocarbamate)$_3$.[45]

In general iron(III) has its greatest affinity for oxygen ligands, although chelating ligands with O and N donor atoms are well known, as are strong field ligands binding through N only. The many amino acid side chains of proteins that can bind through O or N have a ligand field strength of $< 15,000$ cm^{-1}, too small to induce either spin pairing or a high spin-low spin equilibrium.

4. Polynuclear Interaction

The strength of the interaction between the sets of d electrons on different iron atoms of spins S_1 and S_2 that is characteristic of a polynuclear cluster can be expressed[46] by the exchange coupling constant J in the Hamiltonian for the interaction:

$$\mathcal{H}' = -2JS_1 \cdot S_2$$

For $J > 0$, the interaction is called ferromagnetic and for $J < 0$ antiferromagnetic. A few instances of ferromagnetic coupling are known for intramolecular polynuclear clusters,[80] i.e., clusters that are magnetically isolated from other clusters by diamagnetic matter. None of these involve iron(III) ions. For a polynuclear cluster of iron(III) the magnetic interaction is always antiferromagnetic, tending to couple the unpaired electrons on the interacting iron(III) atoms. Antiferromagnetism therefore decreases the magnetic moment per iron from the spin-only value. The strength of the antiferromagnetic coupling determines the extent of this decrease.

For the polynuclear clusters of interest in this study the antiferromagnetic coupling between any two iron(III) atoms does not take place directly through the space between them, but rather indirectly through an intervening bridging unit, e.g., –O– or –OH–. This mechanism for the coupling is known as superexchange.

Physically extended systems or lattices of magnetically interacting iron(III) ions are well known. The interaction can be

ferromagnetic or antiferromagnetic. Examples of both are found among the various mineral phases of the iron oxyhydroxide system. The theoretical treatment of this kind of magnetic behavior is different from the interaction Hamiltonian above. The concepts of magnetic domains and molecular fields are useful in approaching this problem, but the phenomena are not completely understood.[61]

Both these kinds of antiferromagnetism, intramolecular cluster, and lattice types, occur among the polynuclear iron proteins considered in this study.

In addition to lowering the magnetic moment per iron from the spin-only value, antiferromagnetic coupling changes the temperature dependent behavior of the moment. At any temperature there is competition between the order resulting from magnetic effects and the disorder from thermal agitation. In a susceptibility measurement the ordering is induced by an applied field and, additional for antiferromagnetic substances, by the magnetic coupling of the paramagnetic ions. The competition between magnetic ordering and thermal disorder reaches an equilibrium balance at the Néel temperature, T_N. Although the susceptibility increases with decreasing temperature down to T_N, a plot of χ^{-1} against T is non-linear. The antiferromagnetically lowered magnetic moment characteristically decreases with decreasing temperature. It is this behavior that is the most reliable criterion for identifying polynuclear iron(III) species. The room temperature moment

and the steepness of the decrease in the moment as the temperature decreases reflects the strength of the coupling between the iron atoms.

5. Intramolecular Antiferromagnetism

Several complexes of the oxobridged iron(III) system mentioned in the introduction have been characterized by magnetic susceptibility measurements.[47-55] In all cases the temperature dependence can be fitted quite well using the spin-spin interaction model mentioned above. The resulting energy levels include a diamagnetic ground state and thermally accessible paramagnetic excited states. Strong antiferromagnetic coupling may lower the ground state sufficiently to allow the dimeric complex to become diamagnetic at some temperatures. The strongly coupled ($J \sim 100\ cm^{-1}$) dimeric systems $(FeHEDTA)_2O$ and $(FeEDTA)_2O$ behave in this way,[55] becoming diamagnetic at $\sim 30°K$.

In a recent paper on these two dimeric systems, the authors note[55] that the results for all such oxy-bridged systems known can be fitted equally well by two models. Either the $S_1 = 5/2$, $S_2 = 5/2$ or $S_1 = 3/2, S_2 = 3/2$ models, but not the $S_1 = 1/2$, $S_2 = 1/2$ model, fit the data. The extra spin levels of the 5/2, 5/2 model are not sufficiently populated at 300°K to discriminate between the two working models. Electronic spectral results to be discussed later are consistent[55] only with the 5/2, 5/2 model. It is this model that is used in the present study. The temperature dependence of χ for the antiferromagnetically coupled 5/2, 5/2 case is given by equation 1, using the usual notation.[56]

$$\chi = \frac{3k}{T}\left[\frac{55 + 30x^{10} + 14x^{18} + 5x^{24} + x^{28}}{11 + 9x^{10} - 7x^{18} + 5x^{24} + 3x^{28} + x^{30}}\right] + N\alpha$$

where $$K = \frac{Ng^2\beta^2}{3k} \qquad (1)$$

$$x = \exp(J/kT)$$

In this and other studies g has been assumed to be equal to 2.0, consistent with $^6A_1$ iron(III) ions. This value has been confirmed by a recent e.s.r. study of the $(FeHEDTA)_2O$ system.[54] The temperature independent paramagnetism, $N\alpha$, is assumed to be zero. The upper limit for $N\alpha$ of 130×10^{-6} cgs units per mole obtained from the $[(FeEDTA)_2O]^{4-}$ dimer study[55] is less than 1% of the diamagnetic correction for a 50,000 molecular weight protein.

The coupling constant J reflects the strength (in cm^{-1}) of the interaction present. Table 1 shows the effect of different values of J on the magnetic moment (μ) at various temperatures (°K). The difference between the coupling of iron atoms by an oxo bridge and that joined by a dihydroxobridge is apparent from this table.

Table 1

Dimeric System	Ref	$-J(cm^{-1})$	$\mu_{288°}$	$\mu_{150°}$	$\mu_{96°}$	$\mu_{30°}$
$(FeEDTA)_2O$	55	99	1.85	1.16	0.69	0
$(FeHEDTA)_2O$	55	95	1.88	1.20	0.76	~0
(Fe picolinate, $OH)_2$	58	8	5.1	4.55	3.85	2.0

6. Lattice Antiferromagnetism

This theory of antiferromagnetically coupled clusters has been applied quite successfully to the magnetic behavior of trimeric[59] and tetrameric systems.[60,77] An extension of the theory to the case of a linear chain of up to 10 identical ions has been reported.[61] The limits of the spin-spin interaction model become apparent[80] as the number of interacting ions becomes five or more. Except for arrays of high symmetry, the proliferation of different J's prevents an unambiguous determination of the set of energy levels for the system.

As mentioned above, quite different theories are required to account for a polynuclear interaction that is propagated throughout an entire lattice. Lattice type antiferromagnetic materials have a characteristic Néel temperature, below which the behavior of the susceptibility differs from that in the intermolecular antiferromagnetic case. For the latter and for a free ion, the susceptibility is independent of the strength of the applied field. The antiferromagnetic behavior of the lattice coupled case is field strength dependent. A necessary part of any investigation of lattice magnetic phenomena is a field strength study up to magnetic saturation corresponding to the alignment by the applied field of all the moments in a preferred direction.

7. Small Particles--Néel Theory of Superparamagnetism

The magnetic behavior of ferromagnetic and antiferromagnetic materials changes dramatically when the particles become very small, < 100 Å diameter. Neel has pointed out[62] that for

particles of these dimensions the anisotropy energy corresponding to the energy differences of the possible orientations of the direction of ferromagnetism or antiferromagnetism can become of the order of kT. The orientation $\underline{\Delta}$ has sufficient thermal energy to undergo a pseudo-Brownian rotation[63] with a frequency f that can be expressed as

$$f = f_0 \exp - KV/kT$$

K: anisotropy energy per unit volume

V: particle volume

KV is, of course, just an expression of the energy barrier between possible orientations of $\underline{\Delta}$. At some temperature, the blocking temperature, Tb, this energy barrier is $\sim$25 kT. As the temperature drops below T_b, a stable magnetization results from this thermally frozen magnetization and $\underline{\Delta}$ becomes stable, i.e., definitely oriented. This fluctuation of $\underline{\Delta}$ can be used to account for the unusual behavior of small magnetic particles.[64] Its implications for the magnetic susceptibility will be considered here and those for e.s.r. and Mössbauer spectroscopy will be dealt with in the appropriate following sections.

In any particle of diameter less than 100 Å the ions are not well organized into lattice planes, and the magnetic ions can be considered to constitute a single magnetic domain. The two sub-lattices of this "sponge"-like species contain a different number of magnetic ions. This difference can be approximated by $\sqrt{M}$, where M is the total number of magnetic ions in the particle. The particle magnetic moment

is then $\sqrt{M \cdot \mu_\beta}$, where μ_β, is the magnetic moment of the ion. It is oriented with and follows the fluctuations of $\underline{\Delta}$. Using this assumption Néel showed that the magnetic susceptibility of a collection of N such particles containing ions of total spin S is

$$\chi = \frac{Ng^2S^2\mu_\beta{}^2}{3kT}$$

The equivalent formula for an uncoupled system is

$$\chi = \frac{Ng^2S(S+I)\mu_\beta{}^2}{3kT}$$

Consequently in the temperature range above T_b but below T_n the susceptibility of a collection of such antiferromagnetically ordered fine particles will obey the Curie law but with a constant of proportionality below that for the uncoupled system. This constant is that for the whole particle, rather than for the single ion--hence the term superparamagnetism. The experimental observations on fine particles of many systems, i.g., α-Fe_2O_3, α-, and β-FeOOH, are in accord with this theory. The impact of particle size on the magnetic behavior can be appreciated from the observation[66] that while grains of α- and β-FeOOH less than 50 Å in diameter nearly obey the Curie law, the susceptibility of a sample in the massive state is almost temperature invariant.

As the particle diameter exceeds 100 Å, crystalline faces, well defined lattice planes, and magnetic sublattices appear. According

to the Néel theory,[62] either superparamagnetic behavior or an anomalously high antiferromagnetic susceptibility results. A systematic study of the effect of grain diameters from 20 Å to 600 Å on the magnetic behavior of nickel oxide confirms[68] these implications of the theory.

8. Solution Susceptibility Measurements

Magnetic susceptibility studies are usually carried out on a solid sample, yet particularly for metal binding proteins, the solution susceptibility is an important parameter. This can be measured conveniently using the Evans n. m. r. method.[69] The solution under investigation is placed in a capillary tube, coaxially situated inside a normal n. m. r. tube containing the solvent identical to the test solution in all respects save the paramagnetic ions. For protein studies the reference solution ideally contains the metal free protein in a concentration equimolar to that in the sample solution. Alternatively, the diamagnetism of the metal free protein can be measured separately. Both tubes contain a standard proton reference, e.g., t-butyl alcohol (TBA) for aqueous solutions. The paramagnetic ion changes the bulk susceptibility of the sample solution, changing the position of the TBA methyl resonance from that in the reference solution. This shift, Δf, is related to the paramagnetic susceptibility in the following way:

$$\chi = \frac{3}{2\pi m} \frac{\Delta f}{f} + \chi_o + \chi_o \frac{(\rho_o - \rho_s)}{m}$$

Δf: frequency separation (c/s)

f: frequency of the proton resonance (c/s)

m: mass/ml. of solute (g/ml)

χ_o: susceptibility of solute (-0.72×10^{-6} for dilute (2%) TBA solution

ρ_o: density of solvent

ρ_s: density of solution

For dilute solutions the last term can be ignored. A high concentration of paramagnetic ions can introduce further errors by broadening the resonance line. The above equation is valid for spectral shifts observed using the conventional magnet/sample configuration, where the applied magnetic field is transverse to the long axis of the cylindrical sample. Superconducting magnets, such as are used in the Varian HR-220, generate a magnetic field along the long axis of the sample. This different magnetic polarization changes the bulk susceptibility shift of the above equation.[70] It is now twice in magnitude and opposite in sign to that expected for conventional spectrometers. This effect, together with the additional dispersion of chemical shifts at the higher n.m.r. frequency, makes the HR-220 particularly suitable for paramagnetic susceptibility determinations.

The magnetic susceptibilities of the single iron atom in the oxidized and reduced rubredoxin from Clostridium pasteurianum were determined in this way to be 5.85 ± 0.2 and 5.05 ± 0.2 B.M., respectively.[71] In both the reduced and oxidized eight-iron ferredoxin

from C. pasteurianum, the presence of extensive antiferromagnetic coupling was confirmed by similar studies.[72] For ferredoxin and rubredoxin, the temperature dependence (as 1/T) of several proton resonances from the protein identified them as being contact shifted by close interaction with the paramagnetic center.

B. Electron Spin Resonance Spectroscopy

A second technique that has proved useful in identifying certain iron(III) units as polynuclear is electron spin resonance (e. s. r.) spectroscopy.[73] The spectral lines observed arise from transitions among a multiplet of energy levels derived from the electronic ground state of the iron. The splitting is induced by an applied magnetic field creating a first order Zeeman effect of characteristically low energy, $g\beta H$. This is ~ 1 cm^{-1} for an applied field of 10 kOe. The predominant interest in e. s. r. studies of transition metals has been in molecular properties rather than the cooperative phenomena of coupled systems. In fact, dilution of solids and solutions is often used to reduce the exchange interactions, however weak. Low temperatures are usually employed to increase the spin-lattice relaxation time, favoring the observation of the e. s. r. transitions as well defined resonance lines. For the high spin iron(III) of $K[Fe(SO_4)_2] \cdot 12H_2O$ diluted in $K[Al(SO_4)_2] \cdot 12H_2O$ the $^6A_{1g}$ ground term gives rise to the expected g value very close to 2.00.[74]

1. Dimeric Iron(III)

Most dimeric systems[75] that have been intensively studied involve copper(II)[76] not iron(III), but there is a recent report of the e. s. r. spectrum of single crystals of the $(FeHEDTA)_2O$ unit.[77] The major features of the e. s. r. spectra apparently result from a thermally populated S = 2 state and are consistent with the antiferromagnetically coupled 5/2, 5/2 model described for this system in Section II. B-6

above. As the temperature decreases, the complex four line spectrum from the dimeric molecule decreases in intensity with decreasing population of the S = 2 excited state. The presence of two magnetically non-equivalent molecules in the unit cell results in an eight line spectrum being observed in almost all orientations of the crystal with respect to the magnetic field. The line widths are not extensively broadened by magnetic dipole-dipole interaction, since even at room temperature most molecules occupy the diamagnetic ground state. There are few e. s. r. studies of polynuclear clusters containing more than two paramagnetic ions.[78]

2. Polymeric Iron(III)

When the number of iron atoms increases well beyond the two of the dimeric system to 20-30 atoms, this dipole-dipole interaction is expected to be the dominant feature of the e. s. r. spectrum. It is then that e. s. r. can be expected to be a diagnostic tool for identifying polynuclear iron systems. Other explanations for line broadening can usually be rejected by the temperature dependence of the spectrum. Slow tumbling of the large protein molecules can broaden resonance lines, but a temperature increase should sharpen them. Broadening due to spin-lattice relaxation effects is also temperature dependent, but it will decrease with decreasing temperatures. By contrast dipole-dipole broadening results from the physical proximity of magnetic dipoles in a coupled system and unless some structural changes occur it remains effectively independent of temperature.

3. Effect of Particle Size

When the polynuclear iron(III) system also has the dimensions suitable for paramagnetism, the e.s.r. spectrum can be broadened even further. In an analogous way to the magnetic susceptibility results, the e.s.r. absorptions have been attributed to the total magnetic moment of the grain.[62] The additional line broadening observed at temperatures below the Neel temperature can be accounted for by the fluctuations of $\underline{\Delta}$. The temperature dependence of the linewidth, δH, was described by the equation

$$\delta H = A(kV) \exp KV/kT$$

where A is a constant dependent on the grain size. This behavior has been observed by a number of investigators[79] for fine particles of Fe_2O_3 and Cr_2O_3.

C. Electronic Absorption Spectroscopy

An important objective of the present study was to derive a reasonable model for the structure in the immediate vicinity of the iron atoms, i.e., the coordination structure. Magnetic susceptibility and electron spin resonance measurements are valuable probes of the polynuclear interaction between iron atoms, but they are not particularly sensitive to the number and kind of ligand atoms that are bound to the iron. The particular arrangements of ligands that need to be distinguished are the octahedral and tetrahedral arrays of six and four ligands, respectively. The most useful method of investigation in this regard is the electronic absorption spectroscopy of the d^5 electrons of the iron(III) ion. These occur in the near infrared (NIR) and visible (VIS) regions of the spectrum. Absorption bands originating from the set of d electrons are termed ligand field bands. The ligand atoms of interest are oxygen and, to a lesser degree, nitrogen.

Iron(III) is known to occupy both octahedral and tetrahedral sites in various phases of the Fe_2O_3 and FeOOH systems.[9,10] The several models proposed for the coordination structure of the core of the protein ferritin are related to these phases. Models with iron(III) occupying only octahedral sites,[6] only tetrahedral sites,[84] and a mixture of both kinds of sites[35] have been proposed. The coordination structure in this and the other protein systems under study here has been determined primarily by an analysis of the energies of the ligand field bands.

In this section the origin of these bands and of their variation between the octahedral and the tetrahedral environments is explored. The use of the ligand field absorption bands to distinguish between these two symmetries in iron proteins presupposes a thorough analysis of the spectrum of the $[FeO_4]_{tet}$ and $[FeO_6]_{oct}$ units. Excellent spectra of both were reported and analyzed by other workers[105,106] during the course of this study. Their results are discussed in this section.

1. Effects of Various Ligand Fields

The splitting of the energies of the five d orbitals under the influence of a ligand field of octahedral, tetrahedral, and tetragonal symmetries has been presented earlier in Figure 1. As mentioned at that time, section II. A above, the unusual five-coordinate case has been observed only in the series of square pyramidal monohalogen-bis(N, N-dimethyldithiocarbamato) iron(III) complexes.[43] The ligand atoms of the chelate are sulphur atoms. The electronic absorption spectrum in these compounds of ground state with spin S = 3/2 is complex, and the ligand field transitions cannot be definitely identified. These transitions are expected to be quite different in energy and intensity from those in the octahedral and tetrahedral cases. The five-coordinate geometry has never been observed in inorganic complexes of iron(III) bound to oxygen atoms. It was not considered to be important in this study and the following discussion concerns only octahedral and tetrahedral symmetries. Although the temperature dependence of the magnetic susceptibility in the Fe-O-Fe dimeric systems can be

accounted for by antiferromagnetic coupling between either two S = 3/2 or two S = 5/2 ground state ions,[55] ligand field theory excludes the S = 3/2 ground state from octahedral and tetrahedral symmetries. The ligands of interest in this work are weak field ligands unable to induce the iron(III) to establish a S = 1/2 ground state. The subsequent discussion is restricted then to the S = 5/2 ground state which has been found to be the only one that fits the absorption spectrum of the bright red Fe-O-Fe dimers.[55] The energies of the ligand field bands in the dimers are similar to those in typical six-coordinate iron(III) complexes with a $^6A_1$ ground state. This spectrum will be described below. This similarity is reasonable in view of the relative energies of the antiferromagnetic spin-spin coupling ($J \sim 100\ cm^{-1}$) and the ligand field transitions ($>10,000\ cm^{-1}$).

The ligand field created by four ligand atoms arranged in tetrahedral symmetry is predicted[73] by ligand field theory and by simple electrostatic considerations to be less than that of six ligands in octahedral symmetry. Many experimental confirmations of the expected ratio of 4/9 have been reported. In general this means that with a lower ligand field strength a tetrahedral array of ligands will induce ligand field transitions at lower energy than would an octahedral array. As expected from the weaker field, no tetrahedral iron(III) complex has been reported as the low spin, S = 1/2 ground state. However, for the iron(III) electronic configuration, d^5, this is not the case. The energy (E) of the first one electron transition from the ground state configuration

$(t_2)^3(e)^2$ can be simply related to the strength of the ligand field (10 Dq) and to the energy (P) needed to induce two parallel electron spins to pair up with opposite spins. The transition is shown in Figure 2 From the Figure, it is clear that

$$E = P - 10\ Dq$$

As 10 Dq increases, E decreases. The important implication for this work is that the energy required for the first one electron transition in the d^5 configuration is less in a ligand field of octahedral symmetry than in one of tetrahedral symmetry.

2. Energy Level Diagram

The application of a ligand field can split the energy terms of the free ion into the appropriate energy levels of the metal ion. Thus the simple one electron transition described above corresponds to several transitions and hence absorption bands in the metal complexes. The octahedral and tetrahedral ligand fields (the cubic fields) produce the same ligand field energy level scheme from the free ion levels of the d^5 ion. The free ion ground state ^6S is not split by a cubic field. It assumes the $^6A_1$ symmetry label. The first excited state of the free ion ^4G does split into two T states, $^4T_1$, $^4T_2$, and into a degenerate pair, $^4A_1$, ^4E. All retain the spin quartet character of the free ion term. The first three ligand field absorption transitions for the d^5 configuration are the sextet to quartet transitions:

Figure 2

Diagrammatic representation of the energy (E) of the first one-electron transition within the set of d orbitals in an octahedral ligand field of strength (10 Dq). P is the electron pairing energy.

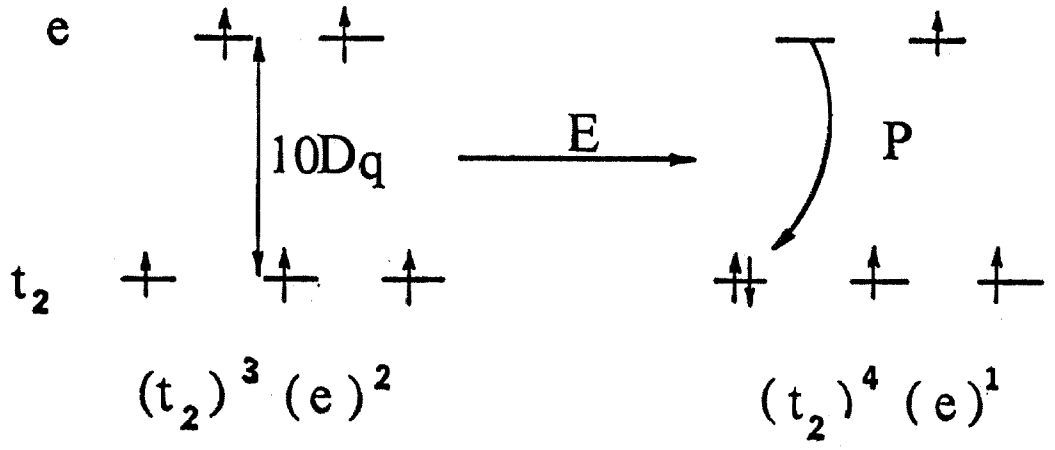

$$E = P - 10Dq$$

$$^6A_1 \rightarrow {}^4T_1;\ {}^6A_1 \rightarrow {}^4T_2;\ {}^6A_1 \rightarrow {}^4A_1,\ {}^4E$$

The extent of this splitting can be calculated[107,108] as a function of 10 Dq, and the two parameters describing the electron-electron repulsion energies, B and C. These diagrams were first calculated by Tanabe and Sugano for cubic fields using a fixed C/B ratio of 4.48.

The behavior of the four lowest energy levels relative to the $^6A_1$ ground state is shown as a function of the strength of the ligand field in Figure 3. The diagram indicates that the $^4A_1$, ^4E level is independent of the ligand field. Ligand field bands are usually broadened by vibrations that modulate the size of 10 Dq. This mechanism of broadening is unavailable to the $^6A_1 \rightarrow {}^4A_1$, ^4E transition and the absorption band is correspondingly narrow. Its unusual behavior in this respect allows it to be readily identified.

These four transitions are from a sextet state to quartet states. Consequently, they are spin forbidden. In octahedral symmetry with its center of inversion, transitions within the set of pure d orbitals are forbidden (Laporte forbidden). This condition is relaxed in tetrahedral symmetry where there is no inversion center and the d and p orbitals are of appropriate symmetry to mix together. The spin forbidden bands are expected to be weak ($\epsilon < 1$) but the intensity in the octahedral case is lowered even further by the Laporte rule ($\epsilon \sim 0.05 - 0.01$).

A description of the energy of the spin forbidden transitions involves both B and C. The three parameters 10 Dq, B, and C are then required to describe the d^5 ligand field transitions. Consequently, at

Figure 3

The dependence on the strength of the ligand field (10 Dq) of the energy of the four lowest ligand field transitions for d^5 iron(III) complexes in octahedral and tetrahedral coordination.

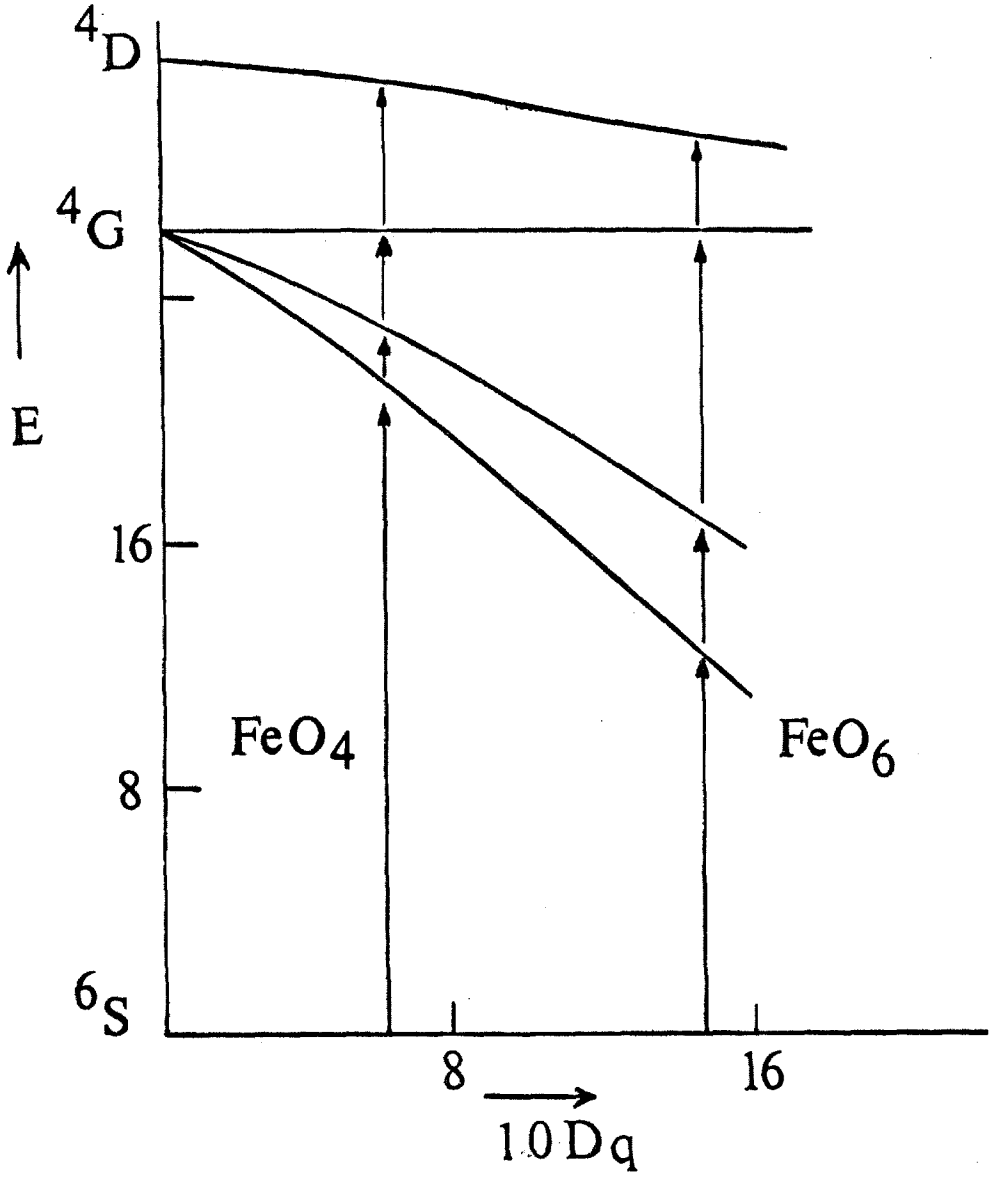
4D
4G
E
16
8
6S
FeO4
FeO6
8
16
10 Dq

least four ligand field transitions must be identified to simultaneously and unambiguously determine 10 Dq, B, and C. The fourth ligand field transition is $^6A_1 \rightarrow {}^4T_2$. In both octahedral and tetrahedral symmetries it is expected to occur close to the ultraviolet end of the visible region. The prevalence of intense charge transfer bands in the ultraviolet is expected to preclude the observation of more than four ligand field bands even in favorable cases.

3. Reference Spectra--$[FeO_6]_{oct}$ and $[FeO_4]_{tet}$

Excellent spectra of iron(III) coordinated to oxygen donor ligands in octahedral and tetrahedral symmetry have recently been reported. The spectrum of $[Fe(H_2O)_6]^{3+}$ has long been obscured by the absorptions of the hydrolysis and polymerization products of iron(III). The ligand field bands for this species have now been observed in a large, pale purple, single crystal of ferric ammonium sulphate.[106] Previous spectroscopic studies of tetrahedral Fe(III) have included $FeCl_4^-$,[109,110] 8-tungstoferrate(III) ion,[111] and β-$NaAl_{1-x}Fe_xO_2$.[112] In the first two cases the important ligand-field bands are somewhat obscured by intense, low-energy absorption, and are split in a complex fashion. The $FeCl_4^-$ spectrum will be discussed in section III-B below. In the third case the Fe(III) coordination is significantly distorted from tetrahedral symmetry.

The tetrahedral species $[FeO_4]_{tet}$ has been examined[105,106] in an iron(III) doped sample of orthoclase feldspar, ideally $KAlSi_3O_8$.

The sample was gem quality, light green in color, in which a small amount of the aluminum in tetrahedral sites had been replaced by iron(III). The two spectra are shown in Figure 4.

In both spectra four low intensity ligand field bands are resolved. The common pattern of two broad bands and a comparatively sharper band at higher energy is apparent. The fairly sharp band is assigned to the $^6A_1 \rightarrow {}^4A_1, {}^4E$ transition. As expected the two spectra show very clearly that the two lowest bands corresponding to the $^6A_1 \rightarrow {}^4T_1$ and $^6A_1 \rightarrow {}^4T_2$ transitions are substantially lower in energy in the octahedral case. The extinction coefficients are low, and those of the octahedral absorptions are generally lower. The identification of four ligand field bands allowed an unambiguous determination of the parameters involved in the Tanabe-Sugano calculations: 10 Dq, B, and C. The data for these spectra together with the parameter values giving the best fit[106] between calculated and experimental energies are shown in Table 2.

The weakness of these ligand field bands as expressed by the small extinction coefficients can make them difficult to observe. Both of the above spectra were recorded on large single crystals. There is an obvious difficulty arising from concentration problems in observing these bands in solution or in an aggregate of small crystals or a lyophilized powder. Reference to this limitation will be made in the later discussion. The intensity of these bands is increased in the case of polynuclear iron. Several instances of this increased intensity of spin-forbidden bands in antiferromagnetically coupled transition

Figure 4

Electronic absorption spectra of the ligand field transitions in FeO_6, recorded as $Fe(H_2O)_6^{3+}$ in iron(III) ammonium sulphate, and in FeO_4, recorded as $[FeO_4]$ in orthoclase feldspar.

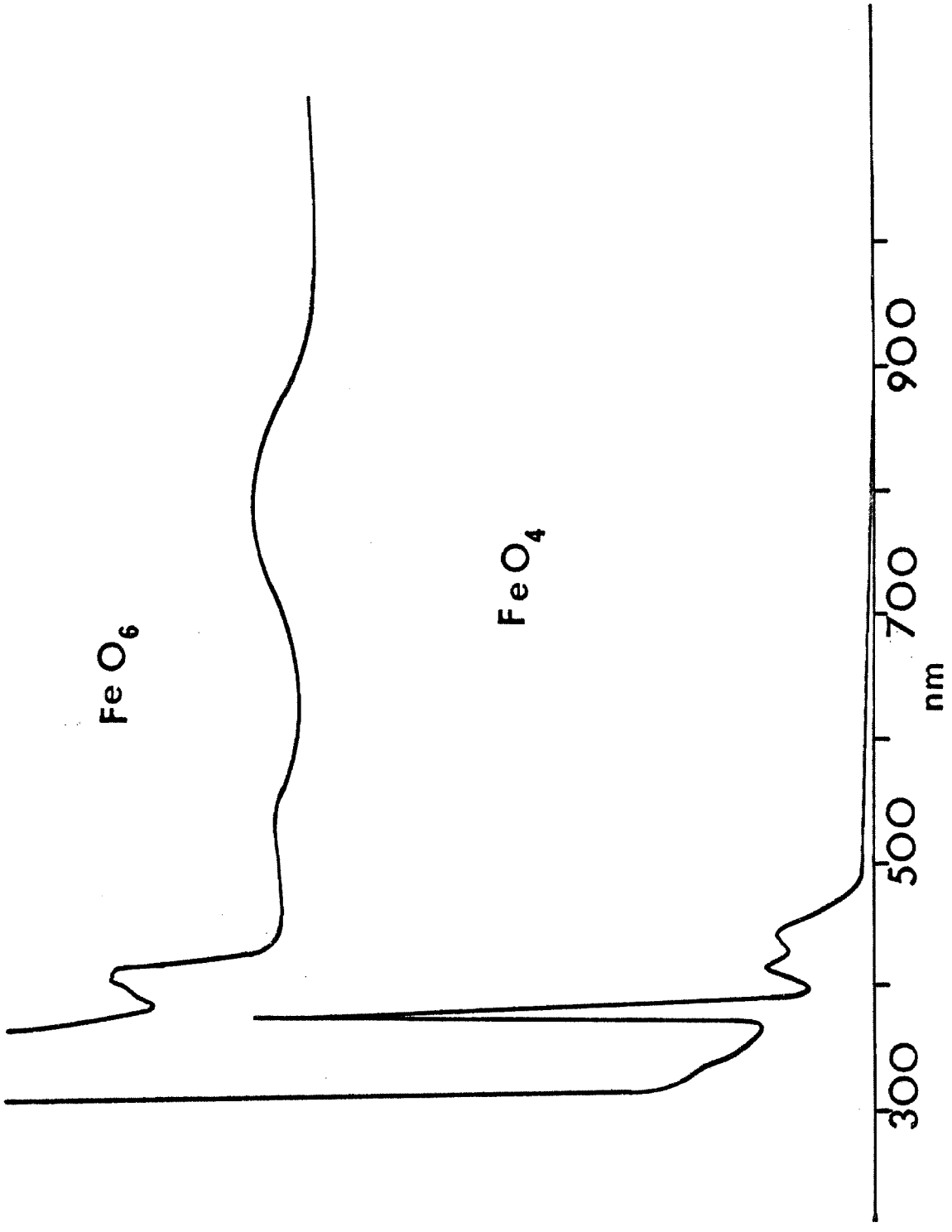
FeO_6
FeO_4
300
500
700
900
nm

Table 2

Transition	$[FeO_6]_{oct}$ λ(nm)	$\tilde{\nu}$ (cm^{-1})	ε	$[FeO_4]_{tet}$ λ(nm)	$\tilde{\nu}$ (cm^{-1})	ε
$^6A_1 \rightarrow {}^4T_1$	795	12,600	0.05	444	22,500	0.73
$^6A_1 \rightarrow {}^4T_2$	550	18,200	0.01	418	23,900	0.76
	413	24,200				
$^6A_1 \rightarrow {}^4A_1, {}^4E$	407	24,600	0.13	377	26,500	4.1
	394	25,400				
$^6A_1 \rightarrow {}^4T_2$	361	27,700	0.1	342	29,200	0.1
Parameter						
10 Dq		13,700			7350	
B		945			540	
C		2960			4230	

metal ions have been reported. They include both lattice antiferromagnetism[113,115] (in the manganese(II) halides, e.g., $MnCl_2$) and intermolecular antiferromagnetism,[55] e.g., $(FeEDTA)_2O$ and $(FeHEDTA)_2O$.

In both cases of antiferromagnetic interaction the band intensities are increased by a factor of 10-50 over the corresponding magnetically dilute systems, i.e., $MnCl_2 \cdot 4H_2O$, and the monomers Fe · EDTA, Fe · HEDTA. This breakdown in the spin multiplicity rule can be taken into account[114] in a description of the antiferromagnetic coupling between nearest neighbors using the spin-spin coupling model described above.

By increasing the intensities of the ligand field bands the polynuclear nature of the iron increases the ease with which those bands might be observed. The extinction coefficients for these bands are still low, however, and can be easily obscured by strong low energy absorption bands.

4. Implications for Protein Spectra

Several features of these reference spectra are important for the spectral studies of the polynuclear iron proteins reported in this work.

a) The apparent color is suggestive of the possible coordination structures of the iron(III). The monomeric octahedral iron(III) is pale violet. The monomeric tetrahedral iron(III) is light green. The dimeric bridged octahedral dimer is bright red. The FeOOH

and Fe_2O_3 phases, and the protein ferritin, are reddish brown in color. Polymeric iron(III) in tetrahedral symmetry has been reported[116] in a quartz phase of iron(III) phosphate, $FePO_4$, formed by high temperature synthesis. The spectrum of this is reported and discussed below, in section III. B. It is also light green-yellow in color.

b) The band pattern for the d^5 configuration is common to the octahedral and tetrahedral cases, yet the widely different energies of the ligand field bands in the two symmetries allows them to be readily distinguished.

c) The relative intensities of the bands in the two symmetries is that expected from theoretical considerations, i. e., tetrahedral > octahedral.

d) From an analysis of the ligand field bands the values of 10 Dq, B, and C that are characteristic for the stereochemistries $[FeO_4]_{tet}$ and $[FeO_4]_{oct}$ have been obtained.

In cases where only three of the ligand field bands are identified, the three parameters 10 Dq, B, and C cannot be allowed to vary simultaneously to give a meaningful fit of the spectrum. The appropriate C/B ratio to assume for the characteristic pattern for the octahedral and tetrahedral symmetries is now known.

D. Mössbauer Spectroscopy

Small perturbations on the nuclear energy levels of iron by the surrounding electrons can be studied by Mössbauer spectroscopy, the recoilless emission and absorption of low energy γ-radiation. The nuclear transition of interest is that between the I = 3/2 and I = 1/2 levels of the Mössbauer nuclide ^{57}Fe, where I is the nuclear spin quantum number. The energy change for the transition is 14.36 keV. A typical requirement for Mössbauer work is 1-2 micromoles of ^{57}Fe which has a low natural abundance of 2.19%. For a protein of 50,000 molecular weight that binds one iron atom, and without isotopic enrichment, this amount of Fe is contained in 2.5 g. The polynuclear iron proteins of this study are characteristically richer in iron than this and are quite suitable for Mössbauer spectroscopy.

The deductions of a structural nature that have been drawn from the results of Mössbauer studies of the protein ferritin and its several structural analogs are still controversial. In this study the Mössbauer spectrum of the most promising of these analogs was recorded. A discussion of the technique and the experimental parameters determined is included at this point preparatory to a later discussion of these results.

In the customary experimental arrangement, the incident energy is varied by including a small relative velocity between the source and sample. The unit of the energy scale is mm/sec. In more conventional terms 1 mm/sec is equivalent to 4.8×10^{-8} eV, about ten times the natural linewidth for ^{57}Fe of 4.7×10^{-9} eV. Four interactions are

possible between the ^{57}Fe nuclide and the electronic surroundings. They are shown in Figure 5.

1. Four Experimental Parameters

a) Isomer Shift--the interaction of the different nuclear charge densities of both the ground and excited states with the electronic charge density at the nucleus produces small changes in these energy levels relative to a standard substance. The isomer shift is related to the s-electron density at the nucleus.

b) Quadropole Splitting--the electric quadrupole of the nuclear excited state (I = 3/2) interacts with the electric field gradients at the nucleus produced by external lattice effects, by unfilled sets of orbitals, e.g., the d orbitals, and by polarization of filled inner shells of electrons. The magnitude of this splitting provides an estimate of the point symmetry about the iron nucleus.

c) Nuclear Magnetic Hyperfine Interactions--unpaired electrons in the outer shells have different exchange interactions with s-electrons of spin quantum number $m_s = 1/2$ than with those with $m_s = -1/2$. The resultant polarization of the s electrons provides a non-zero s-electron charge density at the nucleus creating an internal magnetic field that splits the two nuclear states. According to the selection rule $\Delta I = 0, \pm 1$ six transitions are possible. They can be observed as a six line spectrum when the electronic spin lattice relaxation time is long compared to the characteristic Lamor precession

Figure 5

Effects of three Mössbauer interactions on the nuclear energy levels of ^{57}Fe

(1) The isomer shift resulting from the difference in nuclear energy levels in source (left) and absorber (right) due to differences in electron charge densities.

(2) The quadrupole splitting resulting from the splitting of the excited state by an electric field gradient.

(3) The nuclear hyperfine resulting from the splitting of both nuclear levels by a magnetic field.

Isomer Shift (I. S.)

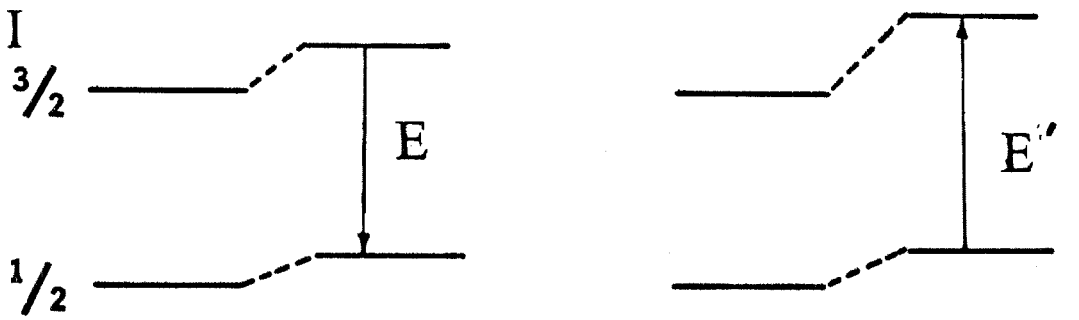

$$I.S. = E' - E$$

Quadrupole Splitting (Q. S.)

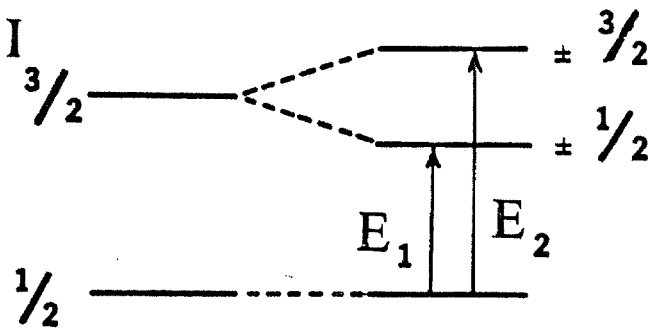

$$Q.S. = E_2 - E_1$$

Nuclear Hyperfine:

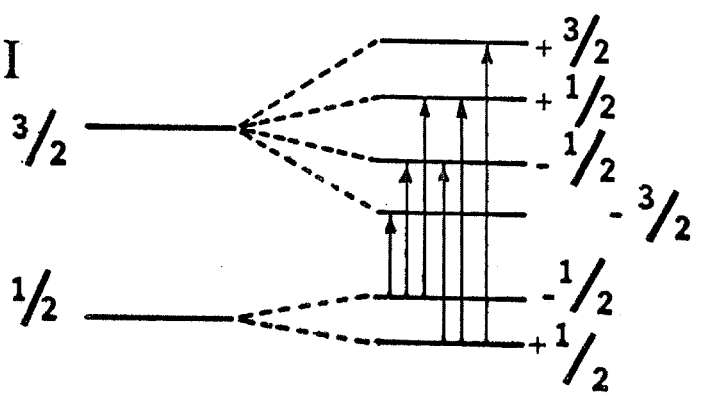

time of the nuclear magnetic moments. This precession time is inversely proportional to the internal field. The usual requirement to observe the hyperfine spectrum for ^{57}Fe is an internal field in excess of 10 kOe,and/or low temperatures. The internal fields observed can be quite large, 500-600 kOe. Iron metal, a ferromagnet, creates an internal field of 330 kOe.

d) Nuclear Zeeman Interactions--the magnetic hyperfine of (c) above is produced by the application of a strong external magnetic field (30-40 kOe).

2. Effects of Particle Size

A second characteristic Mössbauer time is the mean lifetime of the nuclear excited state, 1.4×10^{-7} sec for ^{57}Fe. It is of particular importance in the Mössbauer spectra of the very small particles (diameter $<$ 100 Å) first discussed in section II. A-7 above. With the anisotropy energy comparable to kT the orientation of the magnetic field at the nucleus fluctuates with a relaxation time τ that is an exponential function of the particle volume, V, and the reciprocal temperature, T.

$$\tau = \tau_0 \exp (KV/kT) \qquad K: \text{ anisotropy constant}$$

By lowering the temperature the relaxation time becomes comparable to or larger than the mean lifetime of the nuclear excited state and a magnetic hyperfine spectrum is observed. A distribution in particle size results in a finite temperature range over which the

hyperfine spectrum is established and the usual quadrupole split doublet disappears. This behavior is characteristic of superparamagnetic particles, e.g., fine grains of α-Fe_2O_3,[102] and the core of ferritin.[103]

3. Structural Implications

The isomer shift and the quadrupole splitting can be related to the electronic configuration and stereochemistry of the iron nucleus. Only high spin iron(II) is unambiguously determined in this way. Analysis of the Mössbauer data for other states requires a detailed consideration of all four of the above parameters. Spectra of well characterized compounds can show significant differences. The changes in the isomer shift with respect to stainless steel between high spin iron(II) and (III), low spin iron(II) and (III), and between high spin iron(III) in two stereochemistries are shown in Table 3.

Table 3

Compound	Configuration	Stereochemistry	I.S. (mm/sec)	Ref.
$FeSO_4 \cdot 7H_2O$	high spin iron(II)	octahedral	1.4	(95)
$Fe_2(SO_4)_3 \cdot 6H_2O$	high spin iron(III)	octahedral	0.52	(95)
$K_4Fe(CN)_6 \cdot 3H_2O$	low spin iron(II)	octahedral	0.083	(95)
$K_3Fe(CN)_6$	low spin iron(III)	octahedral	0.000	(95)
$Co(en)_3 \cdot FeCl_6$	high spin iron(III)	octahedral	0.40	(96)
$(CH_3)_4N \cdot FeCl_4$	high spin iron(III)	tetrahedral	0.20	(96)

The quadrupole splitting for high spin iron(II), with the d^6 electron configuration is in the range 2-3 mm/sec while that for high spin iron(III) d^5 compounds is smaller, 0-1 mm/sec. The low spin splittings of both iron(II) and (III) are small, < 0.6 mm/sec. Mössbauer data for a number of monomeric and dimeric iron(III) compounds have been reported.[55] There is little difference in the isomer shifts between the two kinds of compounds, but the quadrupole splitting is usually greater in the dimeric case.

The Mössbauer spectrum of compounds with iron(III) in both octahedral and tetrahedral sites is expected to be broadened and perhaps resolvable into two sets of lines. Examples of both kinds of spectra are known. The following examples involve iron(III) bound only to oxygen ligands, the ligands of prime interest in this work. The ferromagnetic iron garnets $5Fe_2O_3 \cdot 3M_2O_3$ where M is a rare earth or yttrium, have a body-centered cubic structure[97] with two iron(III) sublattices, octahedral and tetrahedral, with an occupancy ratio of 2:3. There is a strong magnetic exchange interaction between the two sublattices and the Mössbauer spectrum is expected to be the six-line hyperfine. In fact for yttrium and dysprosium iron garnets, two hyperfine spectra are readily observed indicating that the local fields at the two lattice sites are appreciably different. The isomer shifts for the two sites differ but the most significant difference is in the effective field at the nucleus.

The Mössbauer spectra of the phases of the iron(III) oxide and iron(III) oxyhydroxide system have been reported.[100,101] Both γ-Fe_2O_3[98] and δ-FeOOH[99] are reported to have iron(III) ions occupying sites of octahedral and tetrahedral symmetry. δ-FeOOH is a metastable phase and forms crystal of varying morphology, leaving some doubt about the exact structure. The two hyperfine spectra of the structurally well characterized γ-Fe_2O_3 can only be resolved by the application of a strong external field (17 kOe). The zero applied field hyperfine field differs only slightly between the two sites. In the δ-FeOOH the two apparently unresolved hyperfine spectra are determined by line shape analysis, and the effective fields are comparable for the two sites. These data for the variation of the hyperfine field are shown in Table 4.

Table 4

Effective Hyperfine Field (kOe)

Compound	Tetrahedral	Octahedral	Temp (°K)
iron garnets	390 ± 10	485 ± 15	295
iron garnets	460 ± 15	535 ± 15	77
γ-Fe_2O_3	488 ± 5	499 ± 9	77
δ-FeOOH	505 ± 5	525 ± 5	77

In any one compound the hyperfine field at the octahedral sites is greater than that at the tetrahedral sites. The variation of each among the compounds is considerable. A similar variation is observed for each site symmetry when the ligand atoms change.[101]

E. X-Ray Studies

The X-ray techniques relevant to the present investigation are the Debye-Scherrer or powder method for fine grained solid samples and the low angle X-ray scattering of solutions. They are considered in turn.

1. X-ray Powder Patterns

These patterns have been widely used in studies of the crystal structure of the core of ferritin.[34] The main experimental difficulty derives from the dimensions of the core, 70 Å, so small that any diffraction pattern produced is expected to be diffuse. The usual procedure[81] in this technique is to bombard an aggregate of finely ground crystallites packed in a narrow capillary with a collimated monochromatic beam of X-rays while the capillary rotates 360° and reciprocates through a small (~5 mm) vertical distance. The diffraction pattern observed is not the spot pattern produced by a single crystal but a superposition of many such patterns producing a series of diffraction lines. The lines correspond to reflections from the lattice planes that scatter in phase as determined by the usual Bragg equation:

$$n\lambda = 2\,d\,\sin\theta$$

Lattice dimensions determine the spacing d and the corresponding diffraction angle θ fixes the line position. The intensity of the line depends however on the chemical composition. Interference between various lattice arrays of the atoms in the cell determines the

intensity. The structural information provided by the diffraction pattern consists of the position and intensity of the diffraction lines, rarely more than twenty in number. The structural information lost in using an aggregate of crystals rather than a single crystal is considerable, but many systems can only be investigated using powder patterns.

The diffracted beam from a lattice plane of spacing d describes a cone of half opening angle 2θ. The longer the wavelength of the radiation used, the greater the θ values and the more dispersed are the diffraction lines. To minimize the absorption and subsequent fluorescence of the incident radiation by the sample the radiation of choice for the study of iron compounds is cobalt ($\lambda = 1.79$ Å) or molybdenum (0.71 Å). The shorter molybdenum radiation has minimum absorption and decreases the cone of diffraction. This unnecessarily crowds together a pattern of many sharp discrete lines but it facilitates the visualization of weak diffuse bands.

A monochromatic beam is obtained by filtering off the β emission from the source, leaving the α_1 and α_2 lines. These are close in wavelength, 0.714 Å and 0.709 Å for molybdenum. The filter used for cobalt radiation is usually iron, and that for molybdenum usually zirconium. For optimum resolution in studies of iron compounds present as particles of small size and/or poor crystallinity molybdenum radiation should be used with a zirconium filter on the incident beam and on the diffracted beam. It was this arrangement that was used in this study.

To obtain sharp diffraction maxima thousands of parallel planes must diffract the beam in phase. This poses a high degree of precision on the Bragg equation. As the crystallite size decreases the number of cooperating planes decreases and the diffraction condition relaxes. As a result the diffraction lines broaden. A completely amorphous substance produces merely a broad halo at a small diffraction angle. In fact, line broadening can be used[81-82] to estimate particle size in the range below ~2000 Å. This broadening leads to serious uncertainties in locating the center of the diffraction line on the film. The scarcity of lines whose positions are poorly defined makes it almost impossible to derive the cell dimensions unambiguously. Such indexing indicates probable dimensions, rather than measures realistic quantitites. The patterns of synthetic and natural analogs are often used in analyzing the pattern produced by an unknown substance. When the observed lines of the unknown are few in number and broadly diffuse, such comparisons have a high degree of uncertainty, as do the chemical inferences drawn from such comparative studies.

The only systems in this study that had crystallinity to produce any diffraction lines were ferritin and hemosiderin. In both cases the lines produced were few in number and diffuse. The diffraction pattern does contain important structural information, but most of the above cautionary comments are relevant to the discussion of the results obtained on these two systems.

2. Low Angle X-ray Scattering of Solutions

Although this technique was not used in this thesis research, two of the compounds studied, the nitrate polymer[84] and the protein ferritin,[86] have been investigated by other workers using this method. The structural conclusions presented in the report on the low angle scattering by the nitrate polymer are at variance with the results of this research. The specific objections to the scattering results will be dealt with in the later discussion. A short description of the technique is presented at this point.

In experiments of this kind[83] a monochromatic and highly collimated X-ray beam is directed onto the solution under study and measurements made of the intensity of that portion of the X-rays scattered at small angles ($\theta \leqslant \sim 5°$) to the beam direction. The scattering curve of relative intensity against θ will usually contain several small maxima superimposed on the side of a curve that rapidly decreases as θ increases from zero to 5°. This curve can be converted by a Fourier transformation into a radial distribution function (RDF) of charge distribution plotted against the separation between the scattering centers. These curves reflect the shape and dimensions of the scattering unit as well as the interactions between them. For a solution of argon the curve provides information on the short range order present. An estimate of the number of nearest neighbors, i.e., the coordination number of argon can be obtained.

For a solution containing particles of small dimensions, ~50-500 Å, the scattering curve can provide information on the particle shape, e.g., a measure of the effective radius of gyration. Such studies have been reported for some spherical viruses and a number of proteins, e.g., ovalbumin.[83] To obtain information about the internal composition of a particle in solution two scattering experiments must be done. The scattering curve of the solvent alone is determined and applied as a correction to the scattering curve of the solution of particles. A Fourier transformation of this difference function is then performed and the ripples in the curve analyzed to derive the interatomic separations for the scattering units. Analysis of the areas under these peaks is used to estimate the number of nearest neighbors around a scattering atom.

Two possible sources of significant error are present in the above procedure for obtaining structural details from a low angle scattering experiment. The correction due to the solvent scattering cannot take into account the changes in this scattering caused by the inclusion of the solute. The scattering reflects the short range order in the solvent, which can be seriously perturbed by the inclusion of a solute. Solute concentrations of several molar are commonly employed. The second difficulty occurs in the analysis of the peak areas to give the coordination number around a scattering center. A recent study[85] used the experimentally determined RDF of argon to compare the four procedures commonly used to derive the coordination number.

The computed coordination number for the saturated liquid varied from 5 to 7. This analysis was carried out on a Fourier derived RDF for a homogeneous liquid, not for the much more uncertain RDF produced by the difference Fourier procedure used in the analysis of the internal structure of a particle in solution.

There is limited access through this technique to the kind of structural information that is of interest in this study. Attempts to derive it are fraught with difficulties, much more so than for the other techniques discussed. However, the technique is extremely useful in obtaining information on the dimensions of particles in solution. A careful and thorough study determined the solution dimensions of ferritin without any iron and with varying amounts of iron present in the core.[86]

F. Vibrational Spectroscopy

The spectral region 0-15,000 cm^{-1} encompasses the far infrared (FIR: 0-400 cm^{-1}), infrared (IR: 400-4,000 cm^{-1}), and near infrared (NIR: 4,000-15,000 cm^{-1}) regions. Most of the important stretching, bending, and rotating vibrations of molecular and lattice origin occur in the FIR and IR regions, both of which can be studied by infrared and Raman spectroscopy. Studies of overtones of some of these vibrations in the NIR region have been quite successfully applied to the analysis of the conformational behavior of polypeptides and polynucleotides in solution.[87] The only part of this spectral region that is of interest in this study is the high energy region, 10,000-15,000 cm^{-1} where the first low energy electronic transitions for iron(III) are known to occur. That spectral region has been discussed in Section II-D above.

1. Infrared and Raman Methods

Infrared and Raman spectroscopic techniques are complementary. Their selection rules differ. Infrared active modes involve a charge in electric dipole during the vibration, while the Raman active mode changes the polarizability. As the molecular symmetry lessens more vibrational modes become both infrared and Raman active, until in the case of macromolecules almost all modes are allowed in both. Instrumental limitations usually restrict the infrared technique to the region 4000-200 cm^{-1} and the Raman to 1000-25 cm^{-1}. The entire FIR range can be studied for infrared vibrations by using interferometry

rather than conventional instrumental design. Blue lasers are extending the effective range of the Raman technique to energies above 1000 cm^{-1}.

When there is a very large number of allowed vibrational modes vibrational spectroscopy becomes limited by the resolution of the instrument and the difficulty of unambiguously assigning bands in a complex spectrum to any particular structural unit of the molecule. At this stage the technique becomes one of empirical comparative analysis between compounds. However structural inferences from characterized spectra to that of an unknown can be tenuous.

2. Protein Effects

For the proteins that bind quite large clusters of polynuclear iron considered in this study vibrational spectroscopy offers a means of identifying the important polynuclear Fe-O-Fe and Fe-OH-Fe structural units. Characteristic vibrational energies of both these units have been identified in inorganic complexes. The asymmetric stretch of Fe-O-Fe is expected[88] at ~850 cm^{-1} and the symmetric at ~230 cm^{-1}.

A weak band at 950 cm^{-1} that moves to lower energy on deuteration has been identified[14] as arising from the $Fe(OH)_2Fe$ unit. The band appears at 970 cm^{-1} in the analogous chromium(III) dimer. The search for these vibrations in a macromolecule is inevitably frustrated by the preponderance in this spectral region of the carbon-carbon stretching, carbon-hydrogen, and nitrogen-hydrogen rocking

vibrations from the polypeptide chain. This frustration is also to be expected for the vibrational modes corresponding to the bonds between iron and the nitrogen or oxygen of amino acid side chains. Even comparative studies between the metal free and the metal bound protein promise little definitive information because of the unknown effect on the protein vibrational energies of the conformational changes induced by metal binding.

Clearly the most promising polynuclear iron protein for study using these techniques would be one that is high in iron content and in which the spectral features arising from iron-iron interactions can be separated from those from the iron-protein binding. Ferritin, by virtue of its structure, fits these requirements. The iron content is high ($>20\%$ by weight) and the iron is contained in a spherical core that effectively insulates most of the iron atoms from direct binding to the protein.

3. Particle Size and Surface Binding

As mentioned in sections II-B and II-C above, ferritin introduces the complications arising from the small particle size of the core, 70 Å. The implications of small particle size for vibrational spectroscopy have not received the theoretical analysis that the magnetic behavior has, but the lack of a well defined lattice in such a small particle is expected to broaden the absorptions making comparative studies difficult. There is no report of a systematic study of the effect on infrared bands of variations in the particle size in this range 25-1000 Å.

Active interest in catalytic processes on solid surfaces has led to many studies by infrared spectroscopy of surface phenomena and adsorbed species.[89,90] The moderate success achieved in this area suggests that specific adsorbed species and their relation to the surface might be identified for the surface area of the 70 Å core of ferritin. The role of phosphate in the core has long been assumed[34] to be that of a surface bound layer between the core and the protein.

Like all spectroscopies, vibrational spectroscopy has its definite limitations. In the present study it offers most promise in analyzing the structure of the core of ferritin.

G. Electron Spectroscopy for Chemical Analysis (ESCA)

This relatively new technique, pioneered by Siegbahn and co-workers at Uppsala,[91] analyzes the energy of the electrons emitted from the surface layer (~100 Å) of a sample irradiated with X-rays. The electron spectrum reproduces the electronic energy level structure of the core electrons, providing excellent values for the binding energies of these electrons. Since the screening of the core electrons and hence their binding energies are affected by the charge distribution of the outer electrons, ESCA also provides information on the chemical structure of the compound. All elements and at least several levels for each element are available for study by this technique. The measured core electron binding energies have been shown[92] to correlate directly with atomic charge calculated by a number of formalisms, e.g., the extended Hückel molecular orbital procedure.

1. Iron and Phosphorus Studies

In this study ESCA was used to provide information on the binding interactions between iron and phosphorous in the protein phosvitin. Typical values for some of the binding energies for electrons from the L and M shells of iron and phosphorous are listed in Table 5.

Table 5

	$L_I(2s_{1/2})$	$L_{II}(2p_{1/2})$	$L_{III}(2p_{3/2})$	$M_I(3s_{1/2})$	$M_{II}(3p_{1/2})$
P	189	136	135	16	10
Fe	846	723	710	95	56

2. Binding Energy Comparisons

The routine use of ESCA to indicate the charge density of an atom presupposes the existence of a chemical shift scale for that element. Such scales exist for oxygen, carbon, and particularly, for nitrogen and sulphur. The chemical shift data for phosphorous are meager. Those for iron are more extensive. A recent report[93] lists about twenty values for the $3p_{1/2}$ binding energies in a variety of metal complexes, ionic salts and mineral compounds. A more limited number of measurements of the $2p_{3/2}$ iron binding energies has been reported.[104] A selection of these measurements is listed in Table 6.

The anticipated trend of an increase in binding energy with increasing formal oxidation state is indicated, e.g., by the $3p_{1/2}$ and $2p_{3/2}$ binding energies of $K_3Fe(CN)_6$ and $K_4Fe(CN)_6$. Compounds containing different ligands cannot be easily related. The $3p_{1/2}$ binding energy for iron pentacarbonyl, $Fe(CO)_5$, is the same for ferrocyanide, $K_4Fe(CN)_6$. The trends are not consistent between the two sets of data. The $2p_{3/2}$ spectral lines are sharper and more readily observed than are the $3p_{1/2}$ ones. The $2p_{3/2}$ binding energies were measured in this study.

Although the pure compounds listed in the above table may have measurably different binding energies,the resolution in both sets of measurements is not better than 0.5 eV. Consequently, the simultaneous determination of the binding energies of closely related compounds in a mixture may be quite difficult.

Table 6

Compound	Iron Binding Energy	
	$3p_{1/2}$	$2p_{3/2}$
$K_3Fe(CN)_6$	55.0	709.0
Fe_2O_3	54.9	711.6
Fe(III)-Cl Phthalocyanine	54.4	
$K_4Fe(CN)_6$;	54.0	707.8
$Fe(CO)_5$	54.0	
Fe(II)-Phthalocyanine	53.0	
Fe metal	52.4	710.0

The implication from these results is that only comparisons between closely related compounds are meaningful. The structural implications of the binding energy of some core electron level measured by ESCA for a compound whose detailed structure is unknown depend critically on the measurement of the equivalent binding energies for a series of closely related compounds. It was this procedure that was used in the present study of the binding energy of iron and phosphorous in relation to their structural roles in phosvitin.

III. RESULTS AND DISCUSSION

A. Transferrin

1. Preparation and Characterization

Iron transferrin was prepared from iron-free commercial egg white transferrin (conalbumin, Nutritional Biochemicals Corp.) that had been exhaustively dialyzed against tris buffer, 0.0005M, pH 7.5, to remove any low molecular weight chelates. The iron was presented to the protein as the iron-nitrilotriacetate complex, pH 7.5. The resulting salmon pink solution was concentrated by pressure dialysis through a membrane (Amicon Corp. diaflo UM-10) under nitrogen (60 p.s.i.), then filtered several times through a millipore filter (0.22 μ). Lyophilization of this solution provided the solid sample used in the magnetic studies.

The transferrin prepared in this fashion was homogeneous by polyacrylamide gel electrophoresis at pH 8.4. The three genetic components with pI values close to 6 were resolved by isoelectric focussing on an LKB 1801 apparatus. The molecular weight was determined by sedimentation equilibrium using a Spinco Model E ultracentrifuge to be 77,500 ± 2,900 at a 95% confidence level.

2. Magnetic Studies

The diamagnetic susceptibility of the iron-free protein was measured directly. It is $-36,000 \pm 200 \times 10^{-6}$ cgs units. For two high spin d^5 iron(III) ions the paramagnetic susceptibility is $\sim 30,000 \times 10^{-6}$ cgs units. The simultaneous presence of these two susceptibilities in

the one compound, e.g., iron transferrin, results in a small room temperature diamagnetism that is difficult to measure precisely. At lower temperatures the paramagnetic component increases, yet its determination is still imprecise. This difficulty is accentuated by the diamagnetic contribution of the coolant gas flow to the signal produced in the magnetometer. The gas density, and hence this diamagnetic contribution, increases with decreasing temperature. The magnetic susceptibility was measured on several preparations of iron transferrin over the range 300-100°K. The value of the magnetic moment per iron over this range appears constant, and is calculated to be 5.0 ± 0.5 B.M.

3. Spectral Studies

The well known feature of the visible spectrum of iron transferrin is a strong absorption at 465 nm that is responsible for the characteristic salmon pink color. Attempts to observe the weak bands corresponding to the spin forbidden ligand field transition were unsuccessful. Although the iron protein is quite soluble, it is not soluble enough to observe these weak absorptions. To produce an optical density of 0.01 in an absorption band of extinction coefficient 0.1, an 8% solution is required.

4. Discussion

The magnetic susceptibility of transferrin has been reported[119] in the range 1,2 - 4.2°K to be that of a simple S = 5/2 ion, i.e., high spin iron(III). The value of the magnetic moment obtained in this work, 5.0 ± 0.5 B.M., tends to confirm that this

description is valid also over the higher temperature range, 100-300°K, but the measurements are characterized by a large uncertainty (± 10%). The coordination structure of the two apparently identical[119] iron binding sites could not be determined by the positions of the ligand field bands. It has long been presumed to be octahedral.

The characteristic absorption band in the visible has been observed[119] in complexes of transferrin with three trivalent metal ions, Mn^{3+}, Fe^{2+}, and Co^{3+}. The extinction coefficient per metal ion in these complexes is 2,000-4,000. A comparison of the energy of this band in these three cases with the appropriate reduction potentials of the metal ions is made in Table 7.

The order of increasing energy is also that of increasing reduction potential for the simple hydrated metal ion. The E^0 values are expected to change when the metals are incorporated into a complex such as the metal-bound transferrin, but the relative order of these E^0 values is expected to stay the same. The trend of increasing reduction potential with increasing band energy strongly suggests that this absorption represents a charge transfer transition from a ligand to the metal. The ligand involved could well be the phenolic ring of tyrosine, three of which have been implicated[120] in each binding site.

Table 7

	Fe^{3+}	Mn^{3+}	Co^{3+}
Reduction Potential, hydrated ion: E^0 (volts)	0.75	1.5	1.84
Absorption maximum: λ (nm)	470	430	405
$\tilde{\nu}$ (cm^{-1})	21,300	23,250	24,700

B. Phosvitin

In the course of this investigation of the interaction between iron(III) and phosvitin three different complexes of iron(III)-phosvitin were prepared. Two of them are green and the third brown in color. For convenience in the following discussion, these three forms are called P- (praeseo), V- (verd), and B- (brown).

The coordination structure of the iron(III) sites and the interaction between these sites were determined by the results obtained from the three important probes of polynuclear iron(III), namely, the ligand field absorption spectrum, the temperature dependence of the magnetic moment, and the electron spin resonance spectrum.

Electron spectroscopy for chemical analysis (ESCA) and ^{31}P n.m.r. spectroscopy were used to study the interaction between the bound iron(III) and the phosphate groups of the serine phosphate residues on the protein.

Two model compounds with iron(III) occupying a coordination site of tetrahedral symmetry were also studied. They were the synthetic quartz-type mineral $FePO_4$[12] and the well-known tetrahedral iron(III) anion $FeCl_4^-$ isolated as the tetraphenylarsonium salt,[124] $\phi_4As \cdot FeCl_4$.

1. Preparation of Iron-Phosvitin

Commercial preparations of phosvitin were obtained from Nutritional Biochemicals. The protein migrated as a single band on electrophoresis in polyacrylamide gels at pH 8.4. Recent studies[125]

of the commercial preparation have shown a significant amount of low molecular weight contaminants containing no phosphorous but absorbing at 280 nm. These contaminants could be removed by gel filtration or dialysis, which were preparative steps used in isolating the iron(III) protein. The amino acid analysis of a sample of phosvitin that had been exhaustively dialyzed against deionized water is shown in Table 8. The results are quoted to the nearest half residue for a molecular weight of 35,000.

a) P-iron phosvitin. The P-form of iron phosvitin was prepared by the direct addition to phosvitin of iron(III) as the nitrilotriacetate chelate. The $[FeNTA]^-$ complex was initially formed by titrating iron(III), as $Fe(NO_3)_3 \cdot 6H_2O$, and NTA in a 1:1 molar ratio to pH 7.5 with dilute sodium hydroxide. The $[FeNTA]^-$ solution (ca 0.12 molar) in about 100 fold molar excess was mixed with phosvitin solution (50 mg/ml). The mixture was allowed to stand at room temperature for several hours and was then passed through a Sephadex G-25 column (2.5 × 40 cm) equilibrated with Tris buffer, 5×10^{-3} M, pH 7.5. Iron(III) phosvitin was collected in the excluded green-yellow fraction, while the excess $[FeNTA]^-$ remained in the included dark red-brown fraction. Lyophilization of this excluded fraction produced the P-form of iron phosvitin as a green powder.

b) Polymerization of iron(III)·NTA. The kinetics of the exchange between iron(III)·NTA and phosvitin are important to the method of preparation. The half life of the reaction, as measured by the

Table 8

CYS	ASP	THR	SER	GLU	PRO	GLY	ALA
1	14	6	121	12	4	12	12.5
VAL	MET	ILV	LEV	TYR	PHE	HIS	LYS
4	1	2	3	0.5	2	7.5	14
ARG							
8							

drop in absorbance at 450 nm, is about 30 seconds. An equilibration time of several hours was therefore adequate to attain complete equilibrium in the preparation of P-iron phosvitin. An extended incubation period complicated the preparation by allowing polymerization of the iron(III)·NTA. After an incubation period of twelve hours or more a brown polymeric fraction was excluded from the G-25 column along with the iron(III) phosvitin. This polymerization is slow compared to that of iron(III) nitrate, which polymerizes within minutes after the addition of the appropriate amount of base.[8]

Two polymeric fractions were isolated from a 1:1 solution of iron(III) and NTA at pH 7.5 that had been left standing for three weeks. The fractionation was achieved by chromatography on a P-60 column (100 × 2.5 cm) equilibrated with tris buffer, 0.005 M, pH 7.5. The first band was eluted at a volume corresponding to that of a globular protein of molecular weight 6000. The second appeared equivalent to a smaller protein of molecular weight below 2000.

On the assumption that the density of these polymers was more like that of the well-characterized iron(III) nitrate polymer than it was of a globular protein, the density of the nitrate polymer (0.45) was used to estimate the real molecular weight of these polymeric fractions. These estimates were 9-10,000 and less than 3000 molecular weight. The most unusual feature of these polymers was that on lyophilization the low molecular weight fraction became a heavy brown powder, but the 10,000 molecular weight fraction became a yellow-green oil. The absorption spectrum of this oil showed no absorption at wavelengths greater than 500 nm. A definite shoulder at 470 nm, and possibly one at 400 nm were observed. These polymeric materials were not further characterized.

c) V-iron phosvitin. A second method of exchanging the iron(III) from NTA to phosvitin was employed to prepare the V-form of iron phosvitin. Jack Heggenauer of the University of California at San Diego kindly supplied a sample for this study. In this method the direct mixing was replaced by dialysis of phosvitin against the iron(III)·NTA prior to gel filtration. The green lyophilized material appeared similar to the P-form in some ways. The analytical results, among others presented below, indicated that the major difference between the P- and V-forms was the increased iron binding capacity of the V-form.

d) B-iron phosvitin. The nutritional relevance of this study of the binding of iron(III) by phosvitin was mentioned in Section I.

The report[31] of the inhibitory effect of an egg rich diet on iron absorption helped stimulate the investigation of the P- and V-forms of iron phosvitin. Any nutritional implications of the chemistry of these forms of iron phosvitin can be applied only to a diet rich in raw eggs. The mundane observation that the Western palate is more pleased by cooked rather than raw egg led to the isolation of the third form of iron phosvitin. This brown, or B- form, was prepared by the method described above for the P-form, with the important modification that the solution of phosvitin was immersed in a boiling water bath for ten minutes prior to the addition of the iron(III) NTA. No precipitate was observed during the boiling nor during the room temperature incubation with the iron(III)·NTA. The rust brown fraction that was eluted at the void volume of the G-25 column was heterogeneous, as determined by the absorption at 280 and 450 nm. It was further fractionated on a P-60 column (100 × 2.5 cm) into the brown iron phosvitin and a colorless component, presumably iron-free phosvitin.

The analytical results obtained for these three preparations were complicated by the presence of an apparently essential amount of water in the lyophilized material. Extensive drying under high vacuum lead to irreversible denaturation as determined by water insolubility. The results for the iron analysis determined by atomic absorptions on samples equilibrated with the atmosphere are listed in Table 9. The number of iron atoms was calculated using an assumed molecular weight for the iron-free protein of 35,000.

Table 9

Iron(III) Phosvitin	Fe(%)	Fe	P/Fe
P-form:	6.83	46	2.07
V-form:	9.6	67	1.48
B-form:	6.91	47	1.99

2. Ligand Field Spectrum

The VIS and NIR spectra of the P-form of iron phosvitin are shown in Figure 6. Those of the V-form are essentially the same. Two distinct shoulders were observed in the spectrum of an aqueous solution (0.005 M tris, pH 7.5) recorded at room temperature. The peak positions were at 447 and 426 nm (22,400 and 23,500 cm^{-1}, respectively). The room temperature spectrum in a 1:1 mixture of ethylene glycol and tris buffer was the same as that in the tris buffer alone. On cooling this mixture to about 150°K, a clear glass was formed. A third shoulder was observed at 400 nm (25,000 cm^{-1}) in the spectrum of the low temperature glass. Extinction coefficients for the three weak bands were estimated by subtraction of a visual extrapolation of the intense UV band from the experimental trace over this region of the spectrum. The absorption of the iron free protein in this region was negligible. A very similar room temperature spectrum was observed with various solutions of iron(III) and phosphoserine (1:1, 1:2, 1:3). The distinct shoulders occur at 457 and 426 nm with extinction coefficients of 0.5 and below. By contrast the spectrum of B-iron phosvitin at room

Figure 6

Visible and near infrared spectra of P-iron phosvitin (8.7 mg/ml) in tris buffer (0.005 M, pH 7.5) at room temperature. The top figure contains the spectra of iron-phosvitin (4.4 mg/ml) in a 1:1 (v/v) ethylene glycol: tris solvent mixture at room temperature (300°K) and low temperature (~150°K).

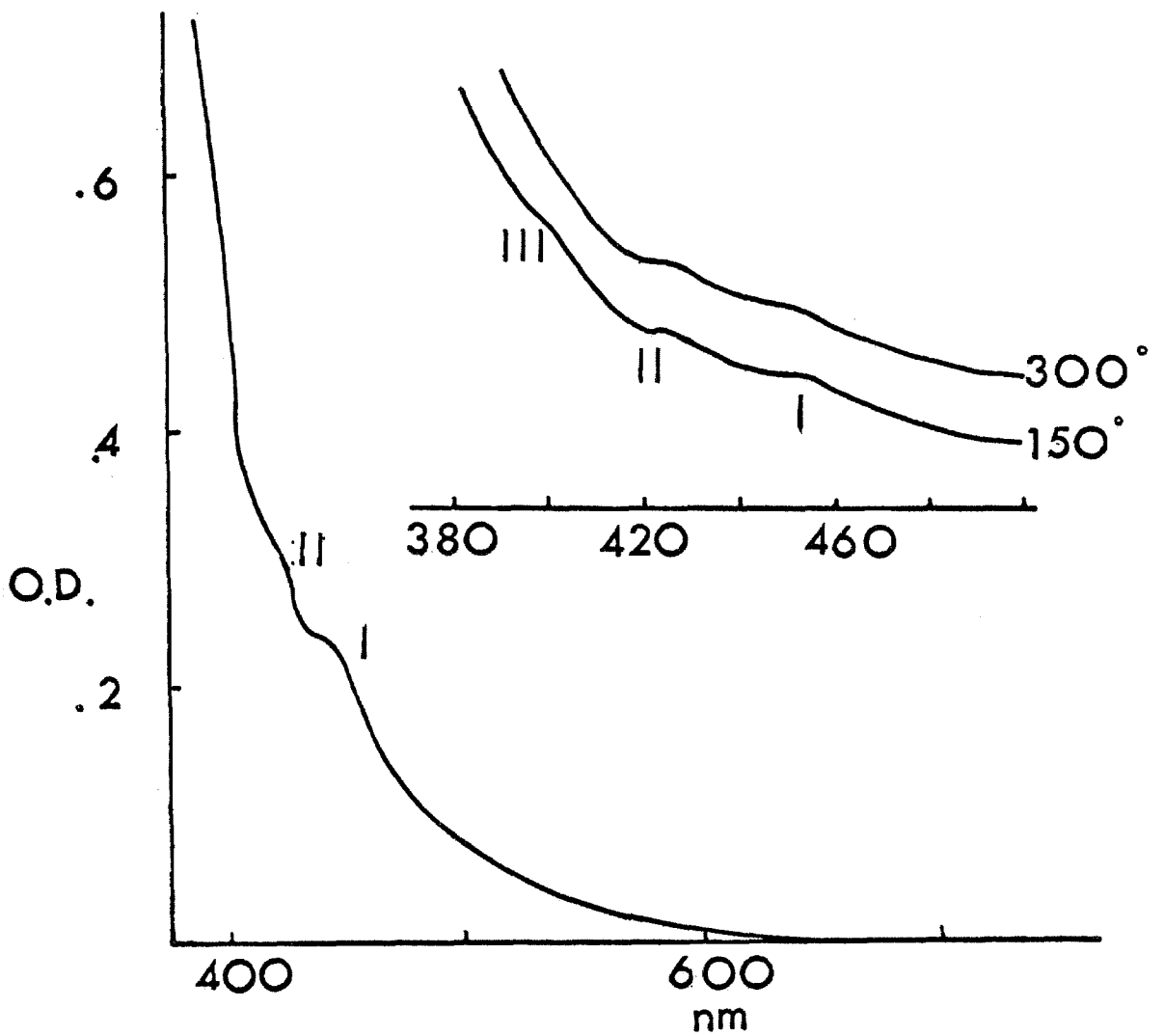
.6
.4
.2
O.D.
III
II
I
400
600
nm
III
II
I
300°
150°
380
420
460

temperature and pH 7.5 exhibited only one weak ligand field absorption band on the end of a strong absorption through the visible region. The shoulder was centered at ~820 nm. The positions and the values of the extinction coefficients per iron for the bands observed in the spectra of the three forms of iron phosvitin are listed in Table 10.

Table 10

		λ	$\tilde{\nu}$	ϵ/Fe
P-, V-forms:	I	447	22,400	5.5
	II	426	23,500	5.0
	III	400	25,000	--
B-form:	I	~820	12,200	~0.3

The VIS and NIR spectra of V-iron phosvitin were recorded at room and liquid nitrogen temperatures in a pellet of potassium bromide (12 mg/214 mg). The room temperature spectrum showed the expected solution bands at 447 and 425 nm with the additional feature of a weak broad shoulder at 810 nm. On cooling to liquid nitrogen temperature three additional bands appeared in the spectrum at 610, 555, and 400 nm, and the 810 nm shoulder became quite distinct. The intensities of the three low energy bands (810, 610, 555 nm) were estimated to be about one tenth that of the three higher energy bands. The band maxima (λ_{max}) and the corresponding energies for these bands are listed in Table 11 . The low temperature spectrum is shown in Figure 7.

Figure 7

The near infrared and visible spectra of V-iron phosvitin (12 mg) in a pellet of potassium bromide (213.5 mg) at liquid nitrogen temperature. The band positions marked occur at 810, 610, 555, 447, 425, and 400 nm.

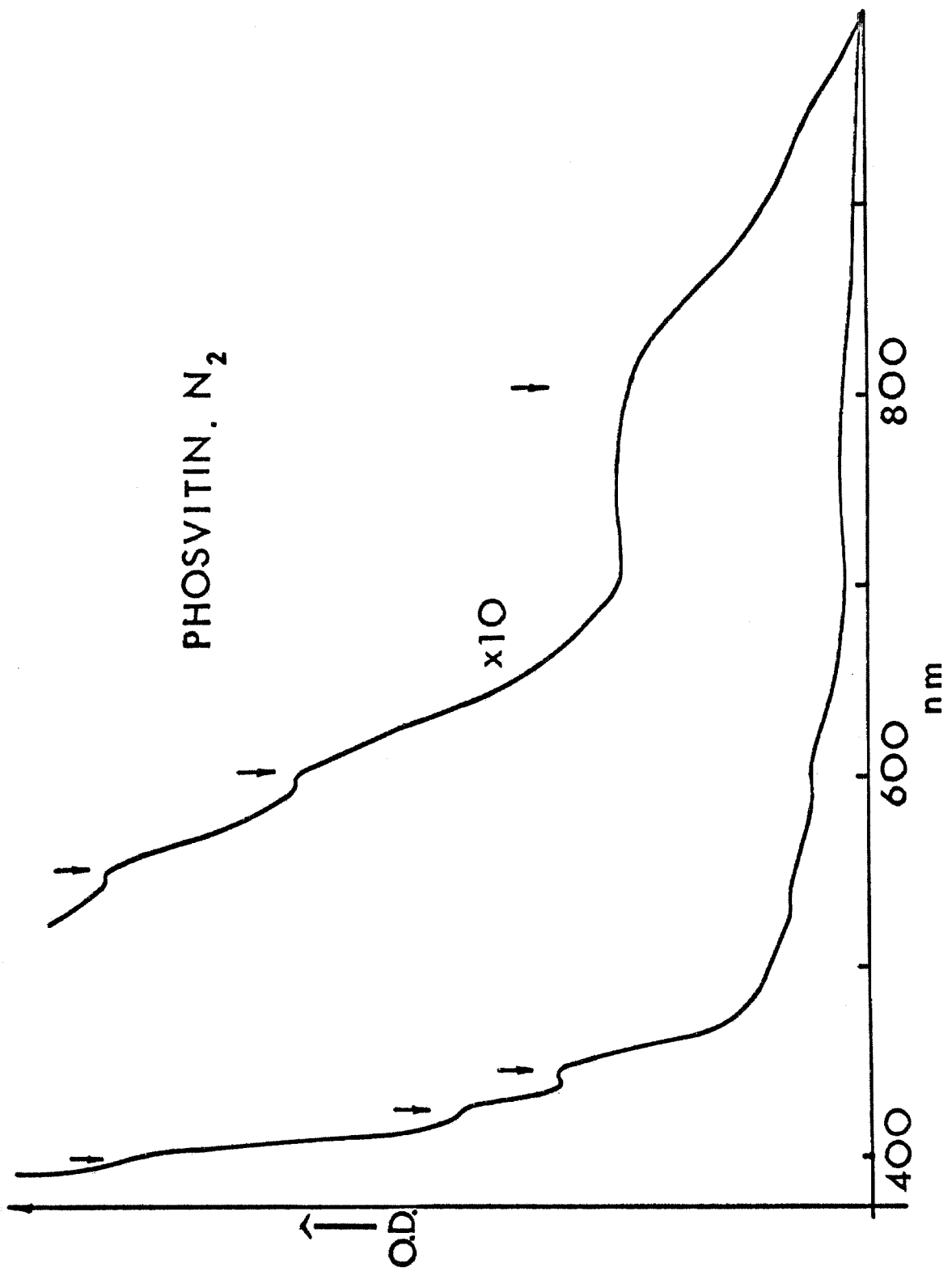
PHOSVITIN. N_2
x10
O.D.
400
600
800
nm

Table 11

λ_{max}(nm)	810	610	555	447	425	400
$\tilde{\nu}$(cm^{-1})	12,350	16,400	18,000	22,400	23,500	25,000

3. Magnetic Susceptibility Studies

a) Solid State. Measurements of the magnetic susceptibility as a function of temperature were carried out on the three forms of iron phosvitin. The temperature dependence of the magnetic moment per iron for each form is shown in Figure 8. The curves are labelled in the following way: I, the P-form; II, the V-form; and III, the B-form. For comparison, curve IV is that calculated by the spin-spin interaction model discussed in section II. A above. The coupling constant, J, between a pair of antiferromagnetically coupled high-spin iron(III) ions, S = 5/2, was taken as -12 cm^{-1} in the calculation. In all four curves the moment decreases with decreasing temperature.

The dependence of the magnetic susceptibility on the applied magnetic field was measured over the range 2-11 kilogauss for V-iron phosvitin. Within experimental error the observed behavior was that of a simple paramagnet, i.e., no field strength dependence of the susceptibility.

b) Solution. The magnetic susceptibility of the V-form of iron phosvitin in tris buffer (0.005 M, pH 7.5) was determined over the temperature range 20°-90°C using a HR-220 n.m.r. spectrometer.

Figure 8

Temperature dependence of the magnetic moment per iron from 300° - 85°K for

I P-iron phosvitin

II V-iron phosvitin

III B-iron phosvitin

IV a dimer of two ions of 5/2 spin, with coupling constant $J = -12\ cm^{-1}$. Calculated by usual spin-spin interaction model.

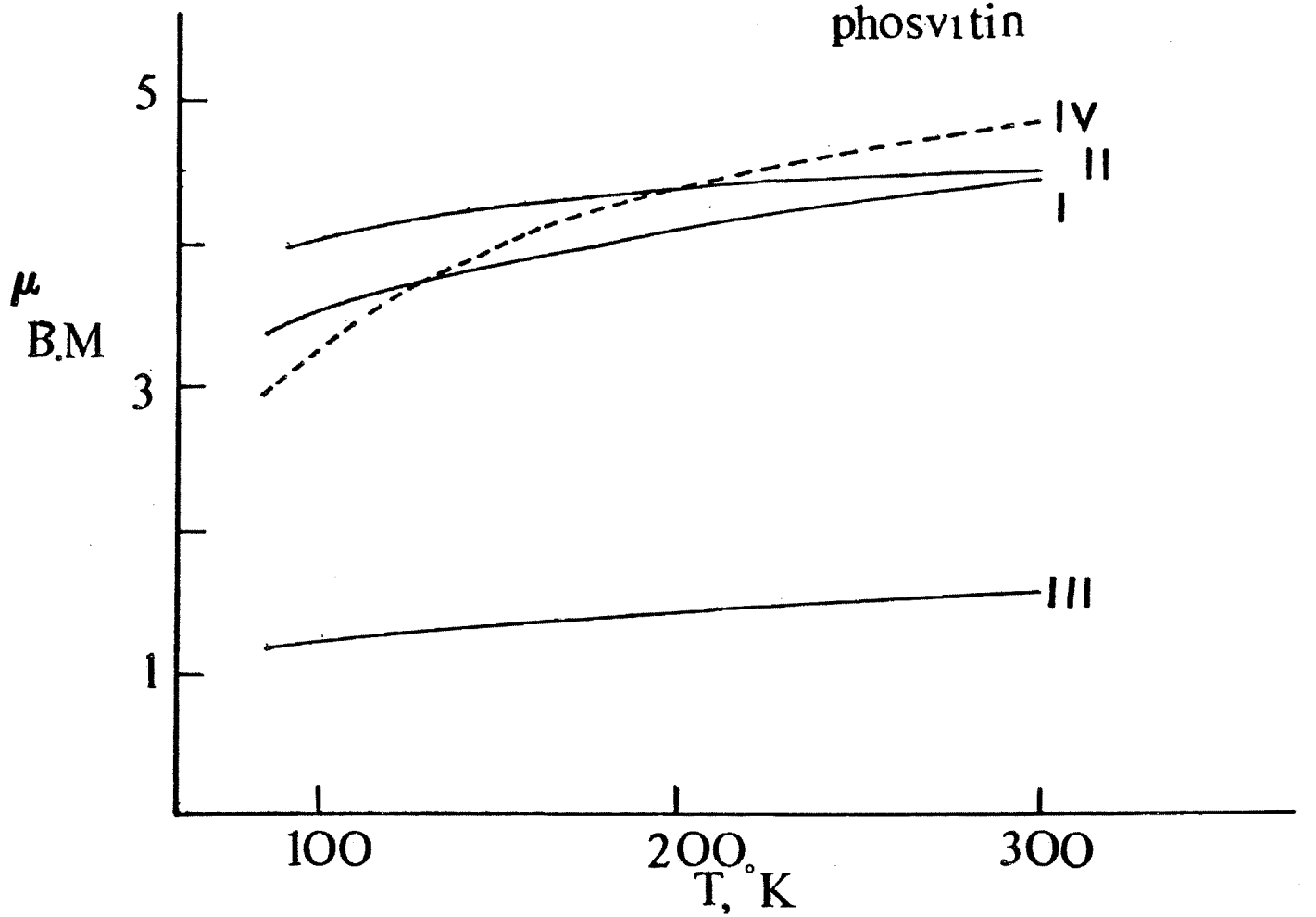
phosvitin
5
3
1
μ
B.M
IV
II
I
III
100
200
300
T, °K

These measurements were made in collaboration with Nancy Beach now with A.I.D., New Dehli, India. In a second experiment the susceptibility of the V-form dissolved in a 1:1 mixture of ethylene glycol and tris buffer was determined from -28° to +88°C. The resonance shift measured was that of the methyl resonance of tertiary butyl alcohol, the reference material present in 5% concentration. The temperature of the spectrometer sample zone was determined to an estimated accuracy of ± 0.5°C from the resonance frequency of the hydroxyl group in ethylene glycol for temperatures above ambient, and from that of the methanol hydroxyl for temperatures below ambient. The contribution to the shift from the diamagnetic protein was calculated from the molar diamagnetic susceptibility determined in the solid state. The iron concentration was determined by atomic absorption. The effective magnetic moment per iron was found to be independent of temperature, within the experimental error of at least 3%, over the entire temperature range studied. The measured room temperature value of the moment in solution was 4.60 B.M. The equivalent solid state measurement was 4.51 B.M. The magnetic moment per iron for P-iron phosvitin in solution and in the solid was determined by the same methods to be 4.56 and 4.45 B.M., respectively.

4. Electron Spin Resonance Spectra

The e.s.r. spectrum of P-iron phosvitin has been reported.[117] That of the V- and B-forms was recorded at

300° and 77°K. Bob Holwerda is thanked for recording the spectra. In all three cases the signal was broad at both temperatures, with a peak to peak width of at least 500 gauss. In the V- and B-forms only, the low temperature spectrum was partly resolved in the low field region. The g values and estimates of the peak widths for the various spectra are listed in Table 12. The spectra at the two temperatures of the V-form are shown in Figure 9. Those of the B-form are shown in the following Figure. The reference signal of DPPH (2,2-diphenyl-1-picrylhydrazyl) at a g value of 2 is included in each spectrum.

Table 12

	P	V	B
g value, R.T.	2.06	2.04	2.03
g value, ℓN_2	2.06	2.03, 2.02	2.04, 2.13
peak width (gauss), R.T.	500	600-700	800
peak width (gauss, ℓN_2	500	600-700	800

5. ^{31}P n.m.r. Study

In an effort to directly identify some interaction between the phosphate groups on the serine phosphate residues of phosvitin and the iron(III) bound to the protein, the techniques of ^{31}P n.m.r. spectroscopy and electron spectroscopy for chemical analysis, ESCA, were employed. A ^{31}P n.m.r. resonance has been observed[125] for the phosphate groups in phosvitin, but even with several hundred scans using a computer of

Figure 9

Electron spin resonance spectrum of a powder sample of the V-form of iron phosvitin at room temperature and at liquid nitrogen temperature (~80 °K).

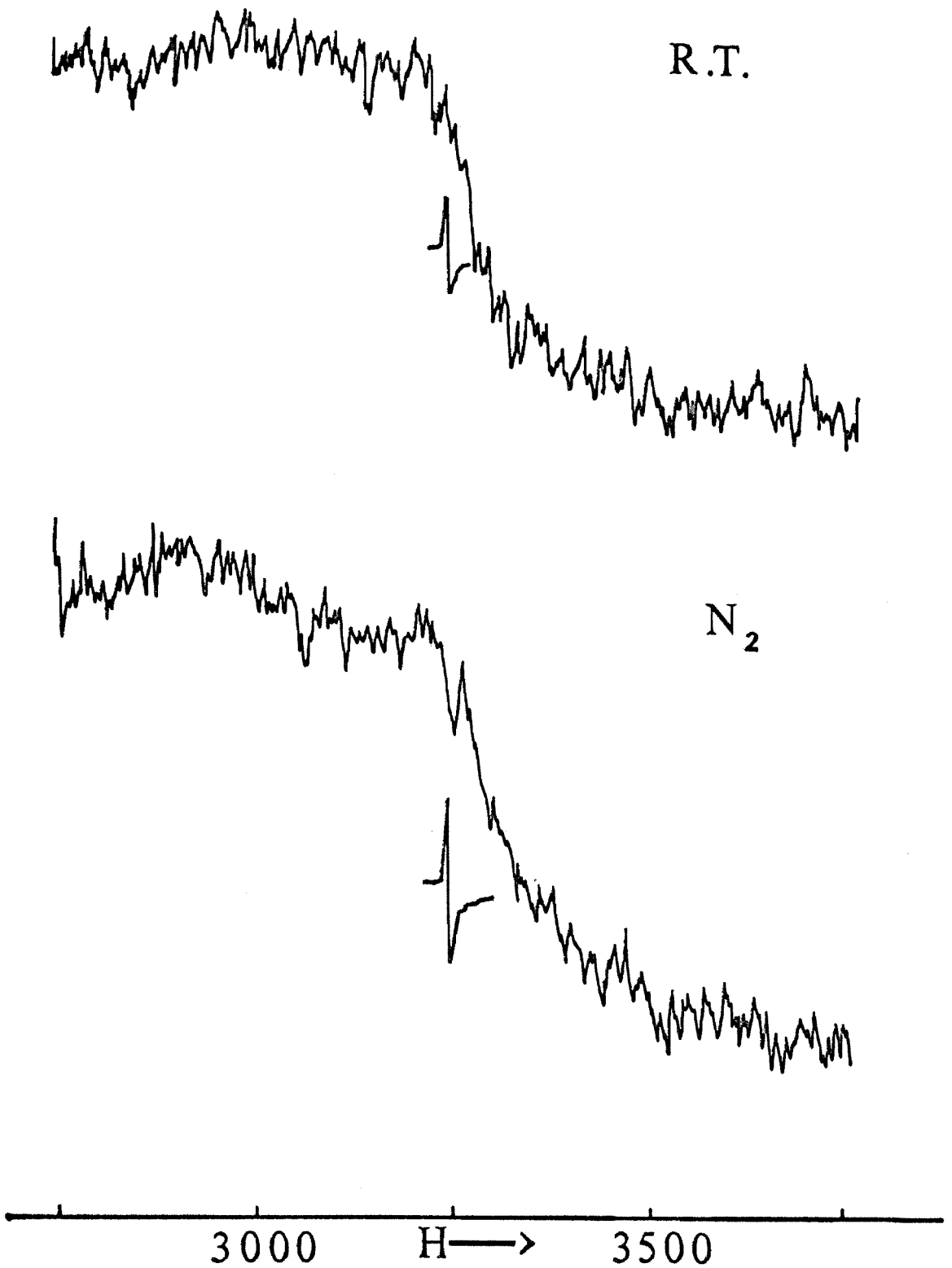
R.T.
N_2
3000
H⟶
3500

Figure 10

Electron spin resonance spectrum of a powder sample of the B-form of iron phosvitin recorded at room temperature and at liquid nitrogen temperature (~80°K).

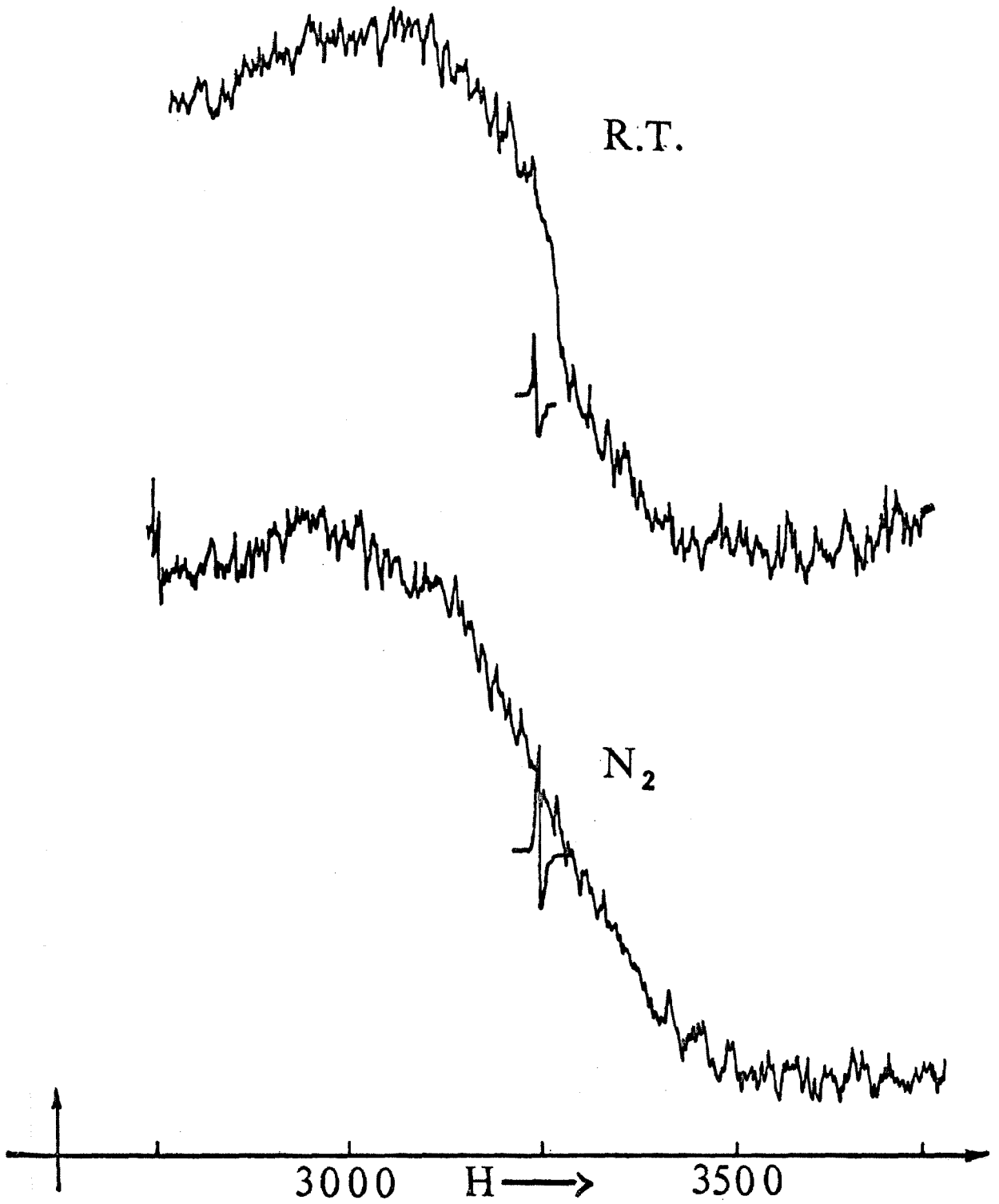
R.T.
N_2
3000
H ⟶
3500

average transients on the HR-220, no ^{31}P resonance of any kind was observed in the V-form of iron phosvitin.

6. Electron Spectroscopy for Chemical Analysis (ESCA) Study

The binding energies of the iron $2p_{3/2}$ and the phosphorus $2p_{1/2,3/2}$ electrons were determined for the iron and phosphorous in V- and B-iron phosvitin, as well as for a number of related and model compounds. Dieter Liebfritz of the California Institute of Technology and Warren Proctor of Varian Associates are thanked for recording the ESCA spectra reported here. The compounds related to iron phosvitin were serine phosphate and iron free phosvitin.

a) Model Compounds. The model compounds were chosen on the basis of structural similarity to the possible iron(III)-serine phosphate interactions.

(i) $Na_2[Co(P_2O_7)(OH)_2]$: The two phosphorous atoms in the bidentate pyrophosphate of this compound have been reported[132] to be structurally equivalent. Bob Holwerda of the California Institute of Technology kindly supplied the sample. The binding energy in the free ligand was also determined, providing an estimate of the change in the phosphorous binding energy in going from an uncomplexed to a bidentate form.

(ii) $[Co(NH_3)_4H_2O \cdot HPO_4]2H_2O$ and $[Co(NH_3)_4PO_4]2H_2O$: These closely related compounds have been reported to contain phosphate

as a monodentate and as a bidentate ligand, respectively. The phosphorous binding energies in both were measured to characterize the difference between these two forms of phosphate binding. The compounds were prepared by a slight modification of the literature methods.[120] Precipitation of the crystals of the second compound was initiated by saturation with sodium perchlorate rather than by methanol addition.

(iii) $FePO_4$: Two phases of iron(III) phosphate are relevant to the present study. The anhydrous quartz type mineral phase,[12] $FePO_4$, contains iron(III) in tetrahedral sites. The hydrated form, strengite,[124] $FePO_4 \cdot 2H_2O$ contains octahedral iron(III). A preparation of $FePO_4$ that was contaminated by a small amount of strengite (as determined by the X-ray analysis discussed below) was included in this section to determine the ability of ESCA to identify a mixture of iron(III) in two sites of different symmetries.

b) Phosphorous 2p electron binding energies. The 2p phosphorous ESCA spectra are shown in Figures 11 and 12. The corresponding binding energies are listed in Table 13. The $FePO_4$ result is listed in the table but has not been included in the figure.

c) Iron 2p electron binding energies. The ESCA spectra of the iron 2p electrons for the V- and B-forms of iron phosvitin are shown with that for $FePO_4$ in Figure 13. The width of the spectral band in spectra B and C of the figure prevented a precise determination

Figure 11

Binding energy of phosphorous $2p_{1/2,3/2}$ electrons as determined by the ESCA technique for

(A) $Na_2[Co(P_2O_7)(OH)_2]$

(B) $Na_2P_2O_7$

(C) $[Co(NH_3)_4PO_4]\cdot 2H_2O$

(D) $[Co(NH_3)_4H_2O\cdot HPO_4]ClO_4\cdot 2H_2O$

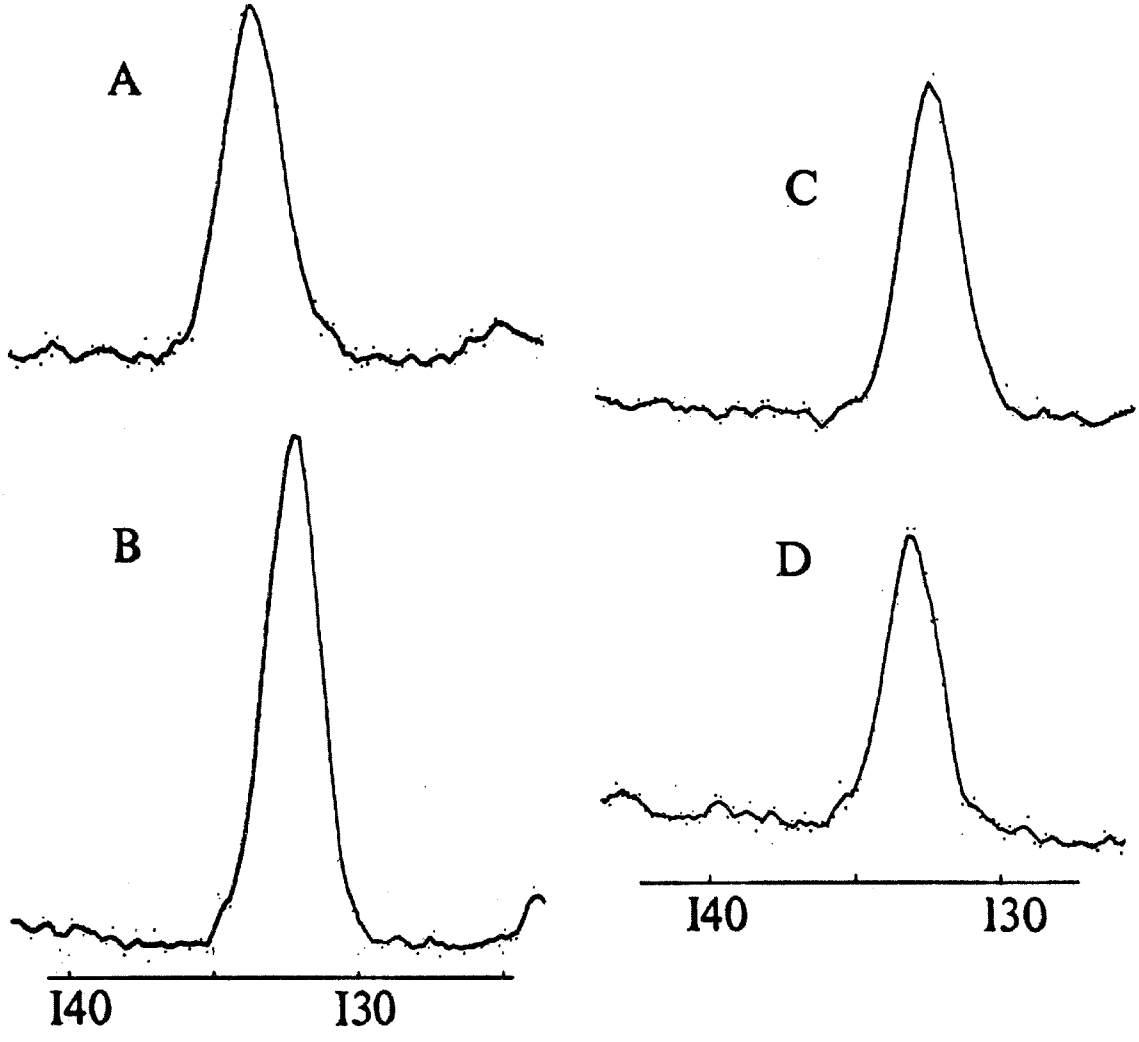
A
B
C
D
I40
I30
I40
I30

Figure 12

Binding energy of the phosphorous $2p_{1/2, 3/2}$ electrons as determined by the ESCA technique for

(A) commercial phosvitin

(B) serine phosphate

(C) V-iron phosvitin

(D) B-iron phosvitin

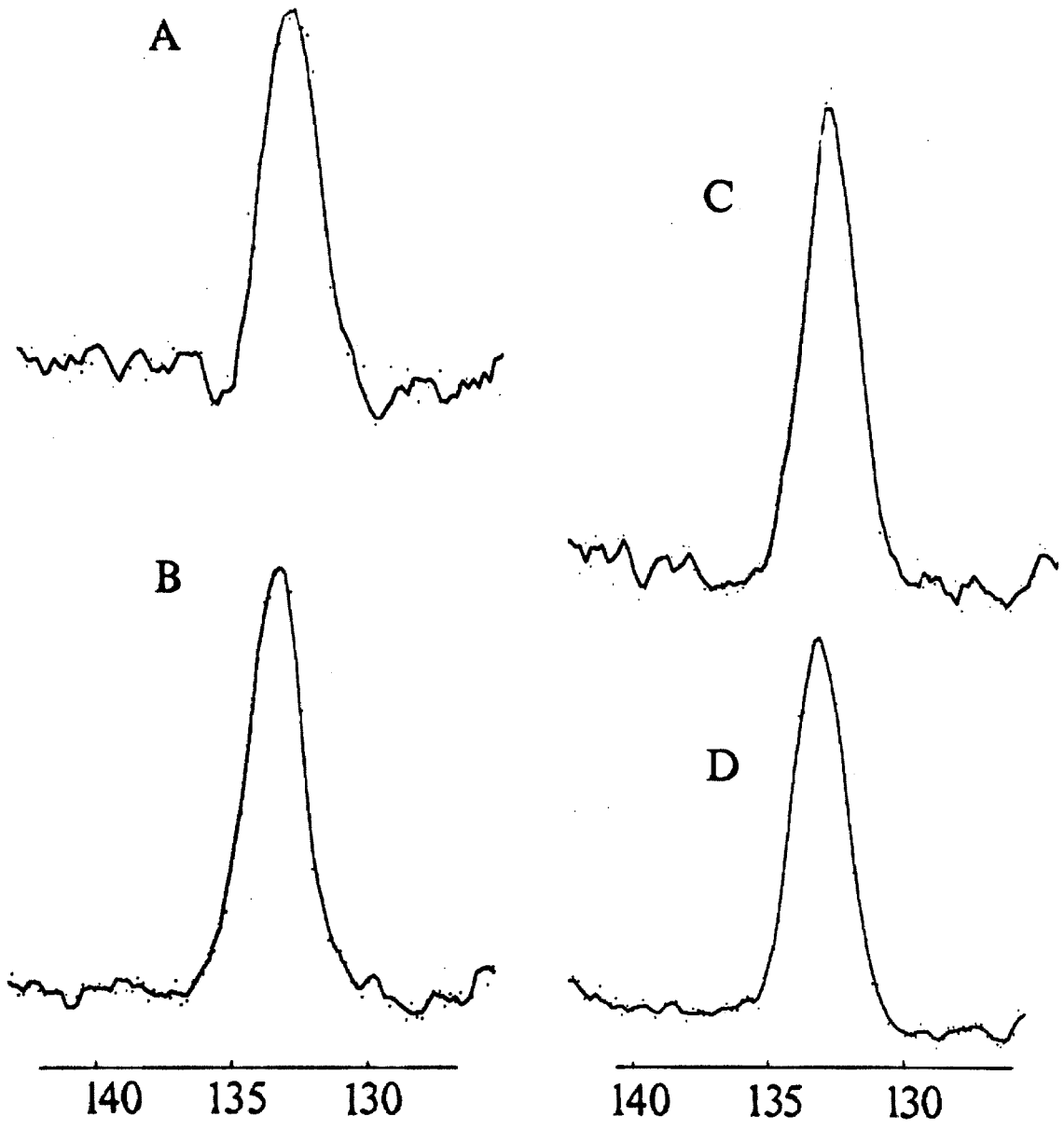
A
B
C
D
140
135
130
140
135
130

Figure 13

Binding energy of the iron $2p_{3/2}$ electrons as determined by the ESCA technique for

(A) V-iron phosvitin

(B) B-iron phosvitin

(C) crystalline iron(III) phosphate, $FePO_4$.

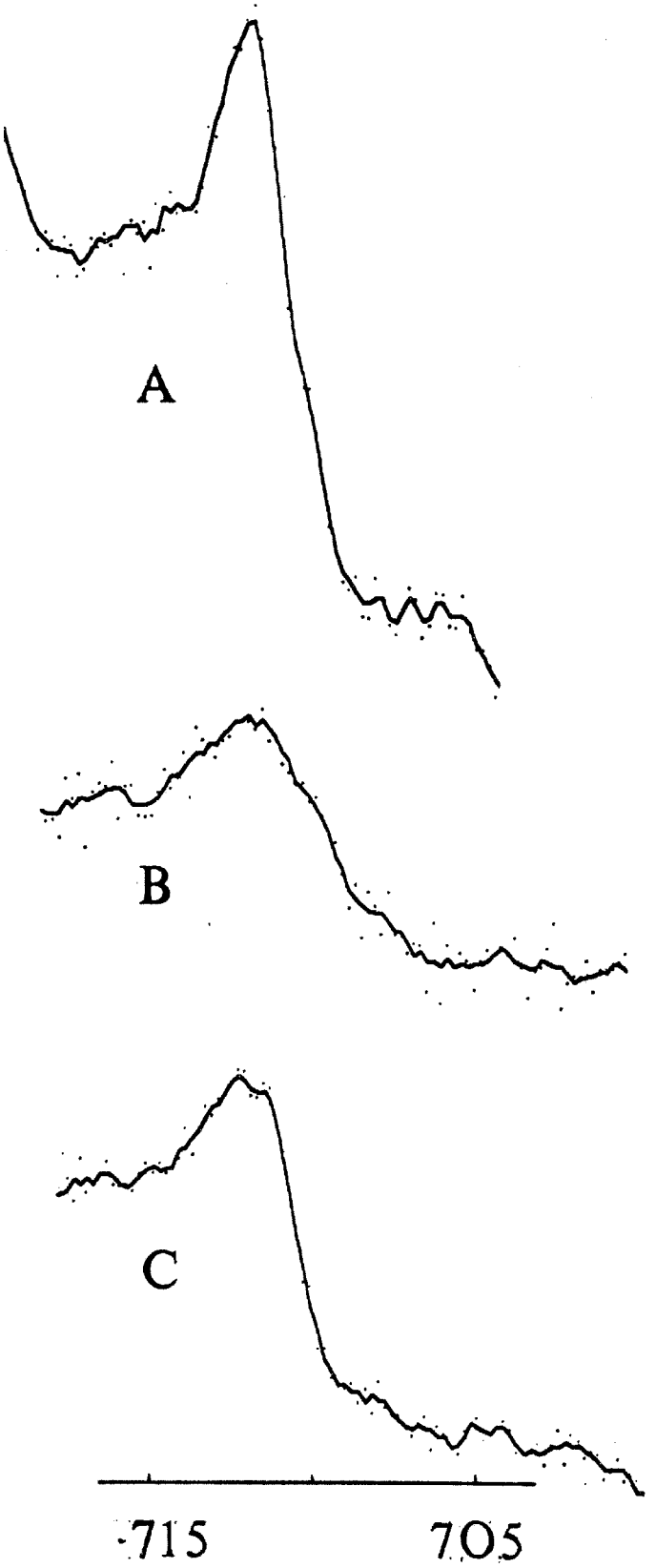
A
B
C
-715
705

Table 13

Model Compounds (see Figure 11)	Binding Energy - Phosphorous 2p Electrons (eV)
$Na_2[Co(P_2O_7)(OH)_2]$	135.2
$Na_2P_2O_7$	132.3
$[Co(NH_3)_4PO_4]2H_2O$	132.1
$[Co(NH_3)_4H_2O(HPO_4)]\cdot 2H_2O$	133.0
$FePO_4$	133.5
Phosvitin Series (see Figure 12)	
Phosvitin	132.7
Serine Phosphate	133.3
Iron phosvitin, V-form	132.7
Iron phosvitin, B-form	133.0

of the band maxima. The energies in all three compounds were nearly the same. More importantly, the spectral band, C, of the compound with iron in two different sites (see 8(f) below) was partly resolved. The binding energies are listed in Table 14.

Table 14

Compound	Binding Energy - Iron 2p Electrons
iron phosvitin, V-form	712
iron phosvitin, B-form	712.2
$FePO_4$	712.2, ~ 711.4

7. Two Tetrahedral Iron(III) Model Systems

The ligand field spectral bands observed in iron phosvitin provided important information on the tetrahedral coordination structure about the iron(III) in the protein (see subsequent discussion). Several of these features have been observed in nonprotein systems. Two such systems, $FePO_4$ and $\phi_4As \cdot FeCl_4$ were studied in some detail.

a) Iron(III) phosphate, $FePO_4$. The mineral phase $FePO_4$ was prepared[12] from freshly precipitated iron(III) phosphate that was exhaustively dried prior to being heated at 600°C for five hours. The X-ray powder pattern of this yellowish powder was recorded using molybdenum radiation and zirconium filters on the incident and diffracted beam.

The visible spectrum of this preparation of $FePO_4$ was recorded at liquid nitrogen temperature as a potassium bromide pellet (5.84 mg/220 mg). The spectrum was not recorded at wavelengths greater than 650 nm because of excessive scattering. The spectrum was complex, at least seven absorption bands being resolved. The lowest energy ligand field band occurred as a weak absorption at 535 nm. Bands at 470 and 413 nm were readily observed. Lying in between these two bands was a complex pattern of four reasonably well resolved absorptions at 449, 443, 435, and 428 nm. The wavelengths (λ_{max}) and energies ($\tilde{\nu}$) of these bands are listed in Table 15.

Table 15

λ_{max}(nm):	535	479	449	443	435	428	413
$\tilde{\nu}$ (cm^{-1}):	18,700	21,000	22,300	22,600	23,000	23,400	24,200

The core electron binding energies were measured for the iron 2p and the phosphorous 2p levels by the ESCA technique. Two binding energies for iron were observed at 712.2 and 711.4 eV. (Table 14 and Figure 13). The phosphorous binding energy was 133.0 eV (Table 13).

b) Tetrachloroferrate anion, $\phi_4As \cdot FeCl_4$. The well known tetrahedral anion of iron(III), $FeCl_4^-$ was prepared as the stable tetraphenylarsonium chloride salt by a method received from

H. L. Friedman at the State University of New York at Stony Brook. The yellow-green crystals were recrystallized from chloroform. Analyses for Fe, As, C, and Cl (Schwarzkopf) indicated a highly pure preparation. The calculated results for the formulation $(C_6H_5)_4As \cdot FeCl_4$ are listed after the determinations for the four elements: 9.97% Fe (9.61); 12.9% As (12.9); 49.7% C (49.6); 24.8% Cl (24.4). The temperature dependence of the magnetic moment was determined from 300° to 85°K. The moment was temperature independent with a value of 5.90 ± 0.1 B. M. This confirmed an earlier report[129] that the ground state of the iron(III) in this compound was high spin, $S = 5/2$.

The ligand field spectrum was readily observed in solutions of acetone or chloroform, and as pellets of thallium chloride. The characteristic absorption pattern for a d^5, $S = 5/2$ ion of two broad absorptions followed by a relatively sharper band at higher energy was observed in the solid and in solution. The most interesting feature of the spectrum was the significant splitting in the first two broad bands in solution even at room temperature. The lowest energy band was further split in the spectrum of the solid sample at low temperature (77°K). The spectrum is shown in Figure 14. The positions (λ_{max}), energies ($\tilde{\nu}$), and extinction coefficients of the bands are listed in Table 16.

Figure 14

The visible and near infrared spectra of tetraphenylarsoniumtetrachloroferrate(II) (20 mg) in a Nujol coated pellet of thallous chloride (400 mg) at room temperature and at liquid nitrogen temperature. The relative intensities of the spectrum recorded in acetone or chloroform at room temperature agree with the pellet spectrum shown.

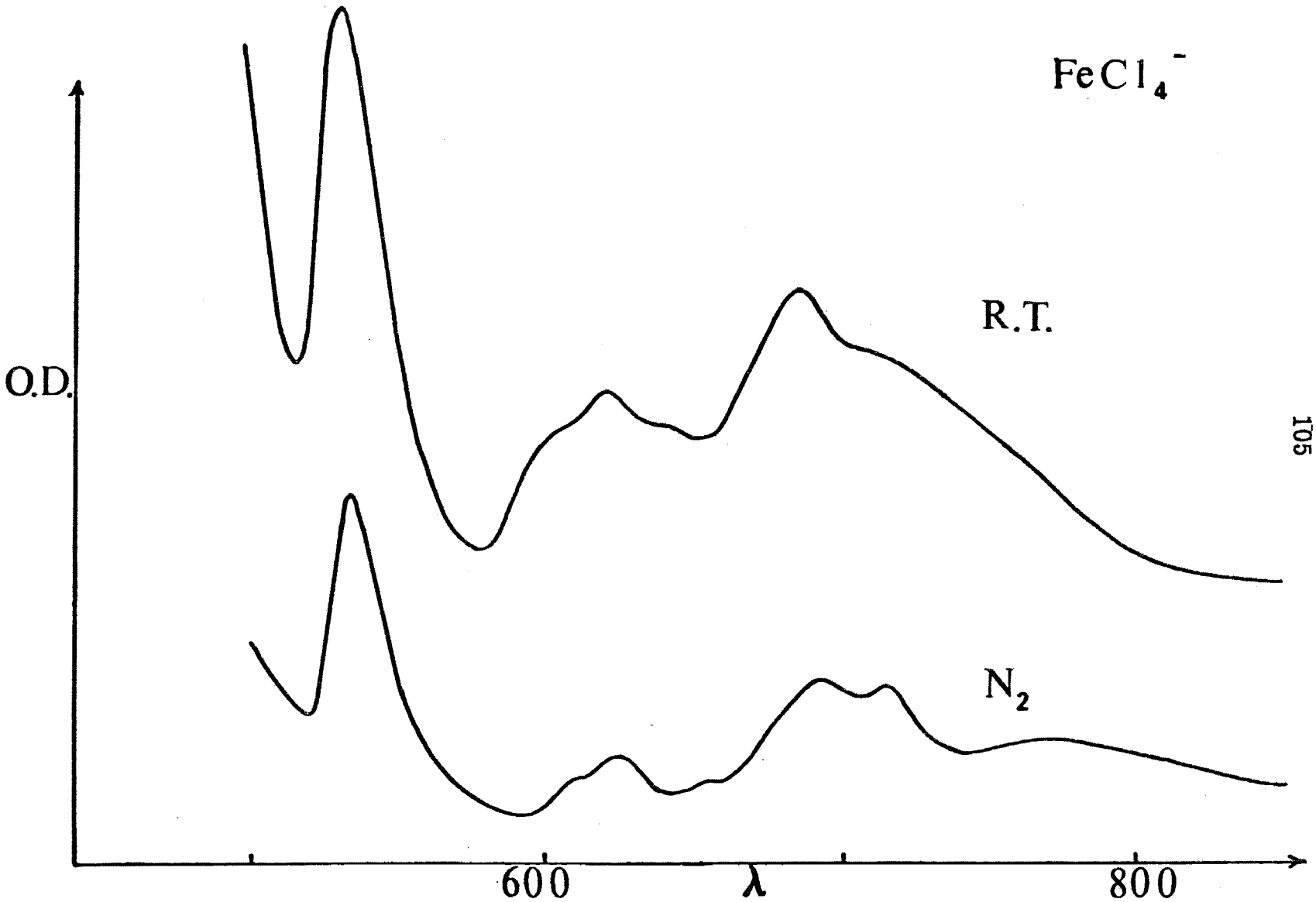
$FeCl_4^-$
R.T.
N_2
O.D.
600
λ
800

Table 16

R.T. (solid, soln)	λ_{max}(nm)	735	685		640	620	597	530
	$\tilde{\nu}$ (cm^{-1})	13,600	14,600		15,600	16,150	16,750	18,850
	ϵ	0.63			0.46			1.51
ℓN_2 (solid)	λ_{max}(nm)	775	715	693	655	628	607	534
	$\tilde{\nu}$ (cm^{-1})	12,900	13,800	14,450	15,250	15,900	16,450	18,750

The possible importance of the totally symmetric iron-chloride stretching mode in the interpretation of these spectral results led to its identification by polarized Raman spectroscopy using a helium laser. The depolarization ratio of the well characterized 314 and 459 cm^{-1} bands of carbon tetrachloride was used to identify the 334 cm^{-1} band as the totally symmetric stretching mode. This confirmed the earlier assignment, based on photographic data. The 334 cm^{-1} band in both polarizations is shown in Figure 15.

8. Discussion

The discussion of the above results will be presented in the following way. The implications of the spectral and magnetic results for the three forms of iron phosvitin will be considered in turn, and models for the coordination structures of iron(III) in the three forms will be presented. The ESCA results will be considered next. The structural information, and the implications for human nutrition, will then be summarized. In a final section, the results obtained on the two tetrahedral model systems, $FePO_4$ and $FeCl_4^-$ will be discussed and the complex pattern of ligand field absorption bands assigned.

a) P-iron phosvitin. Both the temperature dependence of the magnetic moment (Figure 8) and the reported EPR spectrum[117] suggest that the iron(III) present in this form of iron phosvitin is poly-nuclear. The room temperature magnetic moment per iron(III) of 4.45 B.M. is substantially reduced from the high-spin (S = 5/2) value of 5.92 B.M. This intermediate moment is maintained also in aqueous solution. Furthermore, the magnetic moment is not temperature

Figure 15

The totally symmetric iron-chlorine stretching mode of the tetrahedral anion $FeCl_4^-$ recorded in acetone solution at 334 cm^{-1} in the parallel ($\parallel$) and perpendicular ($\perp$) polarization modes, using a Raman laser spectrophotometer.

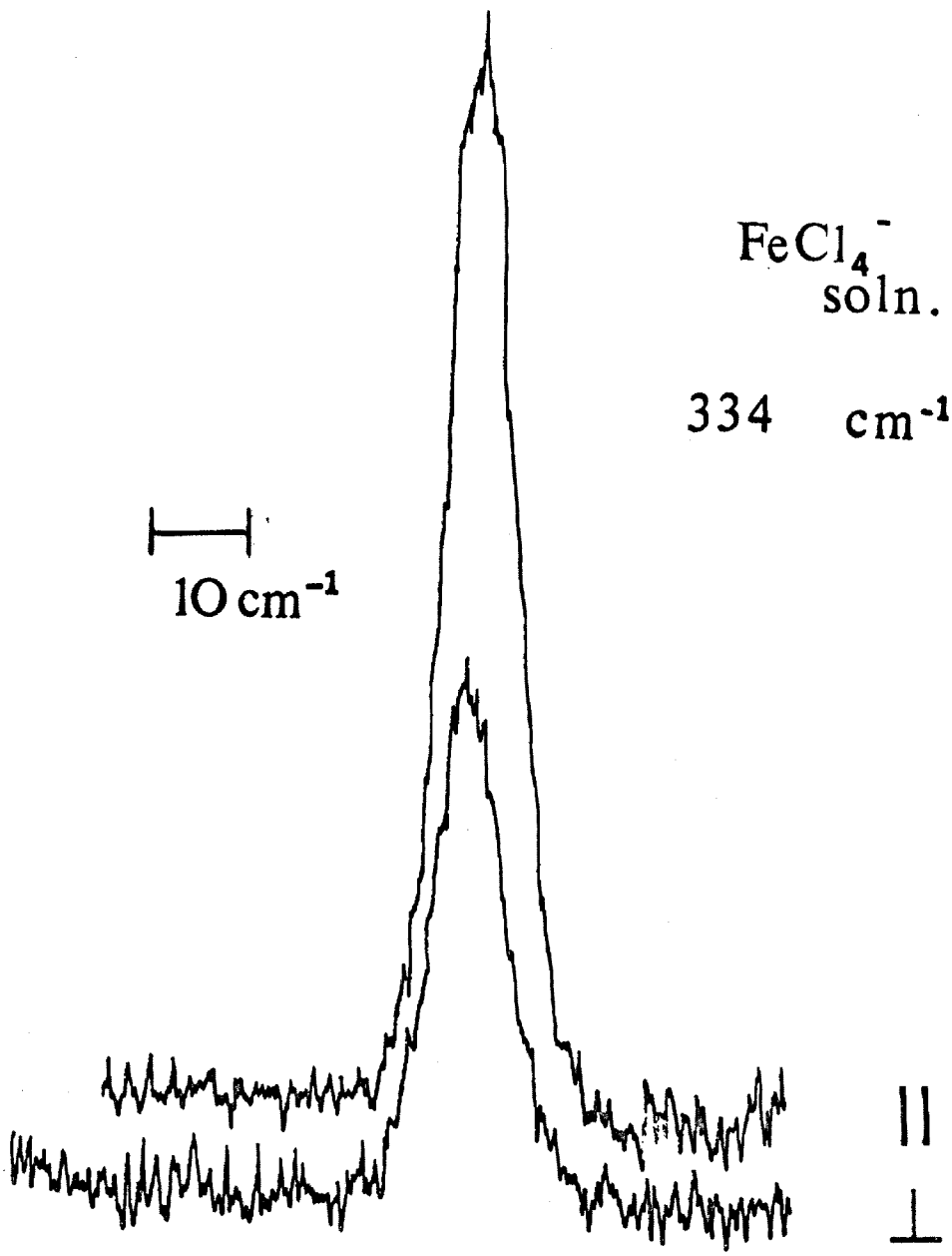
$FeCl_4^-$
soln.
334 cm^{-1}
10 cm^{-1}
||
⊥

independent as would be expected for a mononuclear iron(III) species at each binding site, but decreases with temperature, indicating some antiferromagnetic interaction. The gram susceptibility per iron(III) increases with decreasing temperature over the temperature range studied, indicating that the Néel point is below 85 °K. The general behavior is similar to that observed for iron(III) in simple dimeric systems which can be adequately described by a spin-spin interaction of magnitude J (<0 in the antiferromagnetic case) between two high-spin iron(III) ions. Curve IV in Figure 8 illustrates the case for J = $-12\ cm^{-1}$ ($S_1 = S_2 = 5/2$) and compares the experimental data with the expected behavior for dimeric units. Although it may be concluded from this comparison that some of the iron(III) ions are antiferromagnetically coupled, the model consisting of an array of dimeric units is obviously oversimplified. As might be anticipated from this treatment and the parameters employed, it is possible to fit the magnetic behavior from 300 °K - 85 °K of P-iron phosvitin shown in Figure 8 by a suitable combination of high-spin monomers and spin-spin coupled dimers. The actual mixture required is 25% high-spin monomers and 75% dimers, assuming that the dimers have J = $-25\ cm^{-1}$ and a room temperature moment per iron of 3.88 B.M. The EPR evidence at 80 °K fails to support the presence of significant numbers of monomeric iron(III) ions in iron phosvitin, although any signals arising from them could possibly be hidden by the broad signal from the antiferromagnetic cluster(s).

Further evidence for the polynuclear nature of the iron(III) ions is found in the EPR spectrum. The signal obtained is broad, 500 gauss peak-to-peak at 80°K, and of low intensity. Such broadening is much greater than has been observed in dimeric and trimeric clusters. It is of the same magnitude as that observed for the protein ferritin,[131] which binds several thousand iron(III) ions. The broadness of the band appears to be independent of temperature, suggesting that it results from the local magnetic field produced by nearby magnetic dipoles that consequently alters the total magnetic field at the positions of the neighboring unpaired spins, broadening their resonance lines.

Information concerning the coordination geometry of individual iron(III) centers in the polynuclear complex may be derived from an analysis of the electronic absorption spectrum. The visible spectrum of iron(III) phosvitin shown in Figure 6 has absorption bands at 22,400, 23,500, and 25,000 cm^{-1}, whose low intensities ($\epsilon < 10$) strongly suggest spin-forbidden d-d transitions from a high-spin ground state ($^6A_1$). The two lowest spin-forbidden transitions from a $^6A_1$ ground state decrease in energy as the cubic ligand field splitting increases. Thus for tetrahedral iron(III) these transitions are expected to occur at higher energies than the analogous bands for an analogous octahedral case.

In iron(III) phosvitin, the first two ligand field bands, at 22,400 cm^{-1} and 24,500 cm^{-1}, are very close in energy to those

observed in the reference compound for tetrahedral [Fe(III)O_4], iron(III)-doped orthoclase feldspar (Figure 4). The third band, corresponding to the transition $^6A_1 \rightarrow {}^4A_1, {}^4E$ is not as well resolved as the first two but is also close in energy (25,000 cm^{-1}) to the analogous band in the tetrahedral reference (26,500 cm^{-1}) This close comparison of the spectral bands strongly indicates that iron in phosvitin is in tetrahedral coordination.

Using the C/B ratio of approximately 8 that was found for tetrahedral iron(III), the Tanabe-Sugano diagram for the d^5 configuration has been constructed. It is shown in Figure 16. The calculations were performed using a computer program written by Jack Thibeault of the California Institute of Technology. The peak positions in the iron(III) phosvitin spectrum may be adequately fitted by the parameter values B = 495 cm^{-1} and 10 Dq = 5270 cm^{-1}. The relatively low value of 10 Dq is explicable only in terms of tetrahedral coordination to oxygen-donor ligands. Furthermore, the spectrum under consideration is devoid of peaks in the region 800-1000 nm, where octahedral iron(III) invariably appears. Molar extinction coefficients for spin-forbidden ligand field bands are small, but are a factor of ten larger in the tetrahedral geometry than the octahedral one, because in tetrahedral geometry the transitions are not Laporte forbidden. From the reference spectrum (Figure 4) the measured intensities of the first two octahedral bands are very small, and it is possible that some octahedrally

Figure 16

Tanabe-Sugano diagram of the dependence of the energy levels of the d^5 electronic configuration on the strength of the ligand field (Dq), calculated with the assumption C/B = 8.

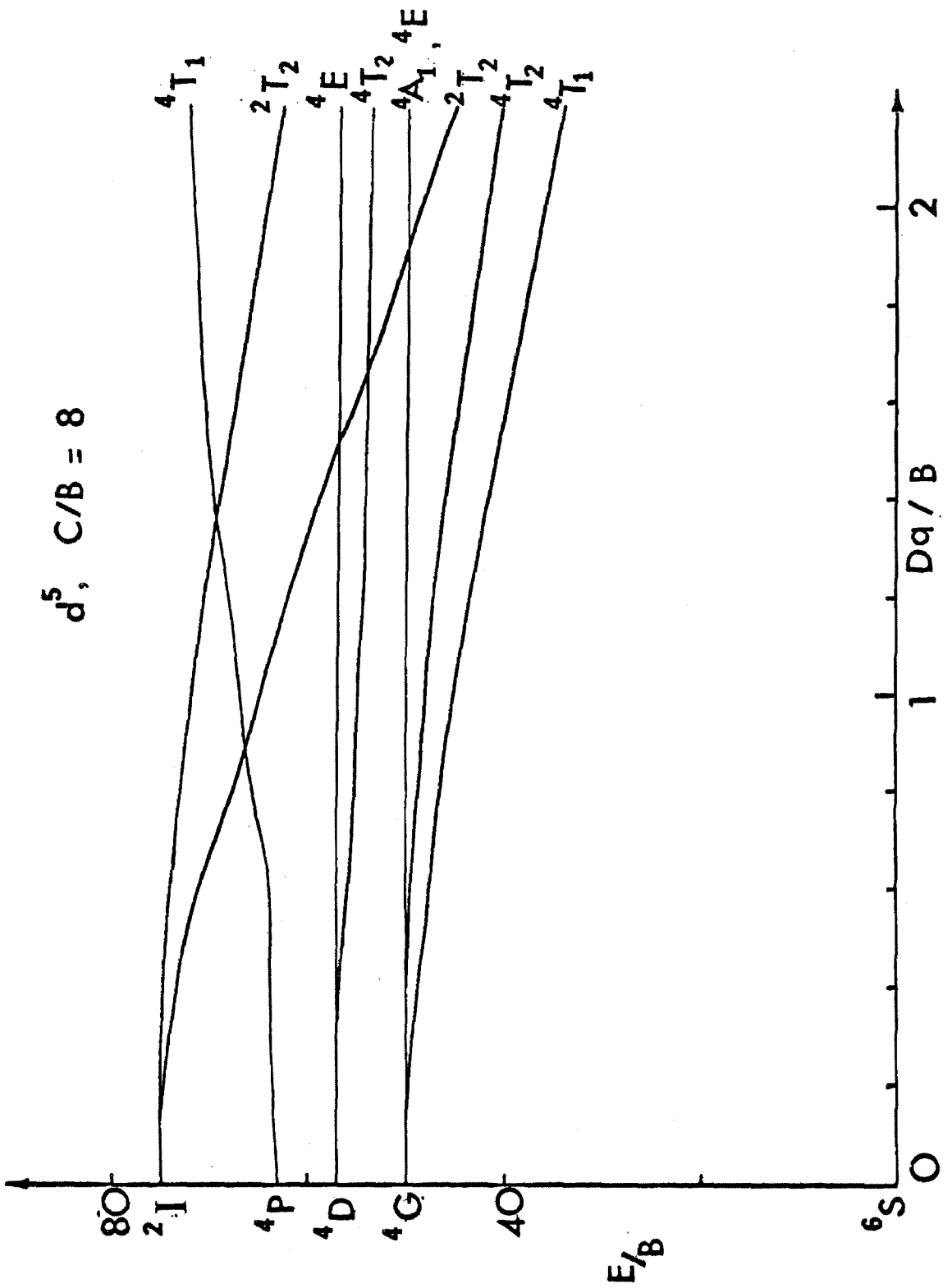
d^5, C/B = 8
$^4T_1$
$^2T_2$
^4E
$^4T_2$
$^4A_1$, ^4E
$^2T_2$
$^4T_2$
$^4T_1$
^2I
^4P
^4D
^4G
^6S
80
40
O
1
2
Dq / B
E/B

coordinated iron(III) ions could escape detection in our spectroscopic experiments. However, the principal conclusion remains that most of the iron(III) ions are tetrahedrally coordinated to oxygen-donor ligands. This contradicts an earlier assumption[141] of octahedral structure. The intensities of the first two transitions in iron(III) phosvitin are almost an order of magnitude greater than those measured in iron(III)-doped orthoclase feldspar. This intensity enhancement is additional evidence for the presence of antiferromagnetically coupled ions.

These results indicate that the iron(III) bound to the P-form of iron phosvitin is tetrahedrally coordinated, probably to four oxygen atoms, and these tetrahedral ions are antiferromagnetically coupled together in clusters that are significantly larger than dimeric.

A number of reports[136-138] have characterized, at least in part, the unusual distribution of serine phosphate residues throughout the protein. These residues are arranged in linear sequences of up to eight residues uninterrupted by other amino acids. This close proximity of the residues is expected to be quite suitable for binding a polynuclear cluster of iron(III) ions.

A more detailed picture of the structure of these clusters can be deduced from the results of a recent conformational study of phosvitin. A detailed study[139] of the optical rotatory dispersion curves and the circular dichroism spectra indicated that at alkaline pH phosvitin has an "unordered" conformation, whereas at very

low pH (~pH 1) the conformation changes to a β-type pleated sheet structure. It was proposed that this transition was induced by the decreased dissociation of the phosphate groups at low pH. In this view, the attendant reduction in the electrostatic repulsions between the charged side chains that are in close proximity to each other allows the transition from an unordered to a β conformation to occur. Observations consistent with this explanation have been reported[140] on the effects of various organic solvents on this conformation.

On this basis the effect of binding iron(III) ions should be to reduce the repulsions between side chains at the pH of interest, 7.5, and induce a conformational change towards the β-structure. The known features of the β-conformation imply that for binding of any one iron(III) by two phosphates to occur, the phosphates would come from two serine phosphate residues that are one residue apart on a single thread of the pleated sheet or from two residues that are on two adjacent threads of the pleated sheet. The phosphate groups could very probably act as bridging groups between adjacent iron(III) ions. The geometry of the binding sites created in this way could well be tetrahedral as observed. The tetrahedral coordination is quite unusual for iron(III) in an aqueous environment at the comparatively high pH of 7.5. It is likely that this β-conformation protects the bound iron from hydrolysis into polynuclear clusters of octahedral iron(III).

b) V-iron phosvitin. This form of iron phosvitin closely resembles the P-form discussed above in the temperature dependence

of the magnetic moment, the e.s.r. spectrum, and in the energies and intensities of the ligand field absorption bands. It does bind a significantly greater number (67) of iron atoms than does the P-form (46).

The room temperature magnetic moment is depressed from the high spin value of 5.92 B.M.. It is 4.51 B.M. in the solid, and 4.60 B.M. in solution. The solution magnetic moment is effectively temperature independent over the range -20 to +90°C. This behavior closely parallels that observed in the solid state, where the moment is 4.50 ± 0.4 B.M. from -20 to +20°C and little change is expected at the higher temperatures. The observed decrease in the magnetic moment as the temperature decreases down to 85°K (Figure 8) is similar to that observed for the P-form, indicating the presence in V-iron phosvitin of antiferromagnetic coupling among the iron(III) ions present. The magnetic susceptibility is independent of the strength of the applied field from 2-11 kiloguass, indicating that there is no lattice-type magnetic interaction present. The width of the e.s.r. signal (Figure 9) is slightly greater in this form, and does not decrease as the temperature is decreased. At liquid nitrogen temperature two g values of 2.03 and 2.02 are resolved in the broad signal.

The ligand field spectrum is identical with that of the P-form (Figure 6) in the energies and intensities of the absorption bands, indicating that in this V-form also the predominant coordination structure of the iron(III) ions is tetrahedral. Quite a different conclusion can be

drawn from the spectrum recorded at 77°K in a pellet of potassium bromide (Figure 7). The tetrahedral bands observed in solution are also observed in the solid pellet spectrum, but three additional bands at 810, 610, and 555 nm are present. These bands are assigned to the appropriate transitions of octahedral iron(III). The 810 nm band is observed even at room temperature, suggesting that the observation of these bands is not the result of the lower temperature attainable in the pellet spectrum. It does suggest that the octahedral sites are induced by the pellet making process (in vacuo, 10^5 p.s.i.) by the addition to the iron, in some of the tetrahedral sites, of the protein bound water known to be present.

The close similarity of the magnetic and spectral data for the P- and V-forms indicates that the iron in the V-form is also present in tetrahedral coordination in antiferromagnetically coupled clusters of polynuclear iron(III). There are in addition important differences between the two forms. The number of irons bound in the V-form is increased by a factor of 1.5 over the P-form. The room temperature magnetic moment is slightly higher, and the broad e.s.r. band is partly resolved at low temperature. These differences can be reconciled by the assumption that there are two kinds of iron binding sites in phosvitin that differ slightly in their accessibility to incoming iron(III) and in their magnetic properties. The different methods of preparation support the difference in accessibility. The iron is presented to the P-form by direct mixing and an incubation period of

several hours, while the V-form results from the slower process of extended dialysis. On the basis of the ligand field spectral results the two kinds of iron sites are tetrahedral. The similarity in the antiferromagnetic coupling in both P- and V-iron phosvitin is emphasized by the close parallel between the temperature dependence of the magnetic moment in both cases. The slight increase in the magnetic moment in the V-form could result from a slightly weaker coupling in those sites that are unique to this form.

In summary, the coordination structure about the iron atom ions bound in V-iron phosvitin is tetrahedral as in the P-form discussed above, but two kinds of iron binding sites can be distinguished on the basis of slightly different magnetic properties and availability to iron(III) ions presented as iron(III)·NTA. Both kinds of sites are occupied by comparatively large antiferromagnetically coupled clusters of polynuclear iron(III).

c) B-iron phosvitin. In contrast to the marked similarity between the P- and V-forms of iron phosvitin, the brown or B-form which binds an amount of iron equivalent to P-iron phosvitin (6.9%) appears to be quite different in many physical properties from both of the other forms.

The room temperature magnetic moment of 1.56 B. M. is depressed far below that of the P- and V-forms. This low magnetic moment decreases further to 1.18 B.M. at 85°K (Figure 8), indicating

that the polynuclear units are larger than dimeric. This is supported by the e.s.r. signal (Figure 10) which is the broadest, 800 gauss, of all three forms of iron phosvitin. This large width is effectively temperature independent. At low temperature, the signal is partly resolved into two components at g values of 2.04 and 2.13.

The ligand field spectrum of a solution of B-iron phosvitin at room temperature shows only one weak ligand field absorption at ~820 nm corresponding to the first ligand field transition of octahedral iron(III). This absorption occurs at the end of a strong absorption that extends throughout the visible, obscuring the higher energy absorption bands of any tetrahedral iron(III) that might be present. This form of iron phosvitin was prepared by a significant modification of the preparative procedure used for P-iron phosvitin. Ten minutes of immersion in a boiling water bath preceded the direct mixing of the phosvitin solution with iron(III).NTA. Both P- and B-forms bind equivalent amounts of iron(III) suggesting that the second kind of iron binding site proposed for the V-form is available to neither of these two forms. The heating procedure appears to change the protein conformation, opening the iron binding sites to hydrolytic polymerization and, consequently, to octahedral coordination.

This form of iron phosvitin, like the other two discussed above, binds iron(III) in large polynuclear clusters, but unlike the other forms, the predominant coordination structure of these antiferromagnetically coupled iron(III) ions is octahedral not tetrahedral.

d) ESCA Results. From the phosphorous binding energies of the model compounds studied (Figure 11) several important observations can be made. The binding energy increased dramatically in going from pyrophosphate in a simple ionic salt (132.2 eV) to pyrophosphate as a bidentate ligand bound to cobalt(II) (135.2 eV). In addition there was a significant difference between the binding energy for phosphate acting as a monodentate (132.1 eV) and as a bidentate (133.0 eV) ligand. These phosphorous containing ligands bind to metal ions via oxygen atoms, with the phosphorous one atom removed from the metal. Significant changes in the phosphorous binding energy are observed among the different binding arrangements. These shifts are in marked contrast to the much smaller shifts observed in the phosvitin series of compounds (Figure 12). The free serine phosphate binding energy did change from 133.3 eV to 132.7 eV on incorporation into the protein phosvitin, but this protein value remained unchanged on binding iron(III) in the V-form and increased only slightly (133.0 eV) in the B-form of iron phosvitin. The structural implication for the iron(III) bound to phosvitin is that it is highly unlikely that the serine phosphate residues act as bidentate ligands to iron(III). The small shift in the phosphorous binding energy of phosvitin on binding iron(III) unfortunately provides no direct evidence for any binding between iron(III) and serine phosphate. The iron(III) ions bound in the V-and B-forms of iron phosvitin differ markedly in their spectral and magnetic properties (8(c) above). The ESCA data indicate that the phosphorous atoms also differ slightly between these two forms.

This difference between V- and B-iron phosvitins is also expressed in their slightly different iron binding energies of 712 and 712.2 eV. The significance of this small difference is unknown. The most interesting iron binding energy data are that obtained on iron(III) phosphate. As discussed in 8(f) below, the X-ray and spectral data on this compound are consistent with the presence of significant amounts (at least 25%) of each of two kinds of iron(III) sites, tetrahedral FeO_4 and octahedral FeO_6. The ESCA results show two iron binding energies that differ by ~0.8 eV. The important implication for the iron phosvitin study is that ESCA can discriminate between these two site symmetries in the one compound. No splitting is observed in the iron binding energy of V-iron phosvitin. The data for the B-form are of lower resolution and no conclusions about different site symmetries can be drawn. These results support the contention made above on the basis of ligand field spectral results that the predominant, i.e., >80%, coordination structure present in V-iron phosvitin and, presumably, in the closely related P-iron phosvitin, is one of tetrahedral symmetry, i.e., $[FeO_4]$.

e) Phosvitin--a summary. The structural information obtained from the studies discussed in the preceding sections can be summarized as follows. In both P- and V-iron phosvitin, the coordination structure of the great majority of iron(III) bound to the protein is the tetrahedral structure, FeO_4. The amino acid side chain that is

predominantly involved in binding to the iron(III) is the $-CH_2-O-PO_3^=$ of serine phosphate. The phosphate groups can act as monodentate ligands or as bridging groups between the iron atoms in the polynuclear clusters. The ESCA results exclude the possibility of the phosphate being a bidentate ligand.

The antiferromagnetic coupling of the iron(III) ions in these forms of iron phosvitin was confirmed by the magnetic and e.s.r. data. The broad e.s.r. absorption indicated that the coupling was extended over several iron atoms, in a polynuclear cluster that was significantly larger than dimeric. The size of these clusters and their distribution are unknown. Speculation on these matters awaits the results of the amino acid sequence determination that is in progress.[142] The protein conformation in iron phosvitin is important in maintaining the unusual tetrahedral coordination. By analogy to the effects of pH and various organic solvents on the conformation of phosvitin, the conformation of iron phosvitin has been deduced to be a β-structure of pleated sheets.

The two green forms of iron phosvitin, P- and V-, bind iron(III) in tetrahedral coordination sites that are coupled together in polynuclear clusters. The V-form binds 50% more iron(III) ions and appears to have an additional kind of iron binding sites to the P-form. The two kinds of sites are distinguished on the basis of slightly different magnetic properties and availability to iron(III) ions presented as iron(III)·NTA.

The third form, B-iron phosvitin, also binds iron(III) ions in large polynuclear clusters but the coordination structure of the iron binding sites is octahedral not tetrahedral.

These results are consistent with the general theory outlined in the introduction that competition between large and small molecular weight chelates is a dominating factor in the regulation of iron uptake in the gut. All three forms of iron phosvitin bind a large number of iron(III) ions in a complex whose binding constant for iron certainly exceeds the reported value[141] of 10^6 calculated on the assumption of a single set of equivalent and non-interacting sites. The stability constant of the complex formed between iron(III) and the phosphate of the free amino acid, serine phosphate, has been reported[143] as $\sim 10^6$. Furthermore, the iron-free protein has been shown to be resistant[33] to the action of proteolytic enzymes.

It would appear that the inhibitory effect of eggs on iron uptake is caused by competition by phosvitin for iron that would otherwise be bound to low molecular weight chelates and so be transferred across the mucosal membrane.

An interesting feature of this work has been the isolation of forms of iron phosvitin that bind large numbers of polynuclear iron(III) ions by preparative procedures that mimic dietary phosvitin in raw eggs (the P- and V-forms) as well as in "hard-boiled" eggs (B-form). The inhibitory effect of both kinds of diet can be understood in the light of this present investigation.

f) $FePO_4$. The identification of the tetrahedral coordination structure of iron(III) in phosvitin, together with the suggestion that the predominant structural interaction between the metal ion and the protein was that between the metal and the phosphate groups of serine phosphate, led to the investigation of the crystalline phase of iron(III) phosphate. The structure of this mineral phase has been reported[12] to be that of the quartz type. Both iron and phosphorous occupy tetrahedral sites, with four oxygen atoms as nearest neighbors. The X-ray powder pattern of the preparation of iron(III) phosphate used in this study identified it as the quartz form of iron(III) phosphate.

The lines corresponding to d spacings of 2.54, 2.20, and 1.72 Å are strong lines in strengite $FePO_4 \cdot 2H_2O$,[128] weak in pure $FePO_4$, and of moderate intensity in this preparation. The enhanced intensity of these lines strongly suggests that this preparation contains some strengite, $FePO_4 \cdot 2H_2O$, a likely contaminant if the dehydration step in the preparation was incomplete. The lines are noted in Fig. 17.

The complex visible absorption spectrum (Figure 17) can be understood on the assumption of a mixing of $FePO_4$ and $FePO_4 \cdot 2H_2O$, which would show absorptions corresponding to both octahedral and tetrahedral ligand field transitions. On this assumption the highest energy ligand field band at 414 nm is assigned to the third ligand field transition of tetrahedral iron(III). This transition occurs near 400 nm

Figure 17

Visible absorption spectrum of iron(III) phosphate (5.84 mg) in a pellet of potassium bromide (220 mg) at liquid nitrogen temperature.

X-ray powder pattern of this iron(III) phosphate using molybdenum K_{α} radiation, an exposure time of 23 hours, and zirconium foil filters on the incident and diffracted beams. The lines, indicated at α spacings of 2.54, 2.20, and 1.72 Å, indicate contamination by $FePO_4 \cdot 2H_2O$.

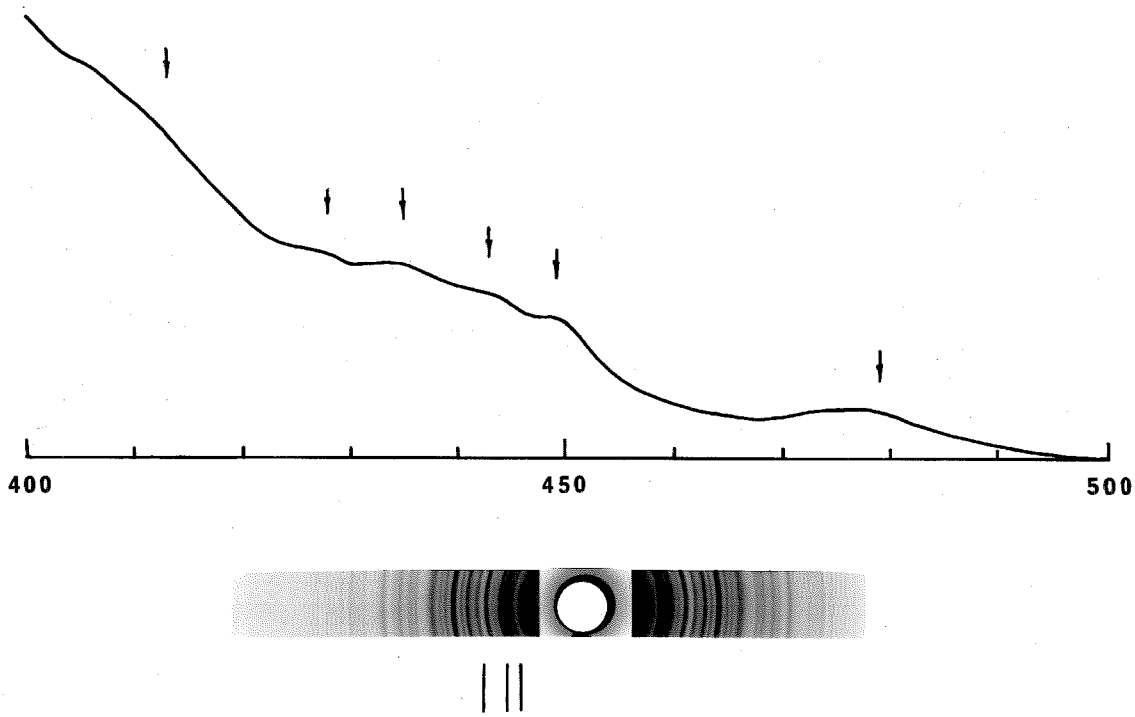
400
450
500

in orthoclase feldspar and iron phosvitin. Using these spectra as analogies the two lower energy tetrahedral transitions are assigned to the discrete 479 nm absorption and to one of the four absorptions of the broad 480 to 430 nm envelope. The three remaining bands in this envelope are assigned to the third transition in octahedral iron(III). This octahedral transition is also split in the spectra of iron(III) ammonium sulphate (Figure 4) and hexaquomanganese(II).[130] The crystalline structures of $FePO_4$ and $FePO_4 \cdot 2H_2O$ are not isomorphous. Any octahedral sites in a preparation of $FePO_4$ are expected to be at least slightly distorted from octahedral, and the absorption band corresponding to the third ligand field absorption would be split. The remaining band, that at 535 nm,is assigned to the second octahedral transition. The lowest energy octahedral band is expected at about 800 nm where the spectrum could not be recorded. The assignments are summarized in Table 17.

Table 17

λ_{max}(nm)	535	479	449 · · 443 · 435 · · 428	413
symmetry	octa.	tetr.	octa/tetr	tetr
transition $^6A_1 \rightarrow$	$^4T_2$	$^4T_1$	$^4A_1, {}^4E/{}^4T_2$	$^4A_1, {}^4E$

Although the spectrum appears complex, a reasonable assignment of all the bands observed can be made on the assumption that the preparation contains iron in both octahedral and tetrahedral sites.

This structure, suggested by the X-ray data, is further supported by the measurements of the binding energy of the iron $2p_{3/2}$ electrons using the ESCA technique. Two components of the ESCA band are resolved at 712.1 and 711.4 eV. The relative intensities of the visible absorption bands assigned to the octahedral and tetrahedral transitions suggest that the sites are present in about equal proportions. The X-ray data suggest however that the tetrahedral sites predominate. The probable implication, already mentioned earlier in 8(d) above, is that ESCA can discriminate between the two slightly different iron(III) coordination sites, FeO_4 and FeO_6, present in significant ($> 25\%$) amounts in any one compound.

g) $\underline{\phi_4As \cdot FeCl_4}$. The most unusual feature of the results obtained on this compound is the complex splitting observed in two of the weak bands of the absorption spectrum (Figure 14). The temperature dependence of the magnetic moment confirms that the ground state of the iron(III) ion was a sextet, namely $^6A_1$. The general pattern of these bands in the spectrum, ignoring for the moment the splitting, resembles that of the tetrahedrally coordinated iron(III) found in orthoclase feldspar (Figure 4). The pattern common to the two spectra is that of two broad bands followed by a sharper band at higher energy. The ready assignment of the comparatively sharp band at 530 nm to the $^6A_1 \rightarrow {}^4A_1, {}^4E$ transition leads to the assignment of the broad envelope from 580 to 660 nm to the $^6A_1 \rightarrow {}^4T_2$ transition, and the 660 to 800 nm envelope to the lowest energy ligand field transition,

$^6A_1 \rightarrow {}^4T_1$. With the one exception of the component at 735 nm whose band maximum cannot be precisely identified at room temperature, the splittings between the various components of the two envelopes stays reasonably constant at $\sim 600\ cm^{-1}$.

The $^6A_1$ symmetry of the ground state excludes, a priori, any contribution to the observed splittings from coupling of the spin and orbital angular moments, and from a ground state Jahn-Teller distortion. This latter distortion is theoretically possible[133] in the two excited states of interest, $^4T_1$ and $^4T_2$. If such a mechanism is operating, as has been observed in several other electronic configurations,[134,135] the splitting is expected to decrease as the temperature decreases. Exactly the opposite behavior is observed for $[FeCl_4]^-$. Another possible origin of these splittings is the presence of a low symmetry component of the ligand field that permanently distorts the ground state away from tetrahedral symmetry. The symmetry in the crystal as determined by X-ray analysis[124] is very close to tetrahedral, and there is no reason to expect that in solution, where the splittings are also observed, that the symmetry should deviate from tetrahedral. A low symmetry component of the ligand field of sufficient magnitude to split the $^6A_1 \rightarrow {}^4T_1$ and $^6A_1 \rightarrow {}^4T_2$ transitions into these components would necessarily remove the degeneracy of the $^4A_1$, ^4E levels. No such splitting in this level is observed.

The only acceptable explanation for these splittings is that they are expressions of a vibrational progression. The spacings of the split bands is reasonably constant, as expected for the stepwise addition of a quantum of vibrational energy to the excited state. This quantum is expected to be that of the totally symmetric A_1 vibrational mode of the excited state. From the observed splittings the energy of this mode is $\sim 600\ cm^{-1}$. The energy of the equivalent mode in the ground state was determined by polarized Raman spectroscopy to be $334\ cm^{-1}$. The increase in energy in this mode in going from the ground to the excited state is not unexpected. The excited states are derived from the one electron transition from the $(e)^2(t_2)^3$ to the $(e)^3(t_2)^2$ electronic configuration (Figure 2). This change corresponds to a decrease in the anti-bonding character of the ground state. Consequently, the iron-chlorine vibrations are expected to be of higher energy in the excited state.

In summary, the $FeCl_4^-$ anion also exhibits the absorption band pattern of a tetrahedral array of ligand atoms bound to iron(III). The band energies are at lower energies than in the FeO_4 case of orthoclase feldspar, but are still easily distinguished from the FeO_6 band energies. The unusual splitting observed in the first two ligand field absorptions is attributed to a vibrational progression in the excited states, where, as expected, the totally symmetric iron-chlorine stretching mode is higher in energy, $600\ cm^{-1}$, than in the ground state, $334\ cm^{-1}$.

C. Gastroferrin

The coordination structure of the iron(III) ions bound to the glycoprotein gastroferrin has been investigated by magnetic susceptibility and ligand field spectral measurements. Mössbauer, electron spin resonance, and infrared spectral results have been reported by another investigator.[117] They will be considered in the following discussion.

1. Preparation

Both iron free and iron bound gastroferrins from two sources, pooled human gastric juices and commercial pig gastric mucin, were kind gifts from Dr. Paul Saltman and co-workers at the University of California at San Diego. The iron-gastroferrin had been isolated by the following procedure.[26] An excess of iron(III) as the chloride was added to gastric secretions at pH 2 and the solution titrated with ammonia to pH 8, where the iron-gastroferrin complex was co-precipitated with iron(III) hydroxide from the excess iron present. The iron(III) hydroxide was removed by treatment with nitrilotriacetate followed by exhaustive dialysis and gel chromatography on G-200. The results presented below were obtained on pig mucin gastroferrin. The magnetic susceptibility data obtained for the human gastroferrin confirm the chemical evidence that the two gastroferrins are very similar.[26]

2. Ligand Field Spectral Results

A rust-brown solution of pig mucin gastroferrin was dialyzed exhaustively against deionized water and a slight cloudiness

removed by centrifugation. Solution spectra were recorded at ambient temperature in 10 cm cells. Since iron free gastroferrin is known to have no absorption at wavelengths greater than 450 nm, the spectral region of interest, the reference solution used was deionized water. The solution was determined to be 1.1×10^{-3} molar in iron by atomic absorption.

Three weak shoulders, at 960, 620, and 490 nm were observed on the side of an intense absorption that spread from the ultraviolet through the visible. Because of the low intensities of the shoulders there is some uncertainty in their extinction coefficients and absorption maxima. The spectrum is shown in Figure 18 and the spectral data collected in Table 18.

Table 18

λ (nm)	$\tilde{\nu}$ (cm^{-1})	ϵ(approx)	Assignment
960 ± 5	10,400 ± 50	5	$^6A_1 \rightarrow {}^4T_1$
620 ± 10	16,200 ± 200	3	$^6A_1 \rightarrow {}^4T_2$
490 ± 10	20,400 ± 400	2	$^6A_1 \rightarrow {}^4A_1, {}^4E$

The energies of these bands are consistent only with octahedral not with tetrahedral coordination around the iron(III) ions. Furthermore the extinction coefficients are higher than expected for the ligand field bands of an octahedral d^5 ion by at least one order of magnitude. This intensity enhancement is consistent with the presence of some polynuclear interaction among the iron atoms.

Figure 18

Visible and near infrared spectra of an aqueous solution of pig mucin gastroferrin (10^{-3}M in iron) at room temperature. The extinction coefficients of the bands at 960, 620, and 490 nm are ~5, 3, and 2, respectively.

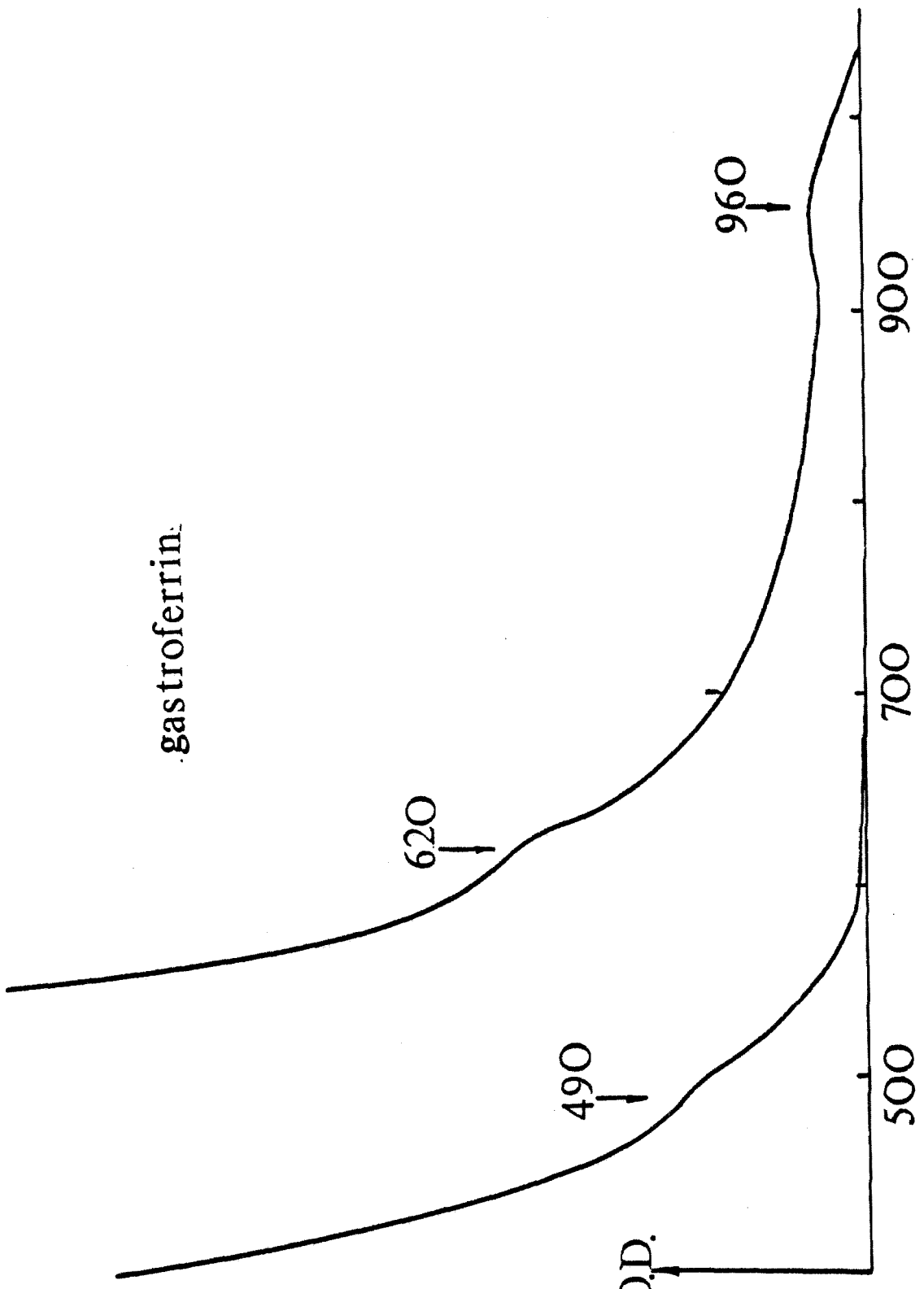
gastroferrin
620
490
960
O.D.
500
700
900

3. Magnetic Susceptibility Studies

The magnetic susceptibility and hence the magnetic moment per iron were determined in solution and in the solid state. Using the usual n.m.r. procedure, a solution of iron gastroferrin, 0.064×10^{-3} M in iron, produced a 5.65 Hz shift at 290°K. The iron-free protein was included in the reference solution. This shift corresponds to a magnetic moment per iron of $3.5 \pm .05$ B.M.

A lyophilized preparation of iron gastroferrin was used for the study of the temperature dependence of the magnetic moment in the solid state. The iron content of $3.95 \pm 0.15\%$ indicates the presence of 180 to 190 iron atoms in the protein of molecular weight 260,000. The molar diamagnetic correction for the protein was determined directly to be $-155,200 \times 10^{-6}$ cgs units. The uncertainty in the iron analytical figure has been incorporated into the calculations for the magnetic moment per iron at various temperatures between 300 and 95°K. The results in the solid and solution are shown in Figure 19.

The solution and solid state results are consistent. The depressed magnetic moment at room temperature of ~3.5 B.M. strongly suggests the presence of antiferromagnetically coupled iron atoms. Even with the error bars shown, the magnetic moment per iron does appear to increase with decreasing temperature. Data at temperatures below 95°K are needed to confirm this behavior.

Figure 19

Temperature dependence of the magnetic moment per iron in gastroferrin (lyophilized powder) from 300° - 90°K. The room temperature solution value is indicated.

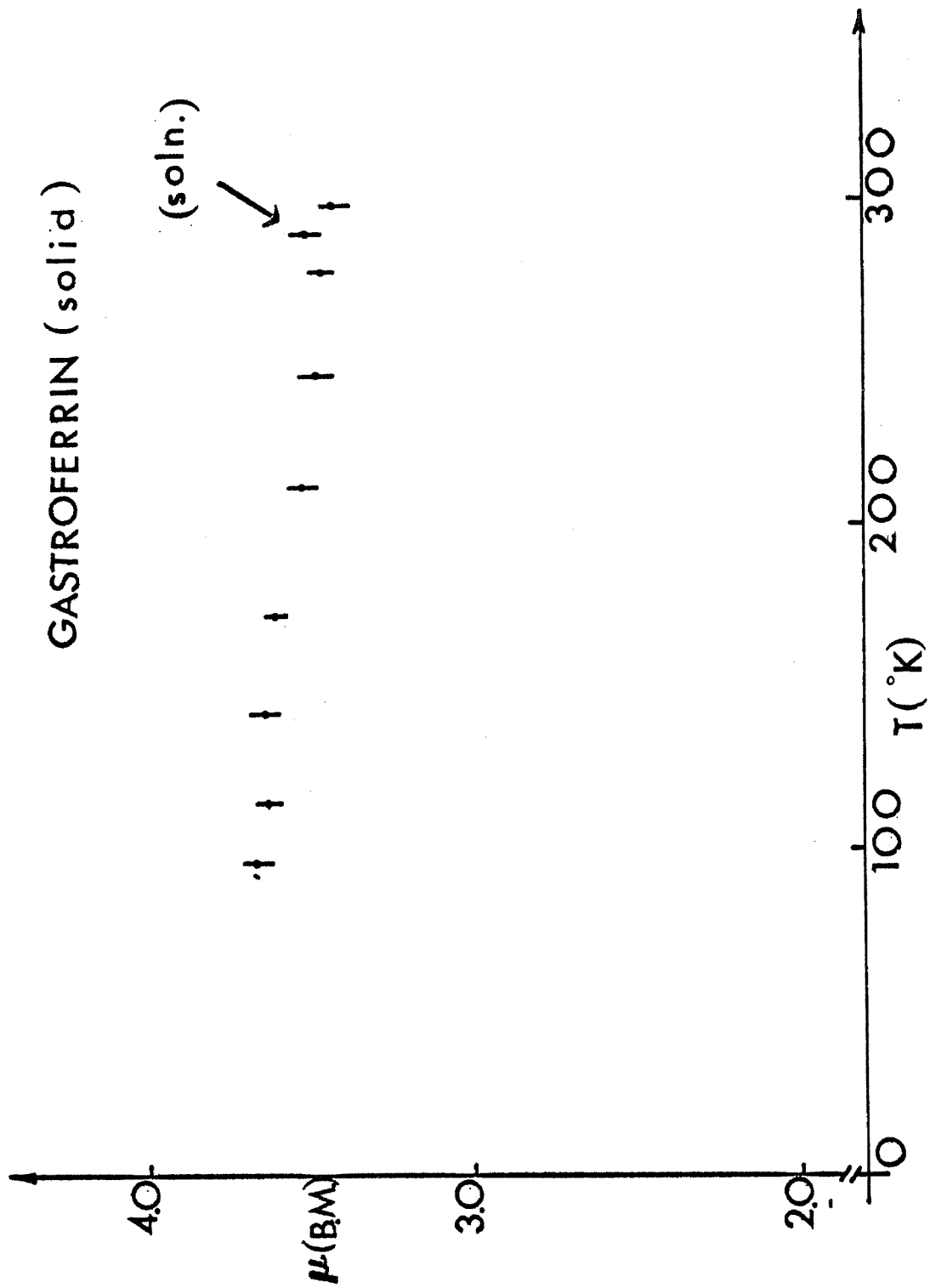
GASTROFERRIN (solid)
(soln.)
4.0
3.0
2.0
μ(B.M.)
0
100
200
300
T(°K)

Another unusual feature of the magnetic properties of this iron-protein was apparent in the study of the magnetic behavior as a function of the applied magnetic field (H) at 298.6°K. For convenience the data are presented as the intensity, I, in arbitrary units, of the output from the magnetometer. For a simple paramagnet the intensity is linear with the applied field and is zero at zero field. The results are shown in Figure 20. At low fields the field strength behavior of the intensity deviates from linear. Line I in the figure is the computed least squares line, $I = 2.118\ H + 0.633$. This line does not pass through the origin. It has an intercept on the H axis of -299 oersteds (gauss). The second line shown, II, joins the high field points, $H > \sim 5$kOe. On extrapolation it does pass through the origin. The deviation of the low field points from linearity is ~10%, greater than the experimental error (~2%).

Although more data are desirable in the important low field region, these results indicate that there is a weak intrinsic magnetic ordering of ~300 oersteds of at least some of the iron atoms in gastroferrin. The effect of this small ordering perturbation is proportionally greater at lower fields where the observed intensity is greater than that of a simple paramagnet. This suggests that the ordering is ferromagnetic in character. The explanation for the observed increase in the magnetic moment per iron with decreasing temperature must take into account this intrinsic ordering.

Figure 20

The dependence of the output from the magnetometer I, in arbitrary units on the strength of the applied field H, in k0e for gastroferrin. The data extend from 1.9 to 10.4 k0e and were taken at 298.6°K.

I: least squares line of best fit, $I = 2.12H + 0.63$. The intercept on the H axis is -300 0e and the correlation coefficient is 0.999.

II: extrapolation of the high field data back to zero field.

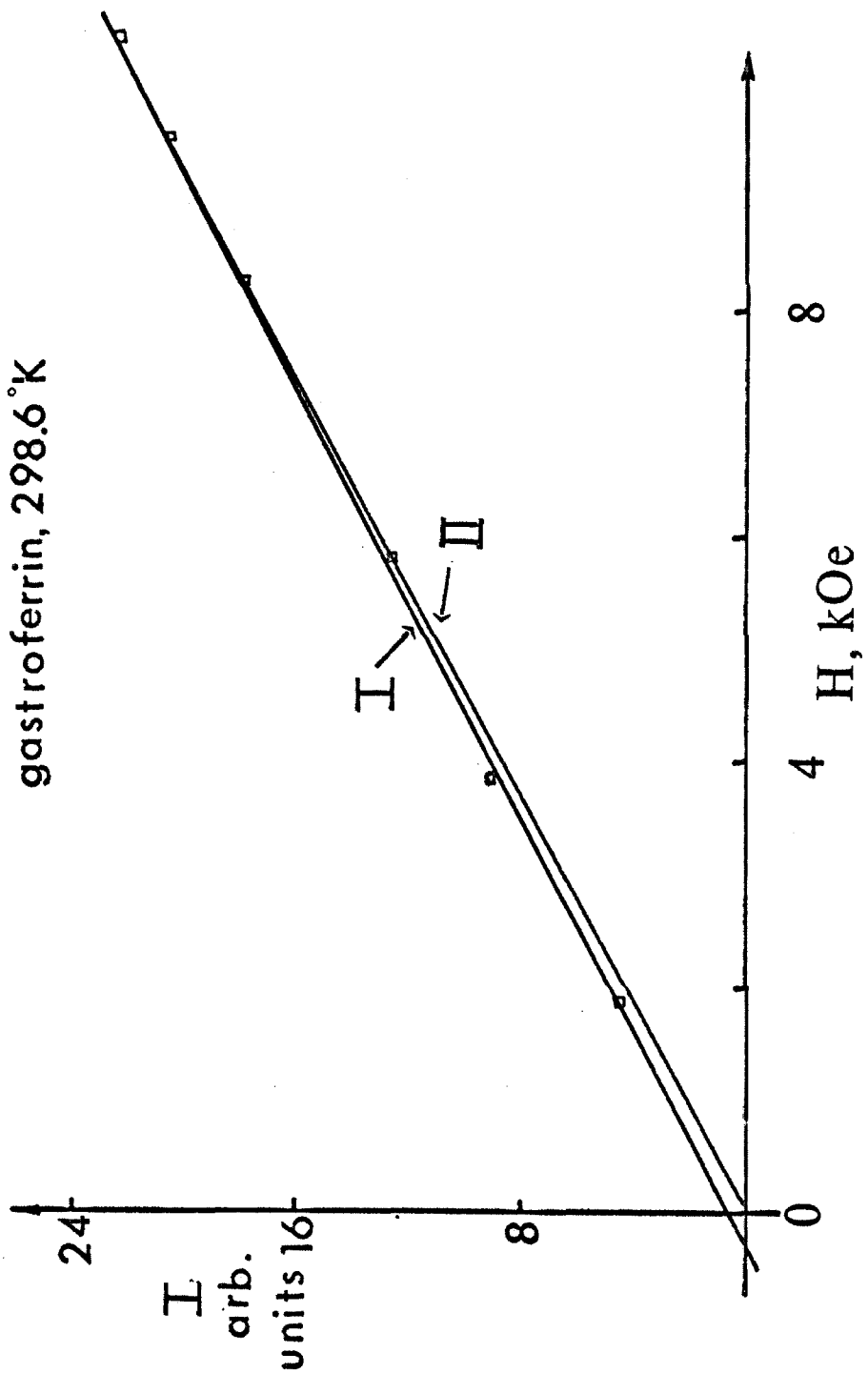
gastroferrin, 298.6°K
I
arb.
units
24
16
8
0
4
8
H, kOe
I
II

4. Discussion and a Structural Model

The spectral results indicate that the coordination structure about the majority of the iron(III) atoms in gastroferrin is octahedral. Any tetrahedral bands occur at higher energies ($\lambda > 450$ nm) and would be obscured by the broad intense absorption centered in the ultraviolet region. The comparatively high extinction coefficients of the ligand field bands are consistent with polynuclear iron(III). The polynuclear interaction is antiferromagnetic, resulting in the depressed magnetic moment of ~3.5 B.M. An additional influence on the magnetic behavior is a small apparently ferromagnetic interaction of ~300 oersteds. Data obtained from other spectral techniques are consistent with these results.

The Mössbauer spectrum at 77°K is a quadrupole split doublet.[117] The isomer shift is 0.19 mm/sec and the quadrupole splitting 0.71 mm/sec. These values are consistent with high spin or antiferromagnetically coupled iron(III). The six line hyperfine splitting observed in magnetically order lattices of iron(III) is ~ 12 mm/sec for an internal field of ~600k0e. The observed ferromagnetic ordering is small even at liquid nitrogen temperature. No splitting or broadening of the Mössbauer resonance lines is expected until much lower temperatures. The e.s.r. spectrum of a frozen solution[117] at 173°K consists of a broad absorption from g = 6.6 to 4.0 with a much weaker sharp absorption at g = 2.3. The broad low field band has a peak

to peak width of 750 gauss, consistent with the presence of polynuclear iron. A structural model for the iron bound to gastroferrin that is consistent with these data can be derived.

The antiferromagnetic coupling between octahedral iron(III) ions confirms that most of the 180-190 iron atoms present are in close proximity to other iron atoms. This is not unreasonable in view of the method of preparation and the high carbohydrate composition of the protein. Many carbohydrates are known to bind iron(III) although a large excess (× 20)of the carbohydrate is required to prevent the precipitation of iron(III) hydroxide at physiological pH. A discrete polymer of molecular weight 65,000 has been isolated from iron(III) fructose solutions.

The preparative procedure of co-precipitation with iron(III) hydroxide suggests that the carbohydrate residues on the protein act in a manner analogous to that of the discrete sugars. The polynuclear iron(III) that forms by hydrolysis is kept in solution at the carbohydrate region by binding to the carbohydrate. In this respect gastroferrin is more efficient than the simple carbohydrates. The mole ratio of carbohydrate to iron in gastroferrin is ~6, not the 20 of the simple carbohydrate system. This increased efficiency could result from the proper orientation of binding groups in the protein. This inhibition of precipitation could occur in several regions of this large carbohydrate rich protein, resulting in a small number of reasonably discrete polynuclear clusters of iron(III) distributed throughout the molecule.

The failure[117] to observe an infrared absorption at 850 cm^{-1} corresponding to the Fe-O-Fe structural unit is consistent with these polynuclear clusters being aggregates larger than dimers. The fructose polymer and many FeOOH phases do not show this absorption.[118] The apparent increase in the magnetic moment with decreasing temperature can be accounted for by a weak ferromagnetic coupling among these clusters.

It is possible that the ordering induced by this coupling has an inverse temperature dependence analogous to that of the susceptibility. This dependence would serve to gradually make it a significant fraction of the strong magnetic field used to obtain the magnetic moment data, 10k0e. It would then increase the observed moment as the temperature decreased. The dimensions of these clusters (< 50 Å diameter) would be in the superparamagnetic range. The expected temperature independent moment of a particle of this size would be modified by the additional perturbation of a ferromagnetic nature.

In summary, the proposed model for the iron bound to gastroferrin consists of a number of reasonably discrete polynuclear clusters of antiferromagnetically coupled iron(III) ions that are themselves coupled in a weakly ferromagnetic way. The coordination about most of the iron(III) is octahedral.

D. Ferritin

The structure of the inner core of the iron storage protein has been the object of many investigations using a variety of physical techniques. These have included electron microscopy, low angle X-ray scattering, high angle X-ray and electron diffraction, magnetic susceptibility, electron spin resonance, and Mössbauer spectroscopy. These studies have been the object of an excellent recent review.[34] Even with results from this wide variety of probes, the structure of the core remains controversial. At the present time four structural models have been proposed. Three of these are based on synthetic materials isolated from hydrolyzed iron(III) solutions, namely, the nitrate polymer,[8] the Towe hydrolyzate,[6] and the van der Giessen gel.[7] A fourth model, based on the proposed structure for δ-FeOOH has been suggested[35] on the basis of X-ray analysis. The experiments reported below mainly concern ferritin and the first two structural models listed. It was not possible to prepare a sample of the van der Geissen gel with the complete X-ray powder pattern reported for this compound. The literature reports on this gel will be considered at the appropriate place in the discussion. The results of several studies on the impure preparation will be briefly mentioned.

A major omission from the above list of physical techniques is absorption spectroscopy of the ligand field bands of the iron(III) ions. A significant difference among the four structural models is the relative

proportion of octahedral and tetrahedral iron(III) ions present. Since oxygen is the only available ligand atom inside the core the choice among the structural models is one among iron(III) exclusively as $[FeO_6]$, exclusively as $[FeO_4]$, and as some combination of the two kinds of sites. The ligand field spectra of these two structural units are quite different and offer a means of distinguishing between the various models and ferritin.

In the study reported here, ligand field spectral results figure prominently. Moreover, the two synthetic models and the protein have been studied, in a comparative fashion, by the temperature dependence of the magnetic susceptibility, infrared spectra, and X-ray powder patterns. In the course of this study the structure proposed, largely on the basis of a small angle X-ray scattering study, for one of the synthetic models, the nitrate polymer (sometimes referred to in subsequent diagrams as the "inorganic polymer") was shown to be inconsistent with observations obtained from other physical techniques. The structural information obtained by each technique will be discussed with the results obtained. In conclusion, a structural model consistent with these results and those reported by other investigators will be proposed for the core of ferritin.

1. Ligand Field Spectra

The characteristic color of ferritin, its structural models, and powders of the phases of FeOOH is reddish-brown, corresponding

to an intense absorption in the blue end of the visible. As a result, only in the near infrared end of the visible can the weak ligand field absorptions of a d^5 ion be observed. The lowest ligand field absorption for $[Fe(III)O_6]$ occurs in this region at 800-900 nm (see Figure 4). The other octahedral absorptions and all the tetrahedral absorptions occur at higher energies where they are expected to be obscured by the intense absorption responsible for the red-brown color. The reference spectra for $[FeO_4]$ and $[FeO_6]$ have been obtained on large single crystals of orthoclase feldspar and iron(III) ammonium sulphate. The compatibility of this solid state with conditions in solution was investigated for the $[FeO_6]$ case by a careful study of the spectrum of iron(III) perchlorate. The hygroscopic purple crystals of the commercial salt were recrystallized six times from perchloric acid (9.6 M) to remove any polymeric species that might have been introduced by hydrolysis by atmosphere water. The spectrum was recorded at room temperature in perchloric acid (0.96 M), and was essentially identical, in the positions, shapes, and intensities of the bands, to that of iron(III) ammonium sulphate.

A number of polymeric iron(III) compounds have been investigated to characterize the spectrum of the $[FeO_6]$ structural unit when it is coupled to other such units in a polynuclear cluster. Horse ferritin was obtained as cadmium-free solutions (Nutritional Biochemicals Corp.). Jarossite, a yellow crystalline mineral of formula

$FeOHSO_4$, can be isolated from one region of the $Fe_2O_3 \cdot SO_3 \cdot H_2O$ phase diagram,[144] and its structure has been determined.[11] An aliquot of the sample that had been used in the structure determination was kindly provided by G. Johansson, Royal Institute of Technology, Stockholm. Each iron atom in the crystal is octahedrally coordinated to two hydroxy groups and four sulphate oxygens. The octahedra which are very close to O_h symmetry are linked together into chains by hydroxide and sulphate bridging groups and these chains are joined to each other by the remaining sulphate oxygens.

α-FeOOH, goethite, is a well known[9,10] mineral phase of wide occurrence whose structure is based on hexagonal close packing of oxygens. Each iron atom lies at the center of a nearly regular octahedron of oxygens sharing three corners with three adjacent octahedra. The hydrogens occupy well defined lattice positions linking two layers of oxygen octahedra. A sample of the natural material from Maryland, U. S. A., was obtained from the Smithsonian Institute (# 117395).

γ-FeOOH, lepidocrocite,[9,10] a naturally occurring mineral, contains iron(III) ions in distorted octahedral sites, $[FeO_6]$. The structure is based on cubic close packing of oxygens. The hydrogens are again well defined structurally. A sample from Horhausen, Germany, was obtained from the Smithsonian Institute (# R9593).

The near infrared spectra of these three minerals, together with those of ferritin and the nitrate (here called "inorganic") polymer

are shown in Figure 21. In all five compounds the spectrum in this region consist of a broad peak centered at about 900 nm with a weak shoulder at 1200 nm.

The close similarity of these spectra strongly suggest that the iron atoms in all five compounds have the same coordination, i.e., octahedral. The weak shoulder observed at 1200 nm is assigned to a vibrational overtone of water and the more intense broad 900 nm peak to the first spin-forbidden transition of octahedral iron(III), $^6A_1 \rightarrow {}^4T_1$. The solution spectrum of ferritin was carefully studied at higher energies to identify other ligand field bands, but any weak bands present were hidden under an intense absorption. Data in the visible region have been reported[118] for α-FeOOH and γ-FeOOH, and were obtained on $FeOHSO_4$, the nitrate polymer and the Towe hydrolyzate.

In contrast to the situation with the oxyhydroxide phases,[118] the spectrum of $FeOHSO_4$ was readily observed up to 400 nm at room temperature. The sequence of two broad and one sharp bands expected for $[FeO_6]$ was observed, with absorption maxima occurring at 940 nm, 500 nm, and a doublet at 428 and 410 nm. The spectrum is shown in Figure 22.

The spectral data were extended into the visible region for two synthetic structural models for the ferritin core, namely, the nitrate polymer and the Towe hydrolyzate. The solution spectrum of the nitrate polymer is shown in Figure 23.

Figure 21

Absorption spectrum in the near infrared of polymeric iron(III) compounds recorded as Nujol mulls and thallous chloride pellets.

(1) ferritin (also as aqueous solution)

(2) inorganic (i.e., nitrate) polymer

(3) $FeOHSO_4$ jarossite

(4) α-FeOOH

(5) γ-FeOOH

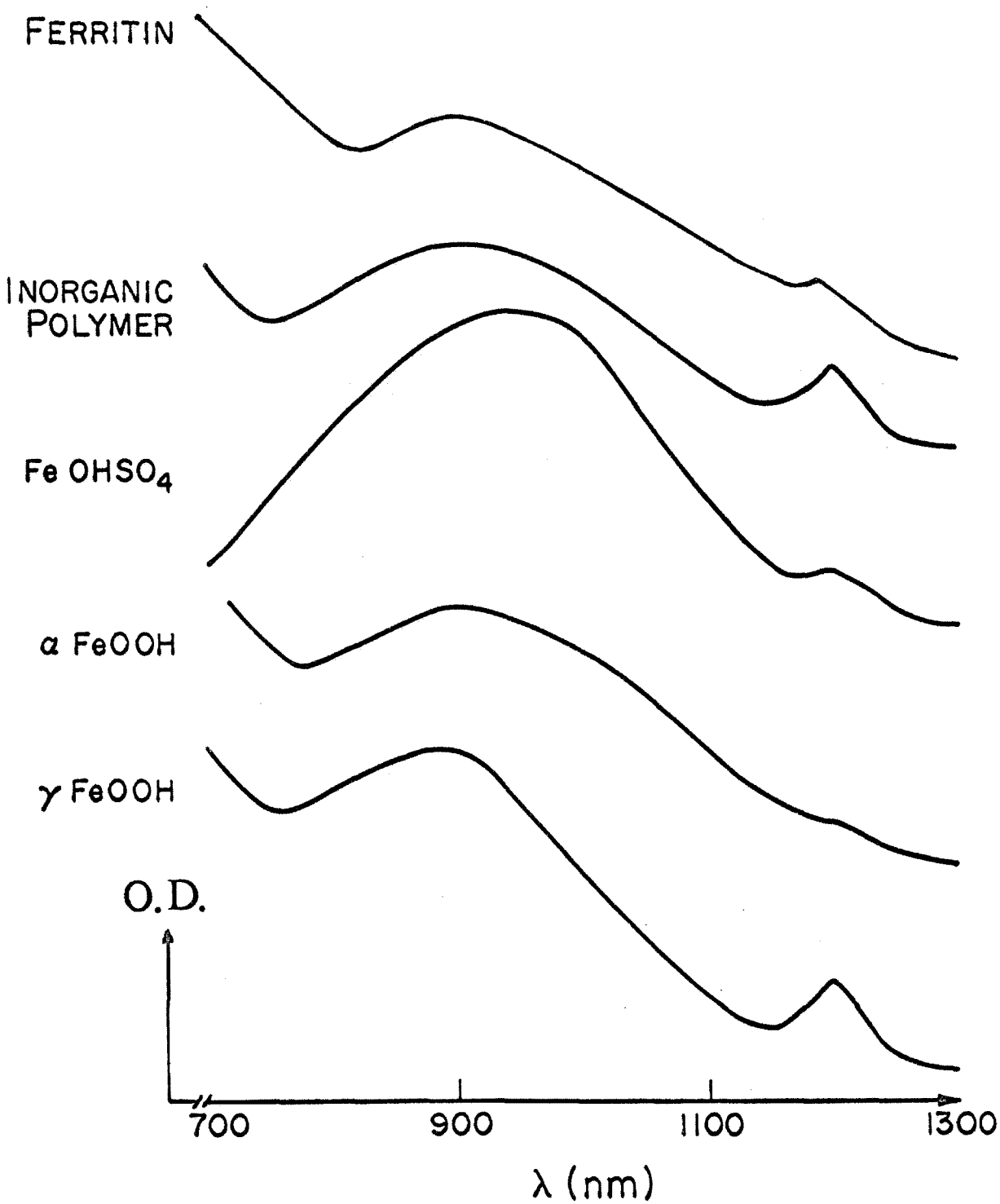
FERRITIN
INORGANIC POLYMER
Fe OHSO4
α FeOOH
γ FeOOH
O.D.
700
900
1100
1300
λ (nm)

Figure 22

Visible and near infrared spectra of jarossite, $FeOHSO_4$, recorded as a Nujol mull. The bands indicated occur at 940, 500, 428, and 410 nm.

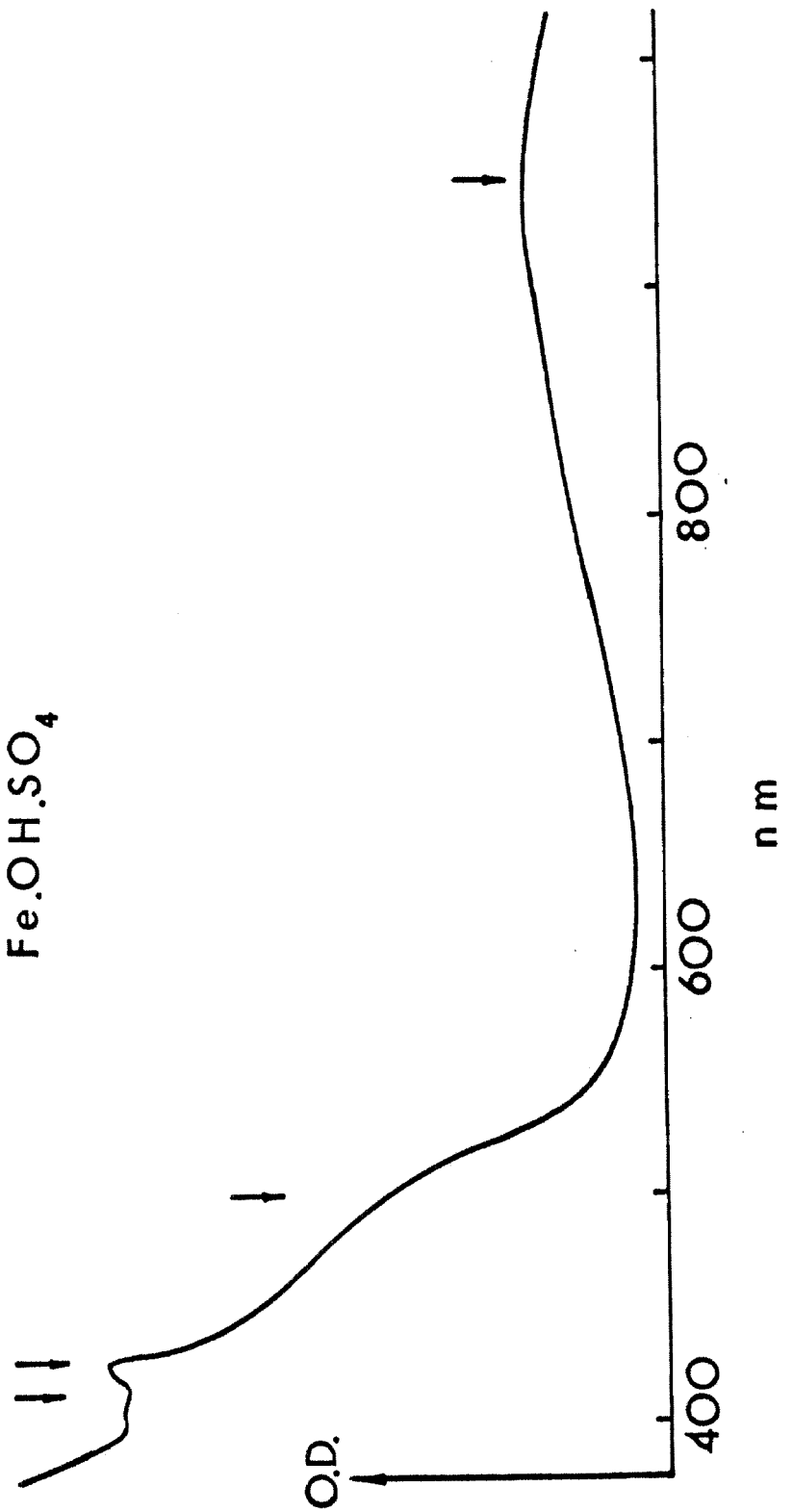
Fe.OH.SO4
O.D.
400
600
800
n m

Figure 23

Ultraviolet, visible, and near infrared spectrum of the nitrate polymer $[Fe_4O_3(OH)_4(NO_3)_2 \cdot 1.5\ H_2O]_x$ in aqueous solution at room temperature.

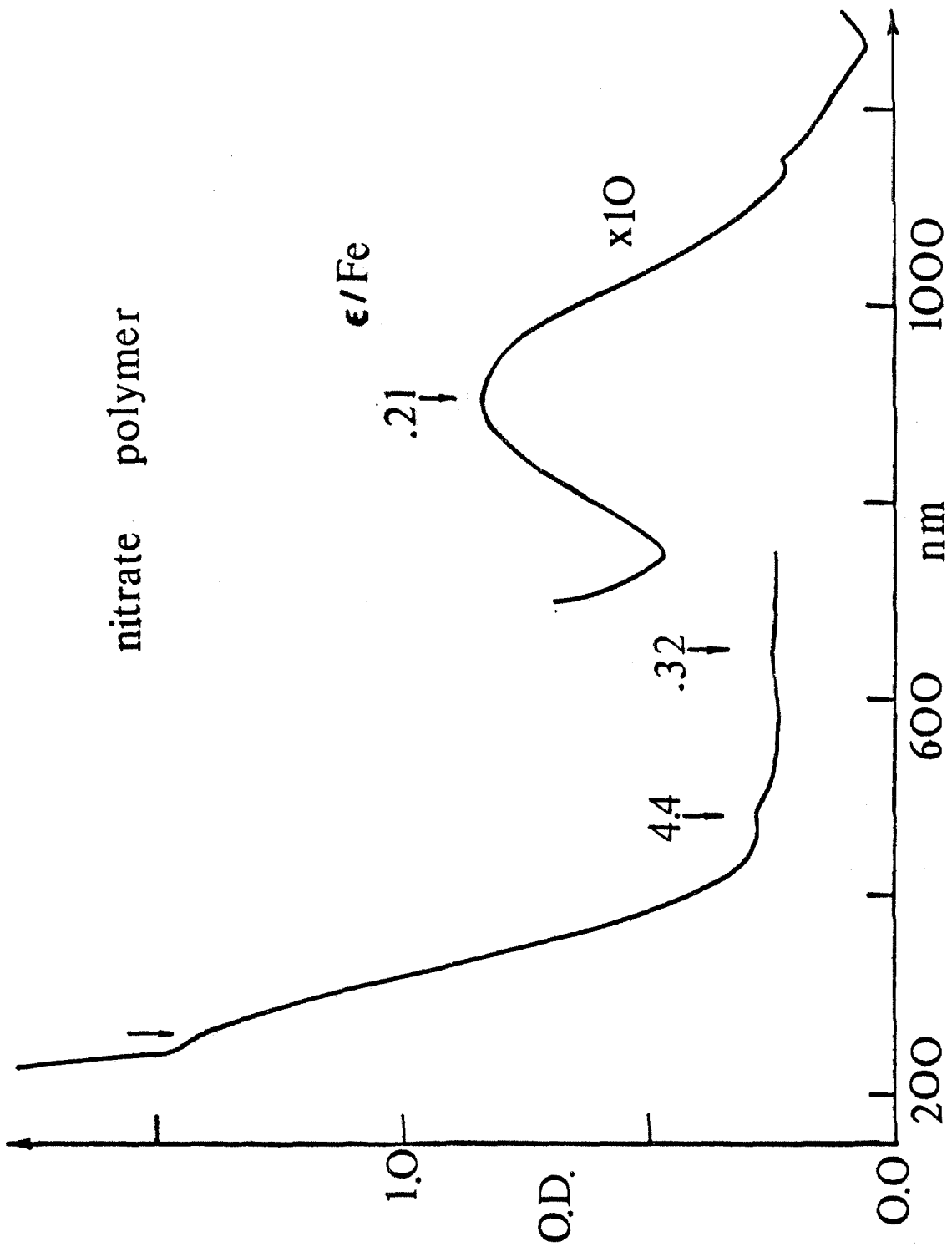
nitrate polymer
ε/Fe
.21
x10
.32
4.4
1.0
O.D.
0.0
200
600
nm
1000

Three weak bands at 900, 640, and 485 nm were observed, with extinction coefficients per iron that were small (<5) but greater than observed in the monomeric iron(III) spectrum, consistent with the presence of polynuclear iron. These bands were assigned to the first three spin forbidden transitions of the d^5 ion. The appropriate C/B ratio of 3.0 used in fitting the spectrum was chosen by reference to the analysis of the hexaquo iron(III) spectrum (C/B = 3.12). Using a Tanabe-Sugano diagram for this C/B ratio that had been calculated by Jack Thibeault of the California Institute of Technology the best fit of the three spectral bands of the nitrate polymer was determined using $Dq = 1130\ cm^{-1}$ and $B = 815\ cm^{-1}$.

The spectrum of the Towe hydrolyzate recorded at liquid nitrogen temperature in a pellet of thallous chloride (4.1 mg/400 mg) exhibited three weak absorptions at 880, 555, and at ~500 nm.

The spectral data and assignments for these compounds containing polymeric iron(III) are listed in Table 19.

2. Liquid X-ray Scattering

The ligand field spectral results and their analysis presented above provide strong evidence that the iron in the nitrate polymer is octahedrally coordinated.

The highest energy octahedral band was observed near where the energy of the first tetrahedral absorption of $[FeO_4]$ is known to occur. The higher intensity of tetrahedral ligand field bands makes it

Table 19

	$^6A_1 \rightarrow {}^4T_1$		$^6A_1 \rightarrow {}^4T_2$		$^6A_1 \rightarrow {}^4A_1, {}^4E$	
	λ_{max}(nm)	$\tilde{\nu}$ (cm^{-1})	λ_{max}(nm)	$\tilde{\nu}$ (cm^{-1})	λ_{max}(nm)	$\tilde{\nu}$ (cm^{-1})
α-FeOOH*	890	11,300	650	15,400	510	19,600
γ-FeOOH*	900	11,100	665	15,000	~535	18,700
Towe hydrolyzate	880	11,400	555	18,000	~500	~20,000
$FeOHSO_4$	940	10,600	500	20,000	428	23,400
					410	24,400
Nitrate polymer	900	11,100	640	15,650	485	20,600
Nitrate polymer (calc)†		10,900		15,850		20,400
Ferritin	900	11,100	--		--	

* From reference 118.

† Calculated using Dq = 1130 cm^{-1}, B = 815 cm^{-1}, C/B = 3.0.

unlikely that they would be covered by the tail of the ultraviolet band when the lower intensity octahedral band was observed.

No bands attributable to tetrahedral iron(III) were observed in the spectrum of the nitrate polymer up to 250 nm. These spectral data provide strong evidence that there is no tetrahedral iron(III) present in the nitrate polymer. This conclusion is in direct contrast to that derived from a liquid X-ray scattering study of a 3M aqueous solution. The radial distribution function has been analyzed to indicate that iron(III) is tetrahedrally coordinated to four oxygen atoms exclusively. The report of the scattering experiment also noted the presence of the first two ligand field bands at 900 and 640 nm. The analysis of this spectrum as that of tetrahedral iron(III) could only be achieved by the assumption of an "unusual and unexpected" ligand field strength of $\sim$1100 cm^{-1}. This is far too large for a tetrahedral field of four oxygens (Dq = 735 cm^{-1} for orthoclase feldspar) even with the presence of the distortion away from tetrahedral that was suggested.

The difficulties associated with the analysis of a radial distribution function (RDF) to provide estimates of interatomic separations and the number of nearest neighbors within a particle dissolved in a solvent have been mentioned in section II. E-2 above. They include,in particular, accounting for the solvent scattering and analyzing for the area under the peaks of the RDF. A 3M solution of the nitrate polymer, a polyelectrolyte, is expected to significantly distort the liquid structure of water from that in the pure solvent, yet it was

the scattering curve of the pure solvent that was applied as a subtractive correction to that of the polymeric solution. The second substantial criticism of the report of this scattering data is that no mention was made of the method of analysis of the area under the peaks of the RDF. The area under the first peak was used as substantial evidence for four rather than six nearest neighbors per iron. It is quite likely[85] that this area measurement is a sensitive function of the mathematical analytical method employed.

The X-ray scattering report also included the Mössbauer spectrum of the polymer over the temperature range 5-300°K. The spectrum is quite similar to that of ferritin, exhibiting the gradual decay of the quadrupole split doublet and the simultaneous gradual appearance of the six-line magnetic hyperfine as the temperature is decreased from 70° to 5°K. The isomer shift and quadrupole splitting are also similar to those observed in ferritin. On the basis of the similarity of the Mössbauer spectra of ferritin and the nitrate polymer, which, from the results of the X-ray scattering experiment, contained tetrahedral iron(III), it was proposed that all the iron in the ferritin core was tetrahedrally coordinated, as $[FeO_4]$.

3. Mössbauer Spectra

A second structural model for the ferritin core is the Towe hydrolyzate isolated[6] from iron(III) nitrate solutions (0.06 M) at 80°C. The crystallinity is sufficient to allow a partial analysis of the structure by X-ray diffraction. The structure is based on hematite,

α-Fe_2O_3 with the iron(III) ions occupying octahedral sites. A sample was kindly provided by Ken Towe of the Smithsonian Institute. The Mössbauer spectrum of this compound was recorded from 300° to 5°K with the assistance of B. Persson and M. Bent at the California Institute of Technology. The values of the usual Mössbauer parameters were similar to those of ferritin and the nitrate polymer. The quadrupole split doublet began to decompose a little above liquid nitrogen temperature, and by liquid helium temperature the familiar six-line hyperfine was well established. There was a slight asymmetry in the several spectra near the origin due to absorption by a beryllium window used in the experimental set-up. This Mössbauer spectrum at various temperatures is shown in Figure 24. The close similarity of the Mössbauer spectra of ferritin, the nitrate polymer (assumed tetrahedral by the X-ray scattering experiment) and the Towe hydrolyzate (octahedral by X-ray analysis) is shown in Table 20.

The isomer shift values are more nearly characteristic of octahedral than tetrahedral iron(III) and the internal field established at 5°K is close to that (515 kOe) of the calibrant hematite, α-Fe_2O_3, which contains octahedral iron(III). The low value of 315 kOe at 70°K suggests tetrahedral coordination but at this temperature the hyperfine is a very minor component of the spectrum. Its measurement is consequently uncertain. The limitations of any empirical correlations of Mössbauer parameters with electronic and structural characteristics of iron were discussed above (II.D), but the evidence from the

Figure 24

The Mössbauer spectrum of the Towe hydrolyzate[6] as recorded in a wax pellet at room (300°K), pumped nitrogen (~40°K), and helium (4.2°K) temperatures.

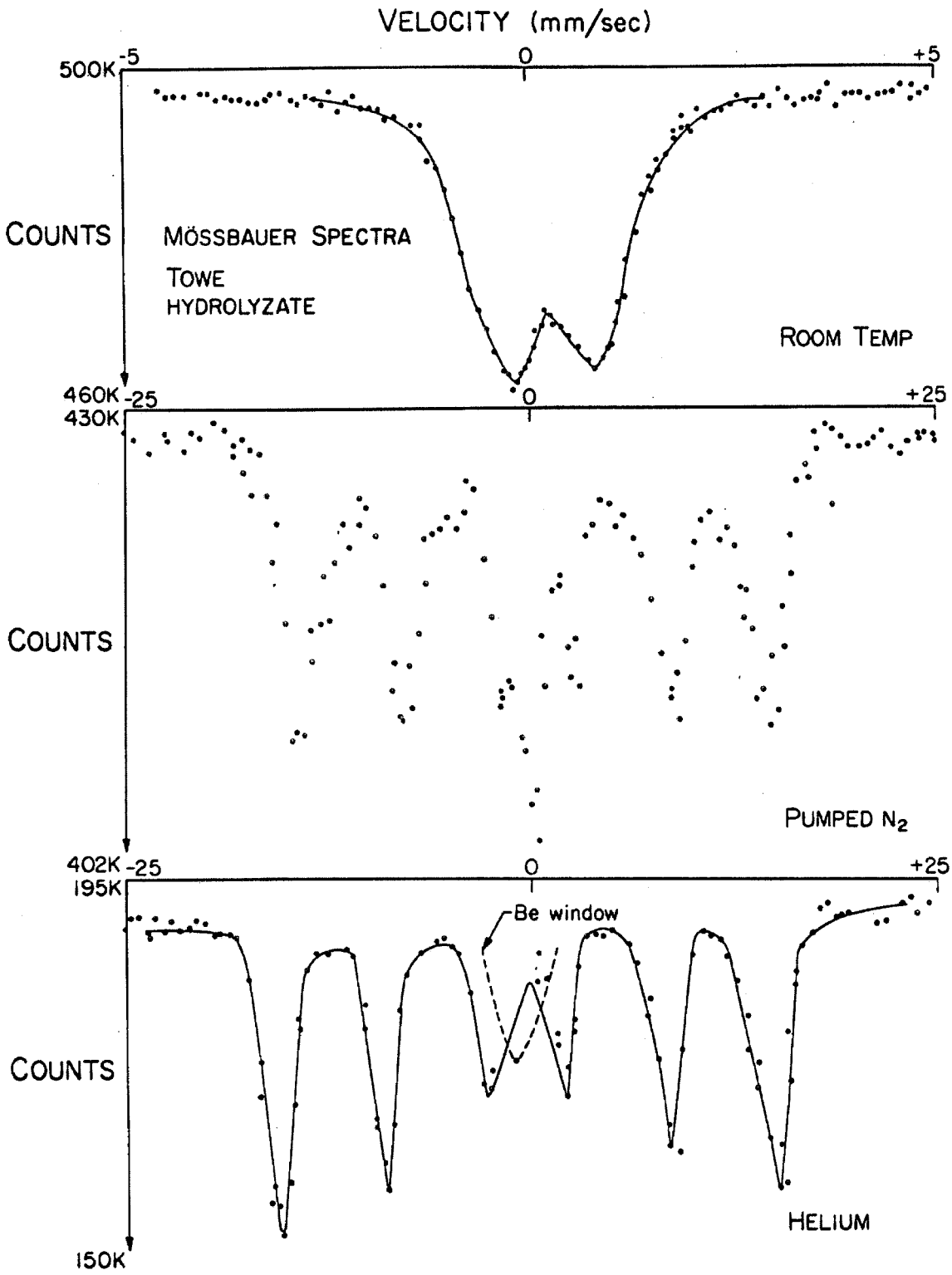
VELOCITY (mm/sec)
500K
-5
0
+5
COUNTS
MÖSSBAUER SPECTRA
TOWE
HYDROLYZATE
ROOM TEMP
460K
430K
-25
0
+25
COUNTS
PUMPED N_2
402K
195K
-25
0
+25
Be window
COUNTS
HELIUM
150K

Table 20

Material (°K)	Isomer Shifts[d] (mm/sec)	Quadrupole Splittings (mm/sec)	Internal Field (k0e)
Ferritin[a](30-300)	0.50 ± 0.05	0.60 ± 0.10	
Ferritin[b](77)	0.47 ± 0.05	0.74 ± 0.04	
Ferritin[b](4.2)			493 ± 10
Polymer[c](298)	0.48	0.67	
Polymer[c](70)			315
Polymer[c](5)			455
Hydrolyzate (300)	0.44 ± 0.01	0.61 ± 0.03	
Hydrolyzate (5)			496

[a] Reference 145.

[b] Reference 103.

[c] Reference 84.

[d] Measured with respect to stainless steel.

Mössbauer suggests that iron(III) in ferritin, the nitrate polymer, and the Towe hydrolyzate is in octahedral coordination. The presence of two different sites is expected to broaden, if not split, the Mössbauer resonances particularly under the influence of a strong magnetic field as is established in these compounds at low temperatures. No such effects were seen. The Mössbauer results and the ligand field spectral data, taken together strongly support the contention that only octahedral iron(III) is present in these structures.

A notable omission from the above discussion has been the third synthetic model for the ferritin core, the van der Giessen gel. The Mössbauer spectral parameters have been briefly reported as similar to those in the table above. Hyperfine splitting at liquid helium temperature has also been observed.[147] However, a detailed report of the Mössbauer results has not appeared. The structure proposed for the gel on the basis of the X-ray powder pattern is based on a cubic cell of side 8.37 Å, yet no arrangement of iron atoms could be found[34] to account for the observed intensities.

4. Magnetic Studies

The temperature dependence of the magnetic moment per iron was determined for the Towe hydrolyzate, the nitrate polymer, $FeOHSO_4$, and γ-FeOOH. These results are shown in Figure 25 with the literature data[58] on the $Fe(OH)_2Fe$ and Fe–O–Fe dimeric systems. Several important features of this diagram should be noted. All room

Figure 25

Temperature dependence of the magnetic moment from 300° - 80°K for a representative group of polynuclear iron(III) compounds. The data for $[Fe(pic)_2OH]_2$ and $enH_2[(FeHEDTA)_2O]\cdot 6H_2O$ were taken from the literature.[14]

(1) $[Fe(pic)_2OH]_2$

(2) Ken Towe hydrolyzate

(3) Inorganic (i.e., nitrate) polymer

(4) $FeOHSO_4$ - jarossite

(5) γ-FeOOH

(6) $enH_2[(FeHEDTA)_2O]\cdot 6H_2O$

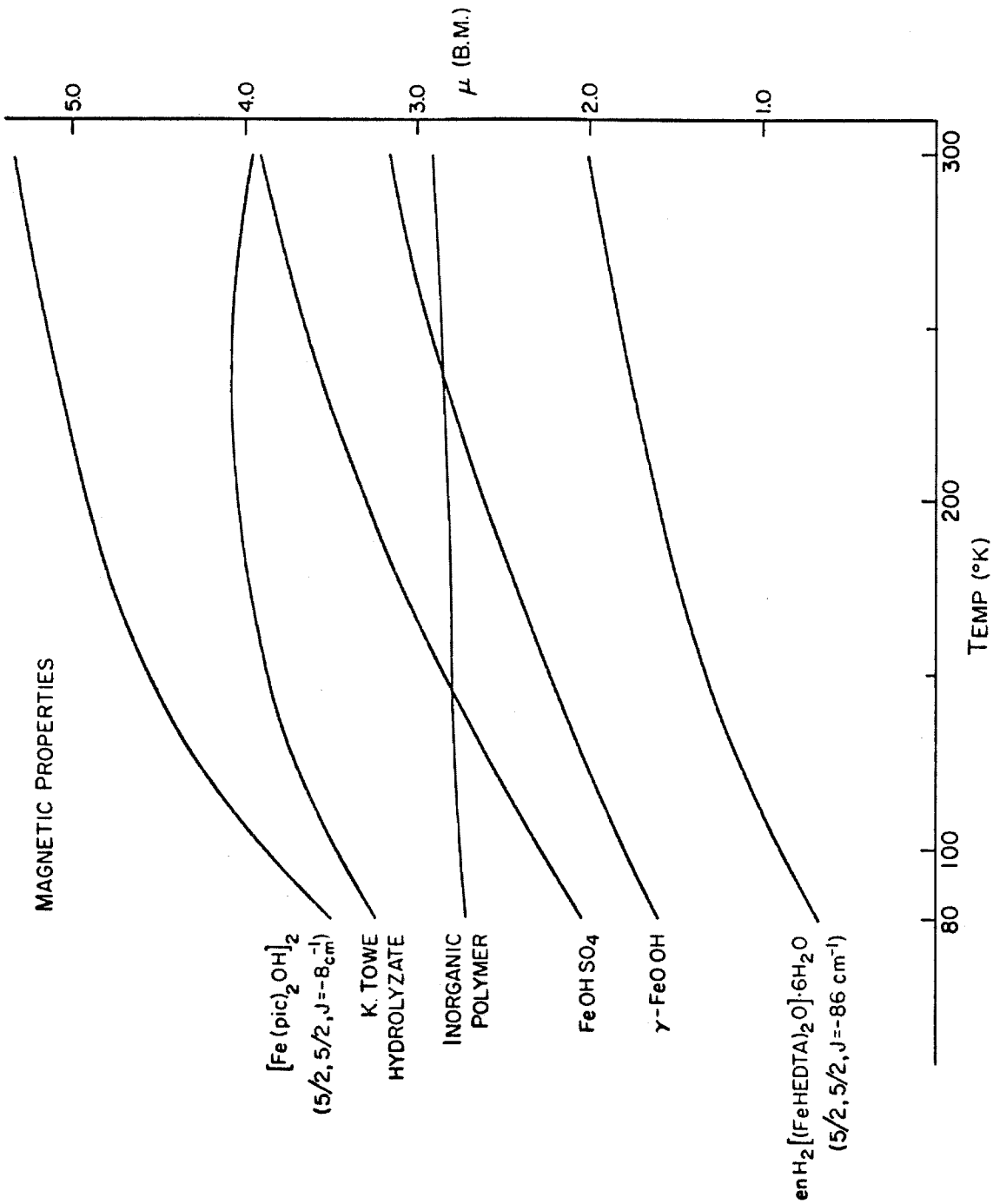
MAGNETIC PROPERTIES
5.0
4.0
3.0
2.0
1.0
μ (B.M.)
80
100
200
300
TEMP (°K)
[Fe (pic)2 OH]2
(5/2, 5/2, J=-8 cm-1)
K. TOWE
HYDROLYZATE
INORGANIC
POLYMER
FeOHSO4
γ-FeOOH
enH2[(FeHEDTA)2O]·6H2O
(5/2, 5/2, J=-86 cm-1)

temperature moments are depressed from the high spin value, indicating antiferromagnetic coupling between iron atoms. In the two mineral systems studied, the gram susceptibility was almost independent of temperature from 300 - 80°K, resulting in a magnetic moment that varied as $\sim T^{\frac{1}{2}}$. This behavior of a decreasing moment with decreasing temperature was also observed in the two dimeric systems studied. The magnetic behavior of the Towe hydrolyzate and the nitrate polymer differed dramatically from that of the other four cases.

The magnetic susceptibility of the iron in the Towe hydrolyzate did not obey the Curie-Weiss law. Moreover, it showed marked field strength dependence between 4 and 10 K gauss that was particularly striking at temperatures below 200°K. The inflection in the plot of magnetic moment against temperature was also observed in the preparation of the van der Giessen gel. The room temperature magnetic moment in this latter gel (at 10 K gauss) was 4.04 B.M., increasing steadily to 4.59 B.M. at 200°K, 4.66 B.M. at 158°K, and then decreasing to 4.60 B.M. at 115°K and 4.48 at 91°K. This magnetic moment has been reported to depend on the strength of the magnetic field.[146] It appears that these two synthetic models of ferritin quite closely resemble each other in their magnetic properties, particularly in their field strength dependent behavior.

This behavior contrasts strikingly with that of the nitrate polymer and of ferritin. The room temperature magnetic moment of ferritin was found to be 3.8 B.M. and effectively temperature independent

down to 80°K, in agreement with other reports. The lower magnetic moment of the nitrate polymer was also temperature independent. A recent study has found a field strength dependence of the magnetic susceptibility of ferritin at high field strengths (30 K gauss) and low temperatures (< 70°K). At field strengths up to 10 K gauss and temperatures down to 80°K which were used in this study, only a slight field strength dependence of the susceptibility was observed in the case of the nitrate polymer and the protein.

The particle sizes of the ferritin core (70 Å), nitrate polymer (70 Å), van der Giessen gel (30 Å), and Towe hydrolyzate (50 Å) are in the range of superparamagnetic particles. As discussed in II. A above, particles of these dimensions are predicted by the Néel theory to obey the Curie law. The presence of a strong magnetic field could determine the fluctuations of the orientation Δ, removing the apparent Curie behavior of the small particle. The distinguishing feature between the two particles that show this small particle effect and the two that do not is the presence of a surface layer of diamagnetic matter. The polypeptide chains coat the ferritin core, while the nitrates coat the nitrate polymer. As a result, both appear in the electron microscope as discrete spheres. In contrast, the Towe hydrolyzate and van der Giessen gel both appear as clusters of the smaller particles. This physical contact can, presumably, affect the magnetic behavior, allowing a particle-particle interaction to be superimposed on the intrinsic

magnetic properties of the particle. It is proposed that this additional interaction accounts for the differences in magnetic behavior between these two compounds and the pair of "insulated" particles.

The ferritin cores can be isolated from the protein by a number of different treatments. On isolation much of the phosphate present in the protein core is lost and the cores aggregate and precipitate. A sample of cores isolated by Chlorox treatment was kindly provided by K. Towe of the Smithsonian Institute. The temperature dependence of the magnetic moment was determined down to 85°K. The behavior was quite different from that of the cores inside the intact protein.

The room temperature moment of 3.37 B.M. was maintained down to 170°K after which the moment decreased to 3.0 B.M. at 85°K. The importance of the organic protein to the magnetic properties is apparent from the results obtained in this and the other studies mentioned above. On this basis the nitrate polymer bears the most resemblance to ferritin. However, it is also apparent that the magnetic behavior is not a particularly suitable criterion for distinguishing among structural models because of the importance of particle size and particle-particle interaction to the magnetic properties.

5. Infrared Spectra

Infrared spectroscopy was applied to the problem of the structure of the ferritin core by an extensive comparative study that included mineral phases of FeOOH, synthetic models of the core, and

protein itself. Ferritin is a particularly sturdy protein and is initially fractionated from other proteins by heat denaturation at 80 °C of all non-ferritin proteins present. Its gross structure is particularly compact, with the core fitted snugly inside the protein shell. Both these observations suggest that any structural information obtained from the infrared spectrum of ferritin recorded in a pellet of potassium bromide (formed in vacuo under pressure) will probably apply directly to the nature protein. On this not unreasonable assumption, the following study was based.

Samples of many of the compounds used in this study were made available to G. Rossman for a study of polymeric oxo- and hydroxobridged systems. The spectra obtained in both studies were identical. Spectra of α- and γ-FeOOH are included with those of β- and δ-FeOOH [118] in Figure 26 reproduced with permission from reference 118. The four spectra show comparatively sharp absorptions near 3500 cm^{-1} indicating the presence of discrete OH. The bands at 796 and 890 cm^{-1} in α-FeOOH and at 1019 cm^{-1} γ-FeOOH are assigned to OH absorption. Overtones of these two sharp bands in α-FeOOH occur as weak and fairly broad bands at about 1645 and 1760 cm^{-1}. In the region below 1000 cm^{-1}, each phase has a characteristic absorption pattern that serves to readily identify it.

The spectra of a colloidal preparation of iron(III) hydroxide, the nitrate polymer, the Towe hydrolyzate, and of ferritin cores isolated by Chlorox treatment are shown in Figure 27, also reproduced

Figure 26. Infrared spectra of iron(III) oxyhydroxides.

A) α-FeO(OH), goethite, 0.91 mg/400 mg KBr pellet, ambient temperature.

B) β-FeO(OH), akagonite, 0.46 mg/400 mg TlBr pellet, ambient temperature.

C) γ-FeO(OH), lepidocrocite, 0.92 mg/400 mg KBr pellet, ambient temperature. Insert shows a 0.50 mg/400 mg TlBr pellet at 78°K in the OH region.

D) δ-FeO(OH), 0.48 mg/400 mg TlBr pellet, ambient temperature.

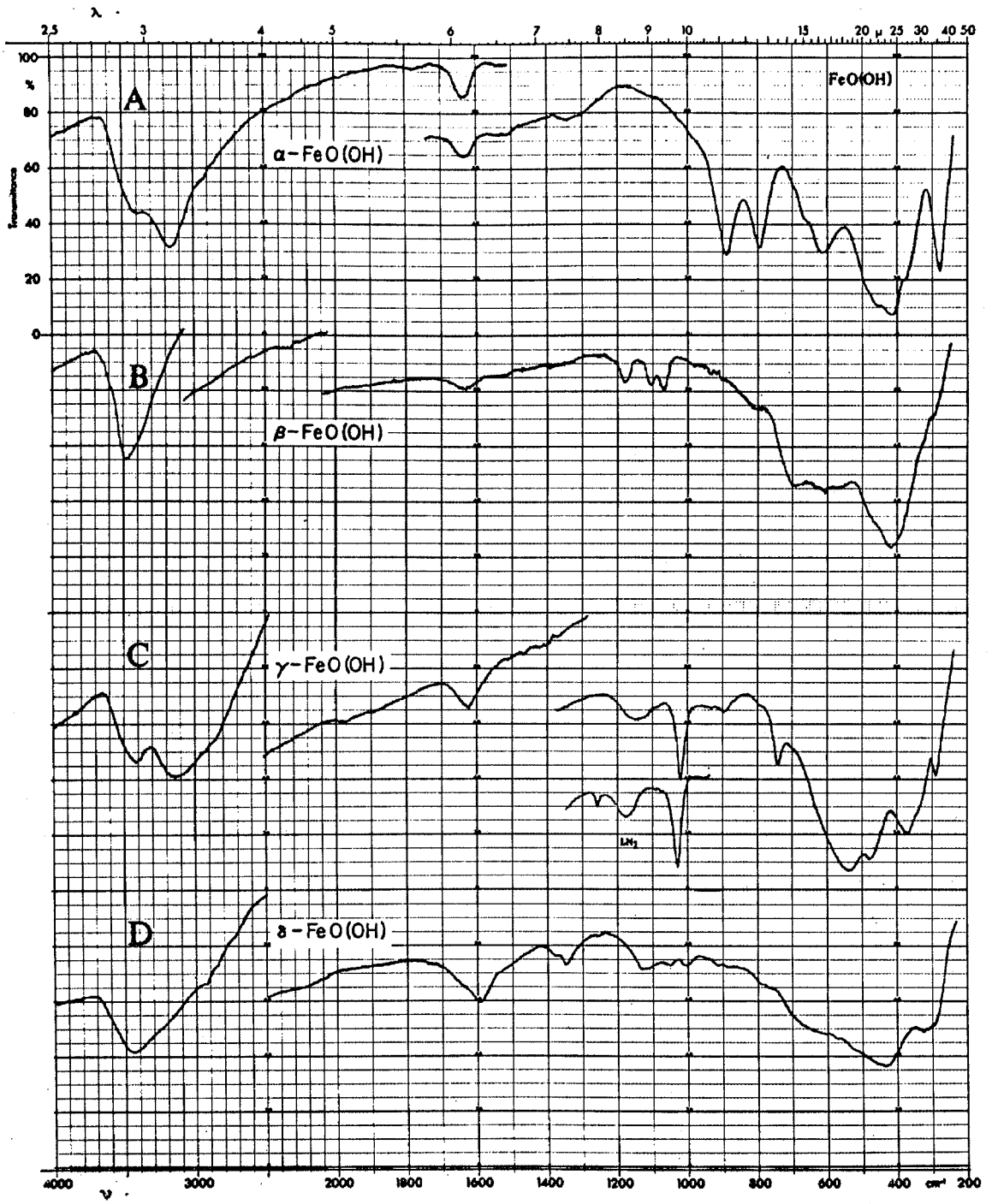
λ
2,5
3
4
5
6
7
8
9
10
15
20 μ 25 30 40 50
100
%
80
60
40
20
0
Transmittance
A
α-FeO(OH)
FeO(OH)
B
β-FeO(OH)
C
γ-FeO(OH)
LN2
D
δ-FeO(OH)
4000
ν
3000
2000
1800
1600
1400
1200
1000
800
600
400
cm-1
200

Figure 27. Infrared spectra of ferritin models

A) "Ferric hydroxide" air-dried overnight. 3.85 mg/400 mg TlBr pellet, ambient temperature.

B) Saltman-Spiro polymer, $Fe_4O_3(OH)_4(NO_3)_2 \cdot 1\frac{1}{2}H_2O$, 0.86 mg/400 mg KBr pellet, ambient temperature

C) Towe hydrolyzate, 0.49 mg/400 mg KBr pellet, ambient temperature.

D) Horse ferritin micelles, 0.64 mg/400 mg KBr pellets, ambient temperature.

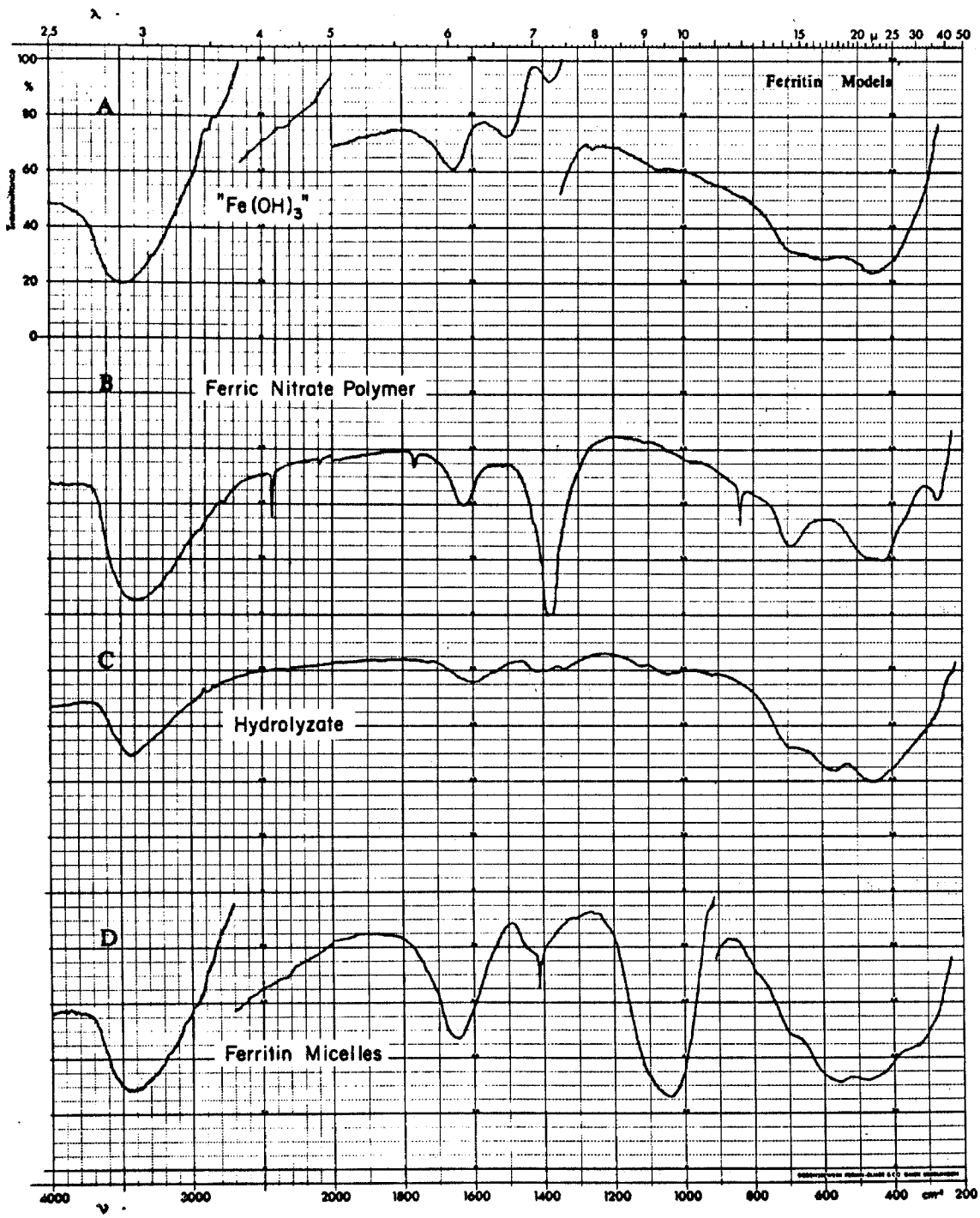
λ
2,5
3
4
5
6
7
8
9
10
15
20 μ 25 30 40 50
100
%
80
60
40
20
0
Transmittance
Fetritin Models
A
"Fe(OH)3"
B
Ferric Nitrate Polymer
C
Hydrolyzate
D
Ferritin Micelles
4000
3000
2000
1800
1600
1400
1200
1000
800
600
400
cm⁻¹
200
ν

with permission from reference 118. The broad overlapping bands below 1000 cm^{-1} contrast strongly with the much sharper ones of structurally well defined mineral phases, e.g., α- and γ-FeOOH. The band at around 3500 cm^{-1} is broad indicating that OH present is not discrete, but is probably present as "lattice" water. In the low energy region below 1000 cm^{-1}, the spectrum of the nitrate polymer is quite different from the three other remarkably similar spectra. All four spectra have bands at about 1640 cm^{-1} that can be attributed to the bending mode of water. The strong band at 1380 cm^{-1} in the nitrate polymer is due to the nitrate and that at 1130 cm^{-1} in the micelles to the phosphate present.

Spectra of ferritin recrystallized from cadmium sulphate (5%), lyophilized ferritin, and hemosiderin are shown in Figure 28. The hemosiderin results are considered in section III. E below. The bands in the crystalline ferritin spectrum are generally sharper than those in the spectrum of the lyophilized preparation. This is particularly significant for the OH absorptions near 3500 and 1100 cm^{-1}. The 3500 cm^{-1} absorption consists of two components in the crystalline ferritin spectrum. The pattern below 1000 cm^{-1} is generally similar in both compounds, closely resembling that of the isolated micelles and the Towe hydrolyzate. The sharp absorption band at 627 cm^{-1} is the most unusual feature of the spectrum of crystalline ferritin. It is not observed in the lyophilized preparation. It is assigned to a phosphate

Figure 28

Infrared spectra of iron storage molecules

(A) crystalline ferritin, 1.15 mg/400 mg potassium bromide, ambient temperature.

(B) lyophilized ferritin, 1.08 mg/400 mg potassium bromide, ambient temperature.

(C) lyophilized hemosiderin, 1.93 mg/400 mg potassium bromide, ambient temperature.

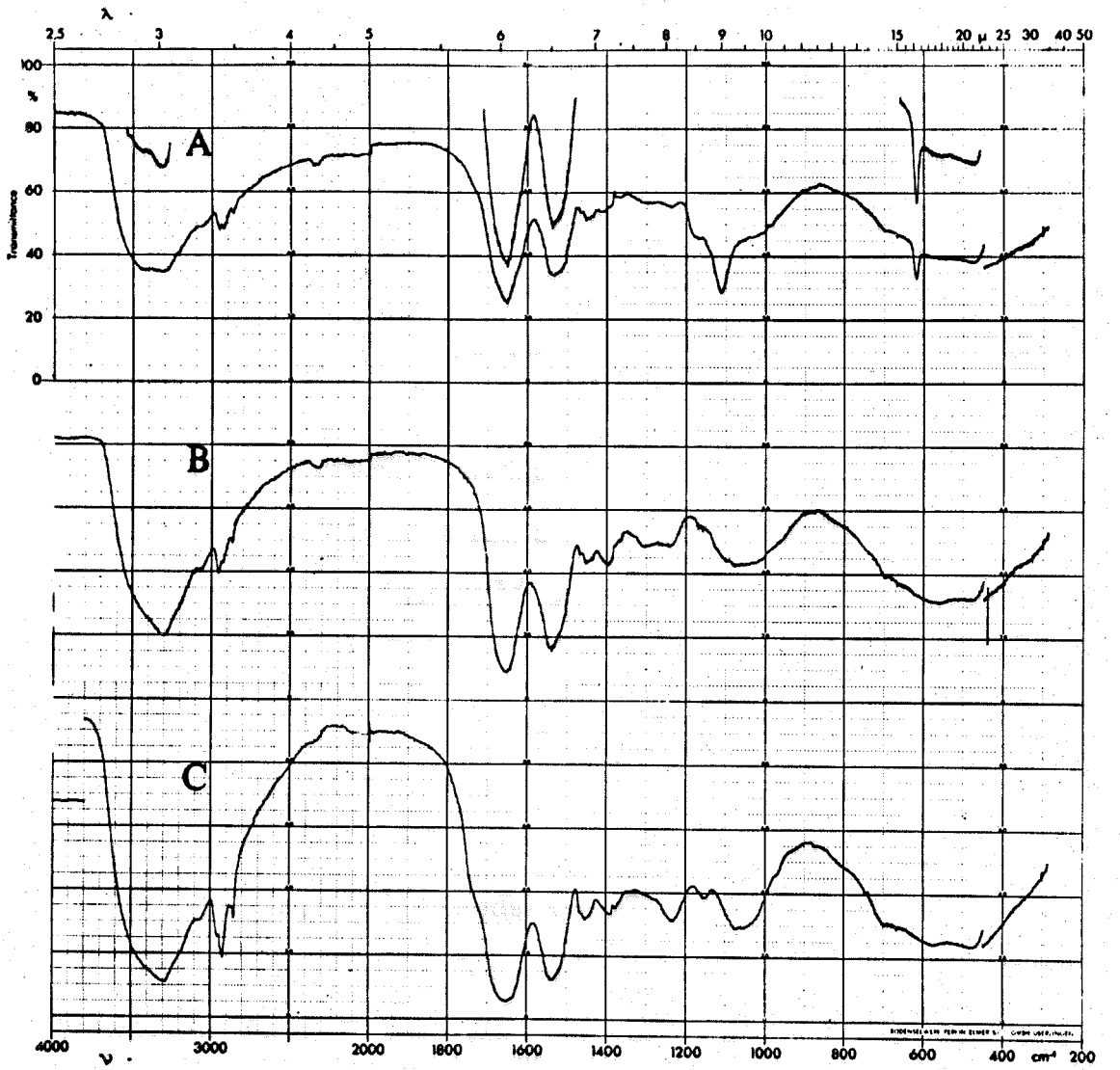
λ
2,5
3
4
5
6
7
8
9
10
15
20 μ
25
30
40
50
100
%
80
60
40
20
0
Transmittance
A
B
C
4000
ν
3000
2000
1800
1600
1400
1200
1000
800
600
400
cm⁻¹
200

absorption, as is the 1110 cm^{-1} peak. An alternate assignment of both these bands to sulphate (from the crystallizing solution) is possible. However, the 1110 cm^{-1} band was also observed as a broad absorption in the spectrum of the sulphate free lyophilized material. Its appearance in this spectrum is attributed to a greater degree of structural definition of the phosphate in the crystalline material. This increased definition sharpens the absorption band, as it does the 1110 cm^{-1} band, and allows it to be resolved from the broad envelope in that region. Both protein spectra show two strong broad absorptions at 1540 and 1650 cm^{-1}. These are assigned to the N-H and C=O structural units of the protein,[149] with the superposition of the -OH absorption on the 1650 cm^{-1} band.

A comparison of the region below 1000 cm^{-1} among this entire range of compounds shows the presence of a pattern of broad overlapping bands in this region for compounds of small particle size. The absorption patterns of colloidal iron(III) hydroxyde, the Towe hydrolyzate, the aggregated micelles, and the two ferritin preparations are all quite similar. The small particles do not contain structurally discrete -OH, although crystallization of ferritin does produce a new band assignable to discrete OH. At this point it should be noted that all attempts to exchange out with deuterium oxide the -OH in the nitrate polymer and the ferritin cores were unsuccessful. Crystalline ferritin also shows much more discrete absorptions assigned to phosphate.

In summary the following points can be made:

a) α-FeOOH and γ-FeOOH are structurally well organized substances that are not suitable models for the ferritin core. However these spectra were recorded on particles much larger than the ferritin core.

A smaller particle size is expected to broaden some of the bands below 1000 cm^{-1} but those due to structurally discrete units, e.g., -OH, are expected to remain sharp. No such absorptions for discrete -OH were observed for ferritin.

b) Of the two synthetic models studied, the Towe hydrolyzate resembles the ferritin core more closely than does the nitrate polymer.

c) Crystallization of ferritin causes greater structural definition of the phosphate groups and, to a lesser degree, of some of the -OH present. Coversely the isolated micelles still contain some phosphate present in poorly defined sites.

6. X-ray Powder Patterns

A comparative study of the compounds investigated by infrared spectroscopy was carried out using X-ray powder patterns. Comparatively long exposure times were generally required. Molybdenum radiation with zirconium filters on the incident and diffracted beams was used to observe the often weak diffuse bands produced by the small particles. The X-ray data obtained in this study for the compounds below are listed in Table 21 . The powder patterns are shown in Figures 29, 30, and 31. Compounds (2) and (3) were kind gifts of

Table 21

1	2	3	4	5	6	7	8	9
					3.38 (m)			
	3.02 (s)	3.02 (s)						
					2.69 (s)			
	2.58 (s)	2.54 (s)	2.54 (s)	2.49 (s)	2.41 (vs)	2.49 (m)	2.49 (s)	2.49 (w)
	2.29 (w)	2.29 (w)		2.23 (m)	2.26 (m)		2.21 (m)	2.22 (vw)
					2.19 (m)			
				1.95 (m)	2.01 (w)		1.98 (w)	
	1.90 (w)	1.87 (w)						
				1.72 (w)	1.72 (s)		1.70 (w)	
					1.55 (s)			
1.49 (w)	1.48 (m)	1.50 (m)	1.47 (s)	1.48 (s)	1.49 (m)	1.46 (m)	1.47 (s)	1.49 (w)
					1.45 (m)			
				1.27 (w)				
				1.05 (w)				
				0.85 (w)	0.90 (w)			

s: strong; m: medium; w: weak;

v: very.

J. Multani, then at the University of California at San Diego.

Figure 29: (1) iron(III) fructose polymer.

(2) iron(III) citrate polymer.

(3) iron(III) nitrate polymer.

Figure 30: (4) van der Giessen gel.

(5) Towe hydrolyzate.

(6) α-FeOOH.

Figure 31: (7) crystalline ferritin.

(8) isolated ferritin cores.

(9) hemosiderin.

Concerning the patterns of the three iron(III) polymers, it is clear that the citrate and nitrate polymers are quite similar in structure, while the fructose polymer appears amorphous. Neither of course has the crystallinity of α-FeOOH (6). The reported pattern of the van der Giessen gel contains a number of other weaker lines that were not observed in this study. The Towe hydrolyzate (5) has several medium and weak lines that distinguish it from the nitrate and citrate polymers. Crystalline ferritin shows only two weak lines. Other lines of equivalent intensity have been reported at 2.24, 1.98, and 1.73 Å in addition to several very weak lines. These extra important lines appear in the pattern of isolated ferritin cores, the Towe hydrolyzate, but not in the nitrate polymer. The hemosiderin results are considered in section III. E below.

Figure 29

X-ray powder patterns of iron(III) polymers using molybdenum K_{α} radiation, long exposure times, and zirconium foil filters on the incident and diffracted beams

(A) iron(III) fructose polymer (23 hours)

(B) iron(III) citrate polymer (24 hours)

(C) iron(III) nitrate polymer (20 hours)

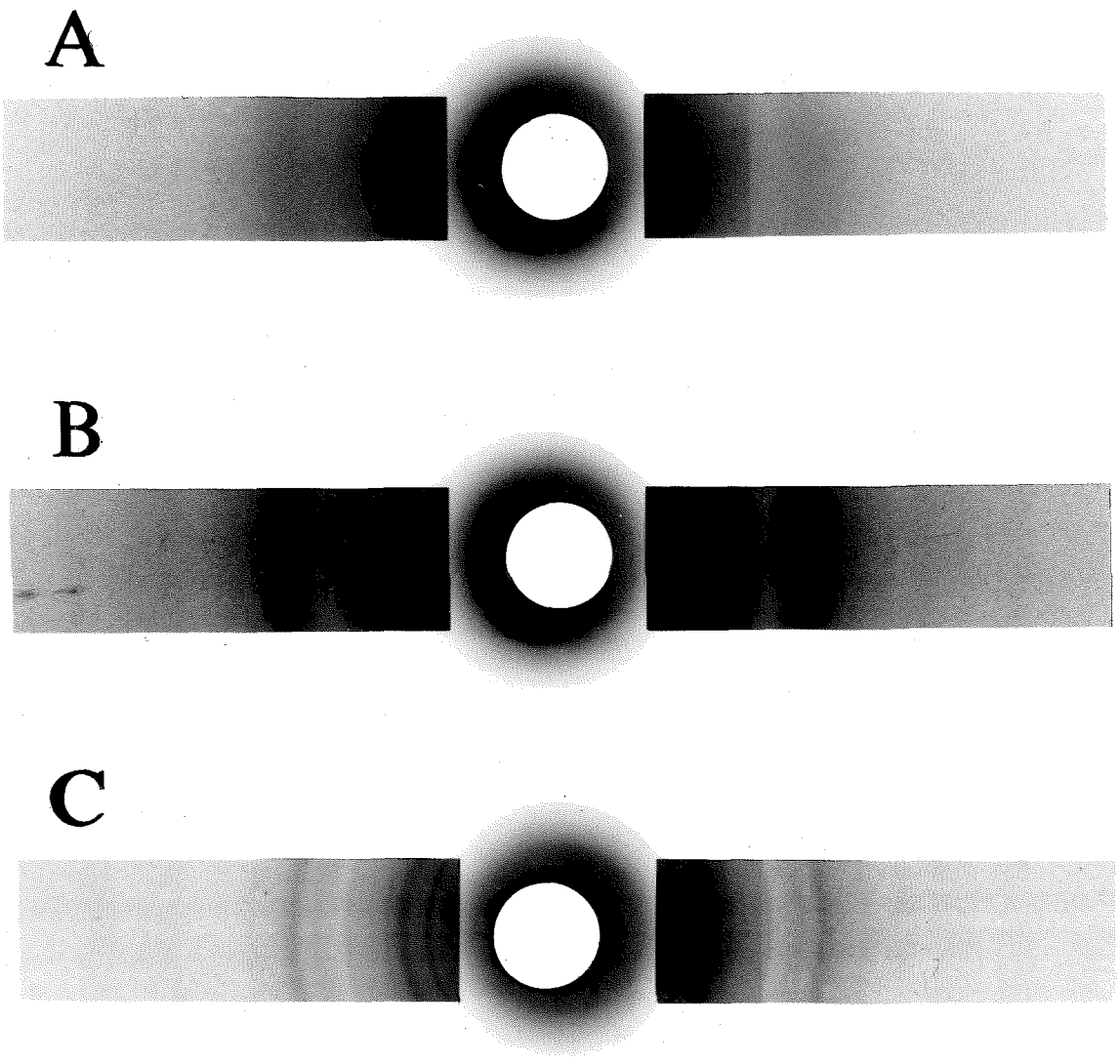
A
B
C

Figure 30

X-ray powder patterns of iron oxyhydroxides using molybdenum K_α radiation, suitable exposure times, and zirconium foil filters on the incident and diffracted beams

(A) van der Giessen gel (31 hours)

(B) Towe hydrolyzate (21 hours)

(C) α-FeOOH (10 hours)

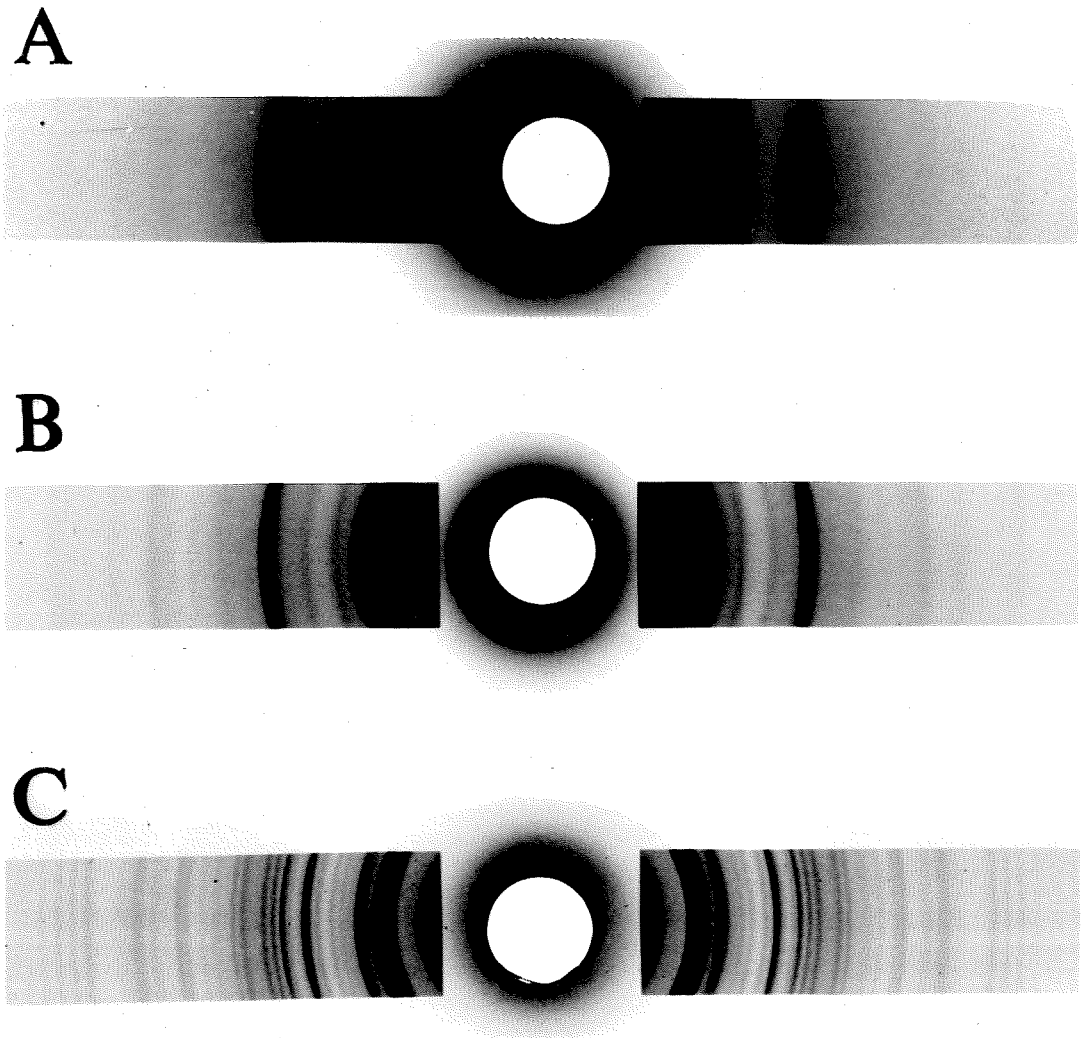
A
B
C

Figure 31

X-ray powder patterns of iron storage molecules using molybdenum K_α radiation, long exposure times, and zirconium foil filters on the incident and diffracted beamd

(A) crystalline ferritin (26 hours)

(B) isolated cores (23 hours)

(C) hemosiderin (67 hours)

A

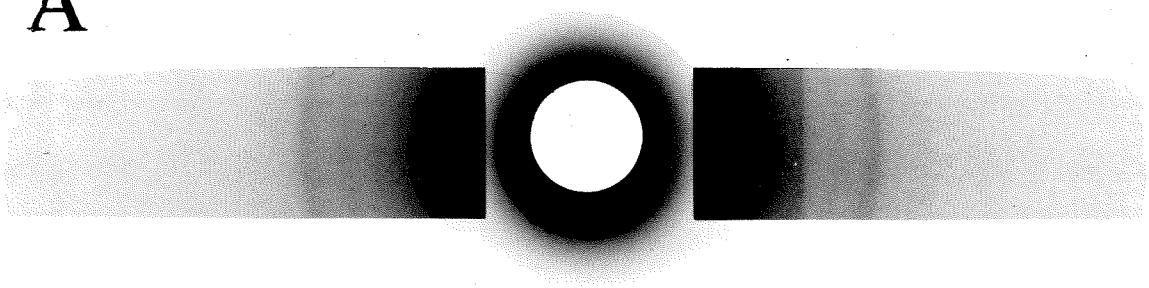

B

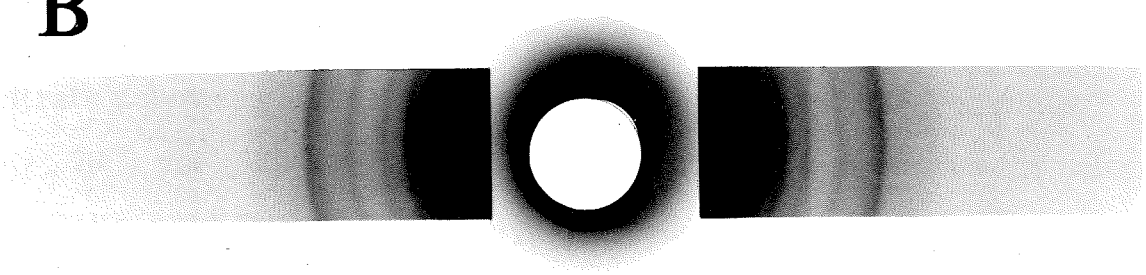

C

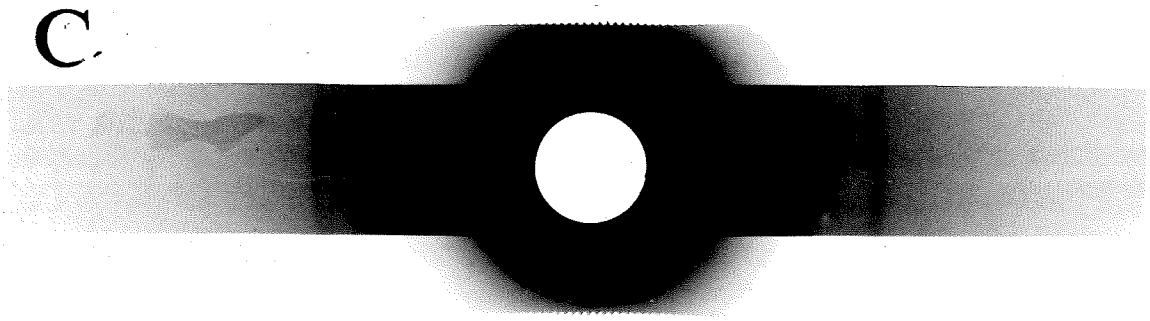

With the exception of α-FeOOH, all patterns have as their strongest lines those at ~2.5 and 1.5 Å. It has been suggested[149] that the same lines as seen by electron diffraction of the nitrate polymer are due to higher order reflections from oxygen octahedra, 5 Å wide, surrounding iron(III) and from the height of layers of these octahedra. This suggestion was based on data from iron oxyhydroxide mineral phases. This coordination structure would be consistent with the spectral and Mössbauer data discussed above. Several important observations can be made from these results:

a) The fructose polymer is amorphous but the nitrate and citrate polymers appear isomorphous. Both are of small particle size 70 Å yet show a high degree of crystallinity in their powder patterns.

b) The Towe hydrolyzate produces a pattern that is close to that reported for ferritin and observed here for the isolated micelles. On isolation and aggregation, the ferritin cores appear to become more crystalline. The crystalline protein produces a very weak pattern under the conditions used.

7. ESCA Study

The phosphorous $2p_{1/2,\ 3/2}$ and iron $2p_{3/2}$ electron binding energies were measured by the ESCA technique. W. Proctor of Varian Associates is thanked for recording the spectra, shown in Figure 32. The phosphorous spectrum is broad and poorly defined, probably as a result of its low concentration in the protein. The band maximum is

Figure 32

ESCA determination of the binding energy in crystalline ferritin of

A: phosphorous $2p_{1/2,3/2}$ electrons

B: iron $2p_{3/2}$ electrons

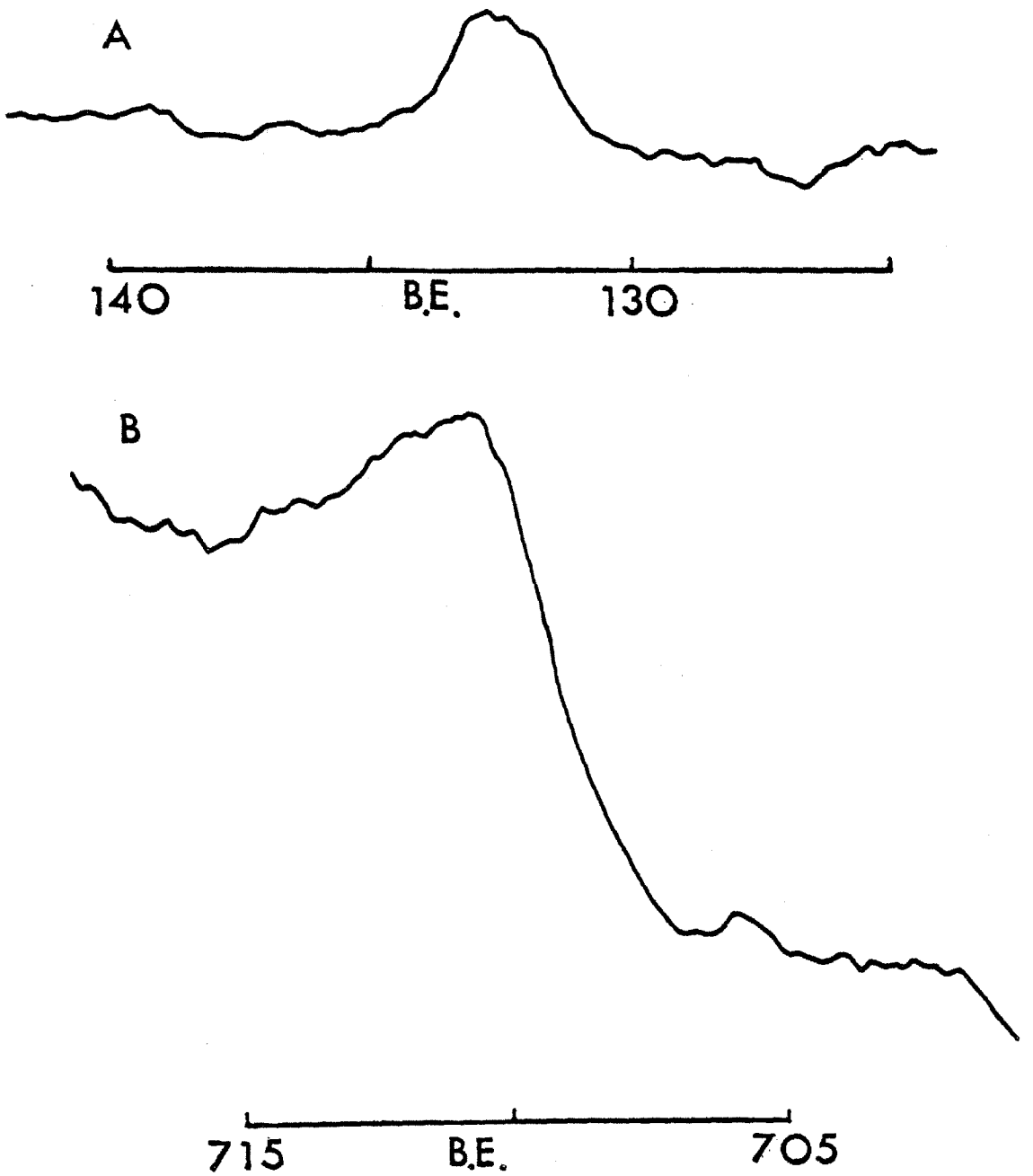
A
140
B.E.
130
B
715
B.E.
705

poorly defined and no structural conclusions can be drawn. The iron spectrum is more interesting, showing what may be two components. The presence of the lower binding energy component is uncertain. Higher resolution data are required. The earlier discussion on ESCA showed that the iron binding energies of FeO_4 and FeO_6 in $FePO_4$ could be resolved if both sites were present in significant amounts. If the suspected two component nature of this band is confirmed, it will provide the first unambiguous demonstration of the presence of two different iron coordination sites in the core of ferritin.

8. A Summary

A variety of structural information has been obtained from the studies reported and discussed above. No one structural model stands out unambiguously as the "best" model, but the evidence does favor the Towe hydrolyzate, containing octahedral iron(III). The nitrate polymer was shown to contain only one iron(III) coordination structure, the octahedral one. It closely resembled ferritin in the temperature dependence of the magnetic moment attributed to the surface coating of diamagnetic nitrate anions. Its iron content is ~one third that of a full ferritin core, signifying a more open structure, which is, none the less, well defined for a particle of 70 Å dimension. The powder pattern lines are not the same as those of ferritin, and the infrared spectrum below 1000 Å also shows some differences.

The Towe hydrolyzate on the other hand differs from ferritin in its magnetic properties but closely resembles it in X-ray and infrared properties. The absorption spectrum is consistent with the octahedral iron proposed. It appears more crystalline than ferritin but nearly equivalent to the isolated cores. The increased crystallinity in the isolated cores can be related to the loss of ordered phosphate during isolation that was observed in the infrared spectra. The interesting suggestion from this is that the phosphate acts in the protein core in a structurally discrete fashion but in the process lowers the overall crystallinity of the core. Surface bound nitrate has sharp absorptions and it is possible that the phosphate acts within the core to coat smaller crystallites of varying shapes, preventing their cohesion into a polymeric sphere analogous to the nitrate polymer. The little data available on the van der Giessen gel from this and other studies indicate that it has many structural features in common with the Towe hydrolyzate. Its uncertain chemical and structural composition makes it a less attractive model than the Towe hydrolyzate for the ferritin core.

A necessary requirement of any structural model is that it contain a significant amount of octahedral iron(III). The spectral results provide no evidence on the presence of tetrahedral sites. Mössbauer spectra suggest the presence of only one site. A preliminary ESCA result may indicate two sites, but requires more careful study.

The arrangement of these octahedral iron(III) units has been suggested above to depend on the phosphate present. The contrast in properties between ferritin and jarossite excludes the possibility that the octahedra are linked in chains as in the jarossite structure. The octahedra are linked in all three dimensions in a very compact fashion, in what can only be called an aggregate of crystallites. This is not to suggest that the ferritin core is composed of discrete subunits. These crystallites are imagined to be structurally intermixed in a variety of orientations, lessening the crystallinity of the core. The resultant structure will consequently never by adequately represented by any of the mineral phases or by synthetic models.

E. Hemosiderin

1. Preparation

Hemosiderin production was induced in five female New Zealand white rabbits by intravenous injections of 800 mg of iron as iron dextran (Imferon, Lakeside Labs, Wisconsin) over a five week period. This preparative procedure follows closely that reported in other investigations.[121] The animals were killed three days after the last injection. Two of the five were found to have unusually large amounts of peritoneal fluid. The livers were removed by careful dissection and perfused with cold saline (0.9%) prior to being frozen in dry ice. The total mass of the five livers was 740 g. After freezing, each liver was wrapped in canvas and put under pressure (15,000 ps.i.), producing a canvas filtered effluent that was pooled prior to further fractionation. The technical assistance of Sandy Webb and Betty Aalseth in the above procedure is gratefully acknowledged.

To remove the soluble ferritin fraction the crude hemosiderin preparation was washed with distilled water and centrifuged (1400 g, 30 min.) until the supernatant was clear. The heavy red brown sediment was suspended in a large volume (× 20) of distilled water and homogenized in a Waring blender. The homogenate was filtered through an increasing number of layers of cheesecloth up to twenty layers. Most of the hemosiderin passed through the cloth and was then further fractionated by washing and centrifugation in distilled water (1400 g, 5 min.) ten times. A portion of this fractionated hemosiderin was freeze dried, producing

a red brown powder that was further dried in vacuo over phosphorus pentoxide, prior to analysis and use in the physical studies reported below. The yield of hemosiderin from the 740 g of liver was just over 1 gram.

2. Analytical Data

The analytical results (Schwarzkopf Lab.) for dried hemosiderin with the corresponding data for rabbit ferritin and hemosiderin reported by other workers[122] are shown in Table 22. After storage for several weeks in a refrigerator, the iron content of the dried hemosiderin was determined to be 12.36% (Galbraith Lab.).

Table 22

	Fe	N	P	S	C
this work	15.08	8.48	1.27	1.03	38.45
hemosiderin	25.8	7.8	3.4	0.84	--*
ferritin	14.9	11.3	1.3	0.90	--*

* Not reported.

The amount of insoluble material in this preparation was determined by first reducing the iron present with sodium dithionite (ox. pot. - 0.1 volt). A weighed amount of hemosiderin was suspended in dithionite (4%) and homogenized manually with a tissue grinder fitted with a teflon plunger (A. H. Thomas Co.). After prolonged agitation for

up to 30 hours the material was filtered through a preweighed millipore prefilter and filter (0.22 μ). In two independent determinations, the amount of the material deposited on the millipore filteres was 75 and 86% of the initial hemosiderin used.

3. Infrared Study

The infrared spectra of hemosiderin was recorded as a potassium bromide pellet in the range 4000 - 300 cm^{-1}. It is compared in Figure 28 with the spectrum of a lyophilized and of a crystallized sample of horse ferritin. This figure is included here as well as in Section III. D above.

4. X-ray Results

The X-ray powder pattern of hemosiderin was only obtained after an exposure of 67 hours to molybdenum radiation, using a zirconium filter on both the incident and the diffracted beams. The patterns produced by hemosiderin, crystalline ferritin, and by ferritin cores released by treatment with Clorox detergent[6] are shown in Figure 31, which also has been included in Section III. D above. The d spacings (in Å) and visual estimates of their intensities are listed in Table 23. The time of exposure used is included at the head of the table.

5. Magnetic Study

The temperature dependence of the magnetic moment per iron was determined from 300° to 85°K. The gram diamagnetic susceptibility of the organic components present was taken as

Figure 28

Infrared spectra of iron storage molecules

(A) crystalline ferritin, 1.15 mg/400 mg potassium bromide, ambient temperature.

(B) lyophilized ferritin, 1.08 mg/400 mg potassium bromide, ambient temperature.

(C) lyophilized hemosiderin, 1.93 mg/400 mg potassium bromide, ambient temperature.

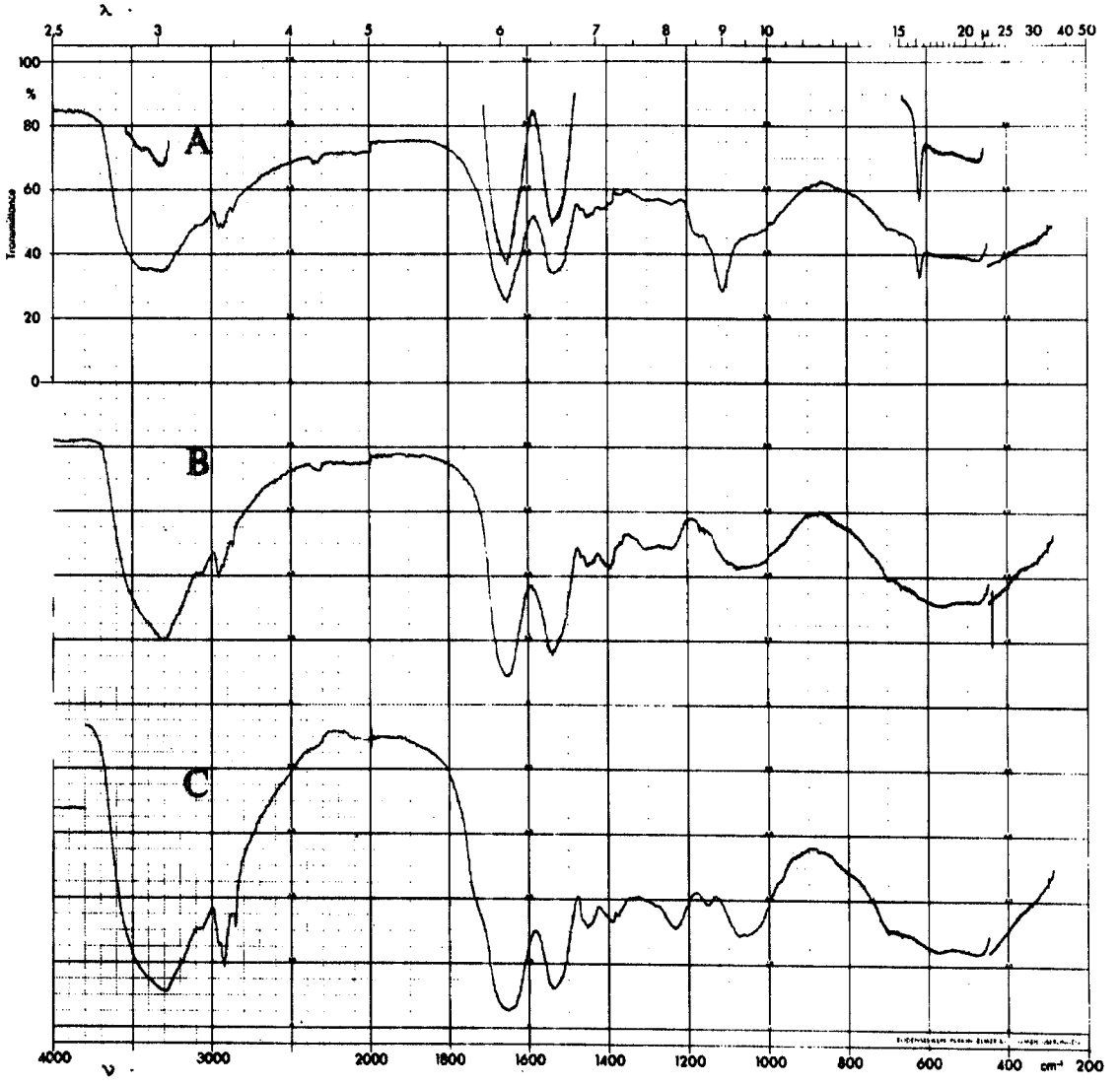
λ
2,5
3
4
5
6
7
8
9
10
15
20 μ 25
30
40 50
100
%
80
60
40
20
0
Transmittance
A
B
C
4000
ν
3000
2000
1800
1600
1400
1200
1000
800
600
400
cm⁻¹ 200

Figure 31

X-ray powder patterns of iron storage molecules using molybdenum K_α radiation, long exposure times, and zirconium foil filters on the incident and diffracted beams

(A) crystalline ferritin (26 hours)

(B) isolated cores (23 hours)

(C) hemosiderin (67 hours)

A

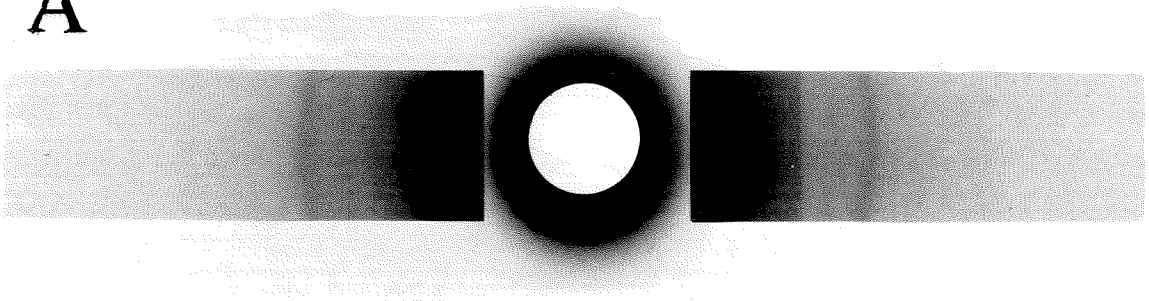

B

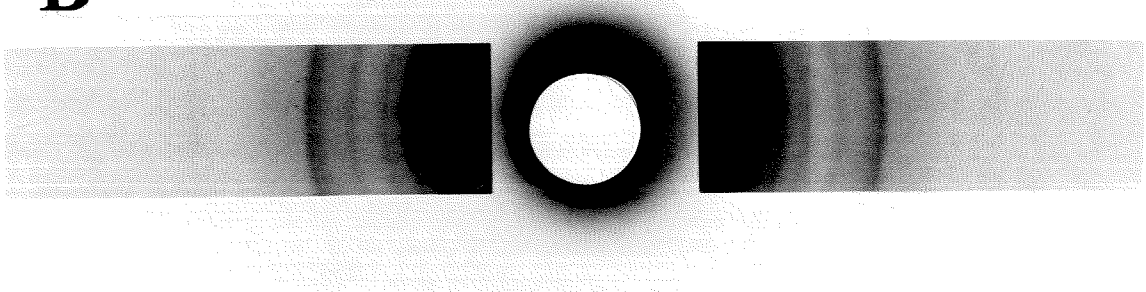

C

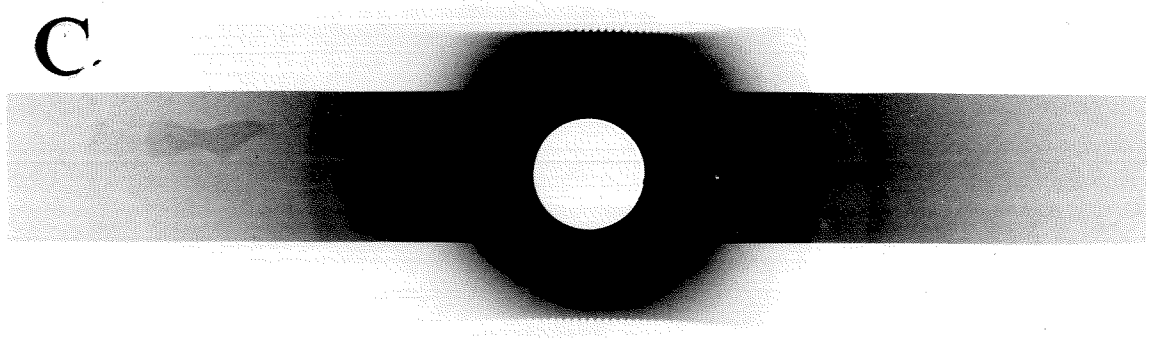

Table 23

hemosiderin (67 hr)	ferritin (26 hr)	isolated cores (23 hr)
d(Å)	d(Å)	d(Å)
2.49 w	2.49 m	2.49 s
2.22 ww		2.21 m
?		1.20 ww
?		1.70 w
1.49 w	1.46 m	1.47 s

w: weak; m: medium; s: strong; ?: may be present.

-0.5×10^{-6} c.g.s. units. The results using both iron analysis data, 12.36 and 15.08%, are shown in Figure 33. Estimates of the errors involved from the iron analysis data alone are apparent from the diagram. A field strength study of the susceptibility from 0.3 to 10 kOe at two temperatures, 298.5 ± 0.5° and 121.5 ± 0.5°K, was made. The results are presented as the intensity of the output signal from the magnetometer versus the applied field. This intensity is a linear function of the field for a simple paramagnet, and is zero at zero field. The experimental results are shown as curves I and III in Figure 34 The lowest field measured was 340 oersteds, and the data have been extrapolated back to zero intensity at zero field. Lines II and IV are the least squares lines of best fit. The correlation coefficient and the magnetic field axis intercept for II, the low temperature case, are 0.997 and -430 oersteds. The corresponding values for the high temperature instance, IV, are 0.999 and -310.

6. Discussion

On the basis of an extensive physical and chemical study of hemosiderin and ferritin it has been suggested[123] that the term hemosiderin be used only if the material is totally insoluble in water. This definition has been applied in this work to allow ready separation of hemosiderin from ferritin. The comparative analytical results of Table 22 indicate that, at least in iron and nitrogen content, this preparation of hemosiderin is intermediate between the hemosiderin

Figure 33

Temperature dependence of the magnetic moment per iron for hemosiderin (freeze-dried preparation) calculated with the two iron analytical results obtained

I 12.36%

II 15.1%

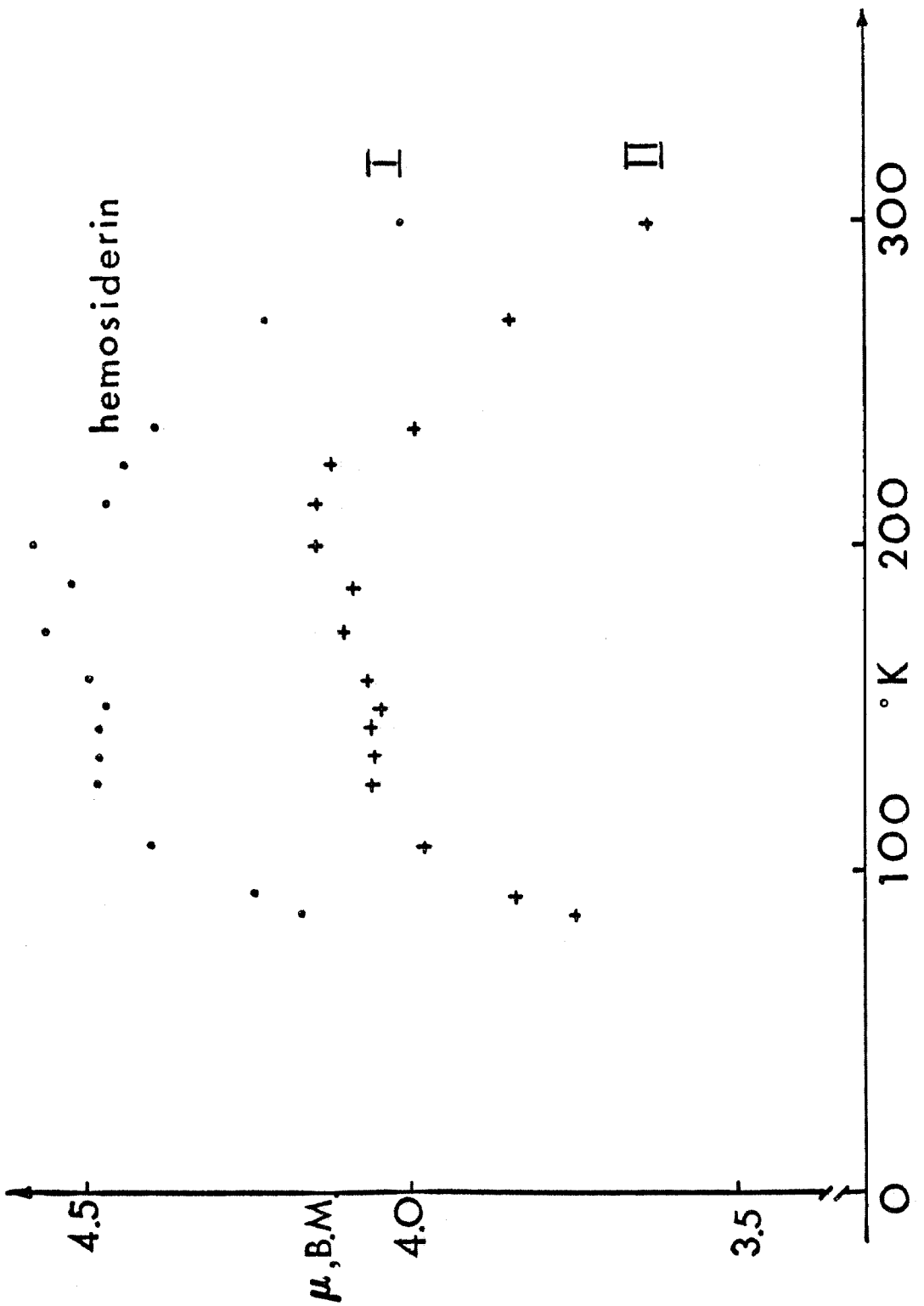
hemosiderin
I
II
4.5
4.0
3.5
μ, B.M.
0
100
200
300
°K

Figure 34

The dependence of the output from the magnetometer I, in arbitrary units, on the strength of the applied field H, in kOe for hemosiderin.

I: experimentally determined behavior from 350 - 10,000 Oe at 122°K.

II. least squares line of best fit, $I = 24.37\ H + 10.47$. The intercept on the H axis is -420 Oe and the correlation coefficient 0.997.

III: experimentally determined behavior from 350 - 10,000 Oe at 298.6°K.

IV: least squares line of best fit, $I = 8.39\ H + 2.58$. The intercept on the H axis is -310 Oe and the correlation coefficient 0.999.

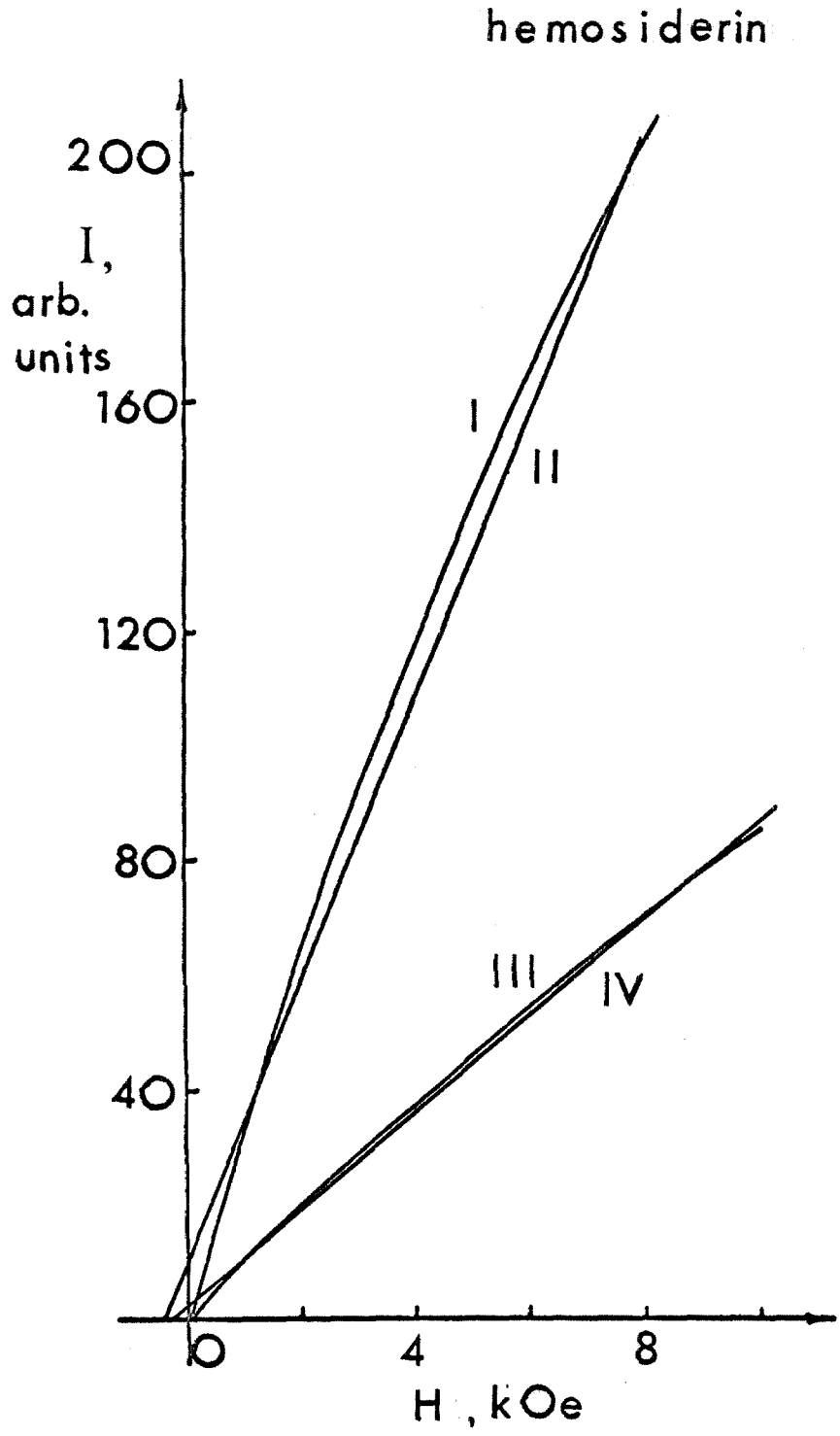
hemosiderin
200
I,
arb.
units
160
120
80
40
I
II
III
IV
0
4
8
H , kOe

and ferritin prepared by others. The comparatively low iron content is matched by a large amount of insoluble matter (~80%) that accounts for almost all of the non-iron components. The insoluble nature of these components suggests that they are denatured macromolecules or cellular debris. Although ferritin and hemosiderin differ in many physical and chemical properties it has been very difficult to prepare hemosiderin quantitatively free of ferritin. Small amounts of fatty acids, cholesterol and other proteins have been reported in various preparations. (1)

The most striking observation from the three infrared spectra shown in Figure 28 is the similarity of the spectra of hemosiderin and lyophilized ferritin. All spectra were recorded as pellets of potassium bromide. The pellet preparation procedure is expected to affect the protein conformation but to have little influence on the ferritin core inside the polypeptide shell. Most of the spectral features of interest are assigned to the inorganic not the organic components of the preparations. In both spectra the absorption bands at 3300, 1650, and 1100 cm^{-1} are broader than those in crystalline ferritin. These bands can be assigned to the asymmetric and symmetric water stretching modes, the water bending mode, and to the iron-bound hydroxyl bending mode, respectively. The sharp 618 cm^{-1} band of crystalline ferritin is absent in the other two cases. The only apparent differences between the spectra of hemosiderin and lyophilized ferritin are the shoulder at 1740 cm^{-1} and the sharpness of the 1233 cm^{-1} band. These features are present only in the hemosiderin spectrum.

These spectral comparisons suggest that the organic component of hemosiderin is primarily protein derived from ferritin. The smaller organic components that have been identified as minor constituents of other preparations of hemosiderin could account for the 1740 and 1233 cm^{-1} spectral features. These bands can be assigned to carbonyl and carbon-oxygen stretching modes that are expected to be observed with small organic molecules. This spectral similarity is the more striking in view of the different water solubility properties of the two substances. Lyophilized ferritin is quite water soluble while hemosiderin is totally insoluble, indicating that the ferritin derived protein present in hemosiderin is probably denatured.

The X-ray pattern of hemosiderin shown in Figure 31 consists of only three weak lines even after prolonged exposure. The weak, diffuse character of these lines indicates a low degree of crystallinity in the preparation. The d spacings are those reported[34] for crystalline ferritin, although only two of them were observed in the ferritin crystals used in this work. These data also support the contention that hemosiderin is derived from ferritin. A comparison of the diffraction pattern of hemosiderin with that produced by protein-free isolated cores indicates that hemosiderin is not just an aggregate of ferritin cores. The isolated cores appear more crystalline than those still inside the protein. It has been suggested above that this increase in crystallinity results from a decrease in phosphate. In this regard,

it is of interest to note that in this and other preparations of hemosiderin the phosphorous content is at least as great as that in ferritin.

Although the room temperature magnetic moment per iron in hemosiderin of ~4 B. M. agrees with values determined by other investigators,[122] the temperature dependence of this moment is reported here for the first time. The unusual behavior is shown in Figure 33. As the temperature decreases from 300° to 200°K, the moment increases. Below 200°K it decreases to a value at 85°K close to that at room temperature. The results of the field strength study shown in Figure 34 indicate that hemosiderin has a finite internal magnetic field at zero applied field of 300 - 400 oersteds. This behavior is similar to that observed for the iron in gastroferrin. The explanation proposed for that case can be applied here, namely, that there is a weak ferromagnetic interaction between clusters of antiferromagnetically coupled iron(III) ions. This explanation may be less valid in the case of hemosiderin because of the poorly characterized nature of the material.

The evidence discussed above from infrared and X-ray studies indicates that hemosiderin is derived from ferritin by denaturation. Denaturation is a nonspecific process that produces, in this case, an insoluble form of ferritin. The structural changes that result in insolubility are undetermined. Consequently any preparation of hemosiderin is expected to be heterogeneous. The temperature dependence of the magnetic properties of this product of denaturation

is particularly sensitive to heterogeneity since it is largely determined by particle size and particle-particle interactions that are both expected to be affected by denaturation. In summary, the evidence suggests that a reasonable model for the structure of hemosiderin is that of an aggregate of ferritin molecules that have been rendered insoluble by some denaturation process. The internal structure of the core remains essentially unchanged from that of the core in ferritin but the protein is rendered insoluble. On this basis the preparation is expected to be heterogeneous, and the difficulty of separating ferritin from hemosiderin is understandable. The theory of hemosiderin being a simple aggregate of cores isolated from ferritin, but without the protein component of ferritin, is inconsistent with the results obtained on the present preparation.

IV. BIOLOGICAL IMPLICATIONS

The results of this study emphasize the widespread occurrence of sizeable polynuclear clusters of iron(III) in biological systems. Prior to this investigation, ferritin was considered to be the only protein to contain polynuclear iron(III) bound to oxygen ligands. This investigation has identified polynuclear clusters of quite different sizes from that found in ferritin. Phosvitin binds 50, gastroferrin 200, irons in a polynuclear fashion. Hemosiderin was shown in this study to be derived from ferritin by denaturation. It does not constitute a further example of a specific polynuclear iron-binding protein. Furthermore, binding can induce unusual coordination structures for the iron(III) bound, e.g., the polynuclear array of tetrahedral iron, $[FeO_4]$, in iron phosvitin at pH 7.5.

As discussed above both "hard-boiled" and "raw" egg phosvitins bind polynuclear iron(III) although in different coordinations. Both can inhibit therefore iron transfer across the mucosal wall by retaining, within the gut, a considerable number of iron(III) ions in a polynuclear cluster. The competition for the iron present in the gut between the protein and low molecular weight chelates is known[1] to be an important part of the control mechanism regulating iron uptake. Gastroferrin also affects iron absorption by binding a polynuclear cluster of iron(III), but the relationship of this binding to the physiological role of the protein, a naturally occurring component of the gut, remains to be established.

In summary, this study, using a variety of physical techniques of the structural and electronic properties of the iron bound to a number of iron proteins has extended the awareness of the presence of polynuclear iron in biology. Polynuclear protein-bound iron can contain as little as 50 iron atoms (phosvitin) or as many as 4000 (ferritin). An intermediate value (200) occurs in gastroferrin. It is anticipated that other systems binding different numbers of iron will be discovered. The storage function of ferritin probably sets the upper limit of 4000 on the size of the polynuclear array. This binding of polynuclear iron by a protein can help explain the effect of such proteins on iron absorption from dietary sources of iron. This effect for phosvitin was shown to be independent of the preparation of the dietary phosvitin, i.e., as "raw" or "hard-boiled". There are, needless to say, many other ways to cook an egg. The influence of various culinary methods on the iron binding capability of phosvitin deserves further investigation.[150]

V. INSTRUMENTAL METHODS

A. Magnetic Studies

Magnetic susceptibility measurements on solid samples (freeze-dried powders) of the iron(III) proteins were carried out on a vibrating sample magnetometer (Princeton Applied Research) fitted with a liquid helium dewar (Andonian Associates) that allows temperature control from room temperature to liquid helium. The apparatus was used only down to liquid nitrogen temperatures in these studies. The sample (0.33 cm^3 in volume) was packed in a Kel-F holder that was fitted to the end of a sample rod assembly containing a copper/constantan thermocouple that fitted into the sample holder and was separated from the sample by only a thin layer (less than 2mm) of Kel-F. A heater inside the dewar assembly boiled the coolant liquid, warming the resulting gas that flowed by the sample, and the heater current was used to vary the temperature continually and automatically. (This feature of the system was designed by G. R. Rossman at the California Institute of Technology.) The thermocouple was calibrated with liquid nitrogen, liquid hydrogen, and liquid helium. Measurements were made using liquid nitrogen to cool the sample from 300°K to about 80°K, over a period of $1\frac{1}{2}$ - 2 hours, long enough to allow the thermocouple and sample to maintain thermal equilibrium with each other.

The magnetometer output, proportional to the susceptibility of the material in the sample region, was continuously plotted versus the

thermocouple reading on a x - y recorder (Hewlett-Packard 7100 BM). The raw data were corrected for the diamagnetism of the sample holder and the effects of the density changes of the gaseous coolant and then calibrated with the room temperature values of the compounds. Room temperature data were calibrated with $HgCo(SCN)_4$, and a sample of high purity annealed nickel metal.

The strength and hysteresis characteristics of the magnetic field were precisely determined with a ^7Li n.m.r. probe. Routine measurements of the magnetic field, as required in the various studies of the field strength dependence of the susceptibility, were made using a transverse Hall probe (F.W. Bell 600 gaussmeter).

Solution susceptibility measurements were made on a Varian HR-200 n.m.r. spectrometer. The sample and reference solutions were contained in the outer and inner compartments of coaxial n.m.r. tubes (Wilmad Glass Co.).

B. Spectroscopic Studies

Absorption spectra in the near infrared (NIR), visible (VIS), and ultraviolet (UV) regions were recorded with Cary 14RI and Cary 17 spectrophotometers fitted with the absorption scales 0 - 0.2 and 0 - 2.0. Room temperature solution spectra were recorded in quartz cells (1 cm, 5 cm, and 10 cm). Low temperature solution spectra were obtained in the VIS-NIR regions using a 1:1 v/v mixture of ethylene glycol and Tris buffer, (0.005 M, pH 7.5) in a Pyrex cell, suspended in

a quartz dewar over liquid nitrogen. The all-quartz dewar was flushed with nitrogen before use and while cooling. At the temperature of measurement (about 150°K) the glycol-salt mixture is a stable, clear glass.

Solid state spectra were obtained on samples prepared as Nujol mulls and pellets of potassium bromide, thallous chloride, or thallous bromide. The pellet solvent was chosen to match the refractive index of the sample. Although the thallous halides have excessive absorbance at wavelengths below ~430 nm, their refractive indices were particularly appropriate to the study of the various iron mineral phases. Low temperature spectra of solid samples were obtained by fixing the pellet in a brass block suspended inside a quartz dewar. The lower part of the block that was not in the sample beam was immersed in liquid nitrogen to cool the sample. Pellet temperatures close to 77°K were obtained in this fashion.

Infrared spectra were recorded on a Perkin-Elmer 225 grating spectrophotometer, using samples in potassium bromide pellets. Raman spectra were recorded on a Cary 81 Raman spectrophotometer fitted with a helium-neon laser (Spectra Physics 125) of output 60 mW. Solution samples were contained in a glass capillary (1 × 70 mm). Depolarization measurements were made by using a half-wave plate between the laser beam and the sample and Poloroid film between the sample and the monochromator.

A Varian spectrometer operated in the X-band region was used to obtain e.s.r. spectra of lyophilized preparations. The magnetic field was regulated by a field dial accessory (V-FR2503).

The ESCA spectra were recorded on a Varian research instrument in the manufacturer's laboratory. The incident radiation was magnesium K_{α}, and the spectrum was averaged over at least twenty scans using a multi-channel analyzer.

X-ray powder patterns were recorded using molybdenum K_{α} radiation filtered through a thin (0.006") foil of zirconium metal. The camera contained this thin zirconium foil over the entire aperture between the film and the sample.

Elemental analyses were carried out by Schwarzkopf Labs, New York, and by Galbraith Labs, Knoxville, Tennessee. Routine solution analysis for iron was carried out by atomic absorption (Varian 303) at the Jet Propulsion Laboratories, Pasadena.

VI. REFERENCES

1. T. G. Spiro and P. Saltman, Struct. Bonding, 6, 116 (1969), and references therein.
2. B. O. A. Hedström, Arkiv. Kemi, 6, 1 (1953).
3. L. G. Sillén, Quart. Rev., 13, 146 (1958).
4. J. Aveston, E. W. Anaker, and J. S. Johnson, Inorg. Chem., 3, 735 (1964).
5. E. Matijevic, J. B. Couch, and M. J. Kerber, J. Phys. Chem., 66, 111 (1962).
6. K. M. Towe and W. F. Bradley, J. Colloid and Interface Sci., 24, 384 (1967).
7. A. A. van der Giessen, J. Inorg. Nucl. Chem., 28, 2155 (1966).
8. T. G. Spiro, S. E. Allerton, J. Renner, A. Terzis, R. Bils, and P. Saltman, J. Amer. Chem. Soc., 88, 2721 (1966).
9. M. H. Francombe and H. P. Rooksby, Clay Min. Bull., 4, 1 (1959).
10. J. D. Bernal, D. R. Dasgupta, and A. L. Mackay, Clay Min. Bull., 4, 15 (1959).
11. G. Johansson, Acta Chem. Scand., 16, 1234 (1962).
12. E. C. Shafer, M. W. Shafer, and R. Ray, Z. Krist., 108, 263 (1956).
13. Ref. 1, Table 1, lists these complexes and their formation constants.
14. H. J. Schugar, G. R. Rossman, and H. B. Gray, J. Amer. Chem. Soc., 9, 4564 (1969).

15. S. J. Lippard, H. Schugar, and C. Walling, Inorg. Chem., 6, 1825 (1967).

16. T. G. Spiro, L. Pape, and P. Saltman, J. Amer. Chem. Soc., 89, 5555 (1967).

17. T. G. Spiro, G. Bates, and P. Saltman, J. Amer. Chem. Soc., 89, 5559 (1967).

18. J. Renner, unpublished. Referred to in reference 1.

19. F. Fletcher and E. London, Brit. Med. J., 1, 984 (1954).

20. C. R. Ricketts, J. S. G. Cox, C. Fitzmaurice, and G. F. Moss, Nature, 208, 237 (1965).

21. J. B. Neilands, Struct. Bonding, 1, 59 (1966).

22. J. C. Brown and L. D. Tiffen, Plant Physiol., 40, 395 (1965).

23. "Iron Deficiency," L. Hallberg, H.-G. Harwerth, and A. Vannotti (eds.), Academic Press, 1970.

24. P. Blaud, Rev. Med. Franc. 'Etrang., 45, 341 (1832). Referred to in reference 1.

25. P. Charley, C. Stitt, E. Shore, and P. Saltman, J. Lab. Clin. Med., 61, 397 (1963).

26. J. S. Multani, C. P. Cepurneek, P. S. Davis, and P. Saltman, Biochemistry, 9, 3970 (1970).

27. P. S. Davis, C. Luke, and D. J. Deller, Nature, 214, 1126 (1967).

28. F. J. Joubert and W.H. Cook, Can. J. Biochem. Physiol., 36, 399 (1958).

29. R. Shainkin and G. E. Perlmann, J. Biol. Chem., 246, 2278 (1971).

30. H. J. Helbock and P. Saltman, Biochim. Biophys. Acta, 135, 970 (1967).

31. P. C. Elwood in "Iron in Flour, Reports on Public Health and Medical Subjects," No. 117, Her Majesty's Stationery Service, London, 1968, p. 1.

32. R. W. Rosenstein and G. Taborsky, Biochemistry, 9, 649 (1970).

33. D. K. Mecham and H. S. Alcott, J. Amer. Chem. Soc., 71, 3670(1949).

34. P. M. Harrison and T. G. Hoy in "Inorganic Biochemistry," G. Eichhorn (ed.), 1971, in press.

35. P. M. Harrison, F. A. Fischbach, T. G. Hoy and G. H. Haggis, Nature, 216, 1188 (1967).

36. J. Seckbach, J. Ultrastruct. Res., 22, 413 (1968).

37. C. N. David, Ph.D. Thesis, California Institute of Technology, 1970.

38. P. M. Harrison in, "Iron Metabolism: An International Symposium," F. Gross (ed.), Springer-Verlag, 1964, p. 40.

39. P. Sturgeon and A. Shoden in reference 38, p. 121.

40. R. Aasa, B. G. Malmstrom, P. Saltman, and T. Vanngard, Biochem. Biophys. Acta, 75, 203 (1963).

41. R. E. Feeney and St. K. Komatsu, Struct. Bonding, 1, 149 (1966).

42. A. Earnshaw, "Introduction to Magnetochemistry," Academic Press, 1968.

43. R. L. Martin and A. H. White, Inorg. Chem., 6, 712 (1967).

44. Handbook of Chemistry and Physics, R. C. Weast (ed. in chief) The Chemical Rubber Co., 1967, p E-109.

45. A. H. Ewald, R. L. Martin, I. G. Ross, and A. H. White, Proc. Roy. Soc. (London), A280, 235 (1964).

46. K. Kambe, J. Phys. Soc. Japan, 5, 48 (1950).

47. H. Schugar, C. Walling, R. B. Jones, and H. B. Gray, J. Amer. Chem. Soc., 89, 3712 (1967).

48. J. Lewis, F. E. Mabbs, and A. Richards, J. Chem. Soc. (A), 1014 (1967).

49. A. V. Khedekar, J. Lewis, F. E. Mabbs, and H. Weigold, J. Chem. Soc. (A), 1561 (1967).

50. M. Gerloch, J. Lewis, F. E. Mabbs, and A. Richards, J. Chem. Soc. (A), 112 (1968).

51. W. M. Reiff, W. A. Baker, Jr., and N. E. Erickson, J. Amer. Chem. Soc., 90, 4794 (1968).

52. W. M. Reiff, G. J. Long, and W. A. Baker, Jr., J. Amer. Chem. Soc., 90, 6347 (1968).

53. A. V. D. Bergen, K. S. Murray, and B. O. West, Austral. J. Chem., 21, 1505 (1968).

54. R. R. Berrett, B. W. Fitzsimmons and A. A. Osusu, J. Chem. Soc.(A), 1575 (1968).

55. H. J. Schugar, G. R. Rossman, C. G. Barraclough, and H. B. Gray, J. Amer. Chem. Soc., in press.

56. Reference 42, p. 77.

57. M. Y. Okamura and B. M. Hoffman, J. Chem. Phys., 51, 3128 (1969).

58. H. J. Schugar, G. R. Rossman, and H. B. Gray, J. Amer. Chem. Soc., 91, 4564 (1969).

59. A. P. Ginsberg, R. L. Martin, and R. C. Sherwood, Inorg. Chem., 7, 932 (1968).

60. M. T. Flood, C. G. Barraclough, and H. B. Gray, Inorg. Chem., 8, 1855 (1969).

61. "Magnetism" III, G. T. Rado and H. Suhl (eds.), Academic Press, 1963.

62. L. Néel, J. Phys. Soc. Japan, 17, Supplement B-1, 676 (1962).

63. J. S. Jacobs and C. P. Bean, in reference 61, p. 271.

64. J. F. Boas, Ph.D. Thesis, Monash University, Australia, 1968. A copy of the appropriate parts of this thesis was generously provided by the author.

65. K. M. Creer, J. Phys. Soc. Japan, 17, Supplement B-1, 690 (1962).

66. T. Takada and N. Kawai, ibid., 691 (1962).

67. K. M. Creer, J. Geomagnetism and Geoelectricity, 13, 86 (1962).

68. J. Cohen, K. M. Creer, R. Pauthenet, and K. Srivastava, J. Phys. Soc. Japan, 17, Supplement B-1, 685 (1962).

69. D. F. Evans, J. Chem. Soc., 2003 (1959).

70. D. H. Live and S. I. Chan, Anal. Chem., 42, 791 (1970).

71. W. D. Phillips, M. Poe, J. F. Weiher, C. C. McDonald, and W. Lovenberg, Nature, 227, 574 (1970).

72. M. Poe, W. D. Phillips, C. C. McDonald, and W. Lovenberg, Proc. Natl. Acad. Sci., 65, 797 (1970).

73. B. N. Figgis, "Introduction to Ligand Fields," Interscience, 1966, c. 11.

74. E. König in "Physical Methods in Advanced Inorganic Chemistry," H. A. O. Hill and P. Day (eds.), Interscience, 1968, c. 7.

75. G. F. Kokoszka and R. W. Duerst, Coordin. Chem. Rev., 5, 209 (1970), and references therein.

76. P. W. Ball, Coordin. Chem. Rev., 4, 361 (1969).

77. L. Dubicki, G. A. Kakos, and G. Winter, Aust. J. Chem., 21, 1461 (1968).

78. E. A. Harris and J. Owen, Proc. Roy Soc. (A), 289, 122 (1965).

79. Reference 64, p. 24, discusses the several investigations of this matter.

80. E. Sinn, Coordin. Chem. Rev., 5, 313 (1970).

81. L. V. Azároff and M. J. Buerger, "The Powder Method in X-ray Crystallography," McGraw-Hill, 1958.

82. H. P. Klug and L. E. Alexander, "X-ray Diffraction Procedures," John Wiley, 1954, p. 504.

83. A. Guinier and G. Fournet, "Small-angle Scattering of X-rays," John Wiley, 1955.

84. G. W. Brady, C. R. Kurkjian, E. F. X. Lyden, M. B. Robin, P. Saltman, T. Spiro, and A. Terzis, Biochemistry, 7, 2185 (1968).

85. P. G. Mikolaj and C. J. Pings, Phys. Chem. Liquids, 1, 93 (1968).

86. F. A. Fischbach and J. W. Anderegg, J. Mol. Biol, 14, 458 (1965).

87. S. Hanlon in "Spectroscopic Approaches to Biomolecular Conformation," D. W. Urry,(ed.), American Medical Association, 1969, p. 161.

88. R. M. Wing and K. P. Callahan, Inorg. Chem., 8, 871 (1969).

89. M. L. Hair, "Infrared Spectroscopy in Surface Chemistry," Marcel Dekker, 1967.

90. L. H. Little, "Infrared Spectra of Adsorbed Species," Academic Press, 1966.

91. K. Siegbahn, et al., "ESCA-Atomic, Molecular, and Solid State Structure Studied by means of Electron Spectroscopy," Almquist Wiksellsboktryckeri AB, Uppsala, Sweden, 1967.

92. J. M. Hollander and W. L. Jolly, Accounts Chem. Res., 3, 193 (1970).

93. L. N. Kramer and M. P. Klein, J. Chem. Phys., 51, 3618 (1969).

94. L. Dubicki, G. A. Rakos, and G. Winter, Aust. J. Chem., 21, 1461 (1968).

95. L. R. Walker, G. K. Wertheim, and V. Jaccarino, Phys. Rev. Letters, 6, 98 (1961).

96. G. M. Bancroft, A. G. Maddock, W. K. Ong, and R. H. Prince, J. Chem. Soc., (A), 723 (1966).

97. R. Bauminger, S. G. Cohen, A. Marinov, and S. Ofer, Phys. Rev., 122, 743 (1961).

98. R. J. Armstrong, A. H. Merrish, G. A. Sawatzky, Phys. Letters, 23, 414 (1966).

99. I. Desza, L. Keszthelyi, D. Kulgawizuk, B. Molnar, and N. A. Eissa, Phys. Stat. Sol., 22, 617 (1967).

100. M. J. Rossiter and A. E. M. Hodgson, J. Inorg. Nucl. Chem., 27, 63 (1965).

101. P. R. Edwards and C. E. Johnson, J. Chem. Phys., 49, 211 (1968), and references therein.

102. W. Kundig, H. Bommel, G. Constabaris, and R. H. Lindquist, Phys. Rev., 142, 327 (1965).

103. J. F. Boas and B. Window, Aust. J. Phys., 19, 573 (1966).

104. D. Leibfritz and W. Bremser, Deut. Chem. Zeitung, 94, 982 (1970).

105. G. H. Faye, Can. Mineral, 10, 112 (1969).

106. H. B. Gray, in "Bioinorganic Chemistry," American Chemical Society, 1971, p. 365.

107. J. S. Griffith, "The Theory of Transition Metal Ions," Cambridge University Press, 1964.

108. Y. Tanabe and S. Sugano, J. Phys. Soc. Japan, 9, 753 (1954).

109. H. L. Friedman, J. Amer. Chem. Soc., 74, 5 (1952).

110. A. P. Ginsberg and M. B. Robin, Inorg. Chem., 2, 817 (1963).

111. D. H. Brown, Spectrochemica Acta, 19, 1683 (1963).

112. T. Birchall, N. N. Greenwood, and A. F. Reid, J. Chem. Soc. (A), 2382 (1969).

113. J. Ferguson, H. J. Guggenheim, and Y. Tanabe, J. Phys. Soc. Japan, 21, 692 (1966).

114. L. L. Lohr, Jr. and D. S. McClure, J. Chem. Phys., 45, 1134 (1966).

115. L. L. Lohr, Jr. and D. S. McClure, J. Chem. Phys., 49, 3516 (1968).

116. E. C. Shafer, M. W. Shafer, and R. Ray, Z. Krist., 108, 263 (1956).

117. J. M. Multani, Ph.D. Thesis, University of California at San Diego, 1969.

118. G. R. Rossman, Ph.D. Thesis, California Institute of Technology, 1971.

119. P. Aisen, R. Aasa, and A. G. Redfield, J. Biol. Chem., 244, 4628 (1969).

120. Reference 41, p. 178.

121. A. Shoden and P. Sturgeon, Annales d'Histochemie, 9, Suppl. 1, 315 (1964).

122. A. Shoden and P. Sturgeon, Acta Haemat., 23, 376 (1960).

123. P. Sturgeon and A. Shoden, in "Iron Metabolism--An International Symposium," F. Gross (ed.), Springer-Verlag, 1964, p. 121.

124. B. Zaslow and R. E. Rundle, J. Phys. Chem., 61, 490 (1957).

125. C. Ho, A. J. Magnuson, J. B. Wilson, N. S. Magnuson, and R. J. Kurland, Biochemistry, 8, 2074 (1969).

126. H. Siebert, Z. Anorg. Allg. Chem., 296, 280 (1958).

127. W. E. Cate, E. O. Huffman, and M. E. Denning, Soil Sci., 88, 130 (1959).

128. Powder Diffraction File, Joint Committee on Powder Diffraction Standards, Philadelphia, Penn., 1970. Entry No. 15-513.

129. A. P. Ginsberg and M. B. Robin, Inorg. Chem., 2, 817 (1963).

130. L. J. Heidt, G. F. Koster, and A. M. Johnson, J. Amer. Chem. Soc., 80, 6471 (1959).

131. J. F. Boas and G. J. Troup, Biochim. Biophys. Acta, 229, 68 (1971).

132. R. A. Holwerda, personal communication.

133. R. W. Jotham and S. F. A. Kettle, Inorg. Chim. Acta, 5, 183 (1971).

134. M. D. Sturge, Solid State Phys., 20, 91 (1967).

135. J. W. Dawson, H. B. Gray, J. E. Hix, Jr., J. R. Preer, and L. M. Venanzi, submitted for publication.

136. R. Shainkin and G. E. Perlmann, J. Biol. Chem., 246, 2278 (1971).

137. H. D. Belitz, Z. Lebensm. Untersuch. Forsch., 127, 341 (1965).

138. J. Williams and F. Sanger, Biochim. Biophys. Acta, 33, 294 (1959).

139. G. Taborsky, J. Biol. Chem., 243, 6014 (1968).

140. G. E. Perlmann and K. Grizzuti, Biochemistry, 10, 258 (1971).

141. G. Taborsky, Biochemistry, 2, 266 (1963).

142. G. E. Perlmann, as told by W. Gibbons, Rockefeller University, New York.

143. R. Osterberg, Arkiv. Kemi., 13, 393 (1959).

144. E. Posnjak and H. E. Merwin, J. Amer. Chem. Soc., 44, 1965 (1922).

145. A. Blaise, J. Chappert, and J. L. Girardet, Comp. Rend., 261, 2310 (1965).

146. A. A. van der Giessen, J. Phys. Chem. Solids, 28, 343 (1967).

147. A. A. van der Giessen, J. Inorg. Nucl. Chem., 30, 1739 (1968).

148. G. Arrhenius, personal communication.

149. K. Nakanishi,"Infrared Absorption Spectroscopy," Holden-Day, Inc., San Franciso, 1962, p. 46.

150. By someone else.

PROPOSITION I

The nature and possible genetic origins of the subunit composition of the transferrins remain controversial. It is proposed that the time dependent effects of various denaturing solvents on the observed molecular weight of transferrin be carefully investigated; that transferrins from species along various branches of the evolutionary tree be studied for their subunit composition; that the amino acid sequences of the fragments produced by cyanogen bromide treatment be determined for a variety of species. An important group of animals to study is that of the most primitive living vertebrates, the cyclostomes, represented by the hagfish and lamprey.

The transferrins are[1] a group of homologous glycoproteins of molecular weight 70,000 - 90,000 that strongly bind two molecules of iron(III) per mole of protein. They have been reported[2] in a variety of vertebrates, and appear to function in iron transfer from storage areas to immature red blood cells.

Several observations suggest that transferrins consist of two similar or identical subunits: (1) Electron spin resonance and temperature dependent magnetic susceptibility measurements indicate[3] that the two iron binding sites are equivalent and non-interacting (2) the carbohydrate portion is arranged as two identical branched[18] carbohydrate chains attached at two different aspartic acid residues along the polypeptide chain[4]; (3) maps of tryptic peptides show many fewer spots than expected from the lysine and arginine content[5,6]; (4) the high molecular weight of ~80,000. Within the conceptual framework of genetic economy, these results suggest that the organism would operate more efficiently by synthesizing two half molecules to be subsequently joined rather than by synthesizing, uninterruptedly, a single chain.

The most probable linkage between any subunits is a disulphide bridge and several investigations of these linkages in the transferrins have been reported. In the first study,[5] reduced and carboxymethylated transferrin isolated from fresh plasma had a sedimentation coefficient in tris buffer of 1.24S, giving a molecular weight of 42-44,000. However, this same preparation was eluted from a G-200 column before the native protein, indicating a molecular weight about twice that of whole transferrin. In two subsequent studies, other investigators decisively refuted this work. In the first study,[1] the sedimentation behavior of the reduced and carboxymethylated preparation was compared with similarly treated single chain proteins, bovine serum albumin (67,800 molecular weight) and pepsin (33,000). Experiments were performed in urea and guanidine hydrochloride to minimize non-covalent interactions between chains. $S_{20°,obs}$ for chicken ovotransferrin, human and rabbit serum transferrin was greater (0.72) than that for either BSA (0.68) or pepsin (0.45). This order is consistent with a single chain transferrin.

The second investigation[7] confirmed these sedimentation results for human serum transferrin and extended the observations to include the intrinsic velocity, gel filtration in guanidine hydrochloride, tryptic fingerprinting, and quantitative terminal amino acid analysis. These additional studies confirmed that transferrin exists as a single polypeptide chain. Varying the time of hydrolysis and the mapping solvent conditions increased the resolution in the tryptic fingerprinting. At least 54 spots were resolved, 70% of the maximum number possible. In the sedimentation studies a small peptide chain of 5-10,000 molecular

weight could be missed but no small chain was seen in gel filtration. There is no corroborated evidence in these transferrins for the existence of subunits linked by -S-S- bonds. Genetic economy seems to be violated. These authors did suggest that, with duplicate iron binding sites and carbohydrate linked peptides, some bits of the sequence could occur in duplicate. Chain synthesis would be derived from the transferrin structural gene duplicated and subsequently fused in the evolutionary past, but whose two halves still maintain significant regions in common. There are at least two other groups of proteins where gene duplication has probably occurred. Ferredoxins,[8,9] non-heme iron sulphur proteins involved in electron transport, are 54-55 residues long and have been isolated from bacteria, plants and green algae. All have similar sequences, suggesting a common archtypal origin. The many bacterial sequences reported show substantial internal repitition in the two halves of the molecule, persuasive evidence for their evolution by gene duplication from a common precursor of roughly half the present size. There is also strong evidence[10] for gene duplication in the structural gene for the light chains of immunoglobulins, Ig G. A primordial gene equivalent to a polypeptide of 12,000 molecular weight has been proposed[10] to account for the simultaneous occurrence of diversity and constancy in these chains.

Genetic changes can have important consequences for a bifunctional protein. A recent report[11] describes the creation by genetic manipulation of a covalent linkage between two enzymes

specified by the second and third structural genes of the histidine operon of Salmonella typhimurium. The two enzymes are separate molecules in the wild type organism. In the mutant they are incorporated into a single enzyme with complete retention of both enzymatic activities. Different organisms exhibit different patterns of control[12,13] for the regulation of the metabolic pathway from aspartate to threonine, lysine, methionine and isoleucine. E. coli has three kinds of aspartokinases and two kinds of homoserine dehydrogenases. Four of these activities are incorporated into two bifunctional enzymes, each with one of the two kinds of activites. By contrast Bacillus polymyxa has only one aspartokinase, and Rhodospirillum rubrum only one aspartokinase and one homoserine dehydrogenase. In the globins genetic duplication[14] without subsequent fusion has occurred several times, giving rise to myoglobin and hemoglobin, and to the various hemoglobin chains.

Evidence for the duplicate nature of the polypeptide chain in egg white transferrin has now been presented.[15] Cleavage of the polypeptide chain at the methionine residues was achieved by cyanogen bromide treatment producing three fragments of molecular weight 21,000, 9400, and 7000 in the molar ratio 1:1:1. Two moles of each fragment were produced per mole of whole protein.

A very recent observation,[16] as yet unpublished, on pigeon serum transferrin supports the existence of transferrin subunits. Migration of the protein in 1% SDS-acrylamide gels corresponds to that of a protein of molecular weight 80,000. After standing for a week in 1% SDS, the migration is that of a 40,000 molecule. The preparation

has been reduced and alkylated as in the studies above but it seems that the subunits created in this way interact so strongly that their dissociation in the denaturing SDS is quite slow.

In order to clarify the significance of the earlier experimental results, it is proposed that the time dependent effects of the various denaturing solvents on the observed molecular weight of transferrin be carefully investigated. None of the three studies discussed above makes any reference to any time dependent phenomenon. Further, to obtain a more definitive picture of the nature and possible genetic origins of the subunit composition of the transferrins, it is proposed that a wide-ranging investigation of transferrins from other species along different branches of the evolutionary tree be initiated. Two areas of investigation are apparent. First, sedimentation studies in denaturing solvents and gel electrophoresis in SDS would identify the presence of sub-units. Second, various transferrins would be treated with cyanogen bromide and the resulting peptides sequenced. Most transferrins for which amino acid analysis data are available[2] have about 10 methionine residues. This is the number found in egg white transferrin, which produces peptides of suitable size for comparatively easy sequence work.

An important group of animals to investigate is the cyclostomes, the most primitive living vertebrates which have evolved independently since earliest vertebrate origins. They are represented today by the hagfish and lamprey. The lamprey hemoglobin[14] is an evolutionary carryover from the time prior to the production of α and β chains. It

has only one chain. A lamprey transferrin containing about 12 methionine residues has recently been reported.[17]

A final consideration in comparative inter-species studies of genetic differences is the rate of acceptable mutations in the protein. These rates have been correlated[14] with biological function. Cytochrome c, which has to mesh with other macromolecules on the mitochondrial membrane, has changed more slowly than the globins, which interact with smaller molecules. The fastest rate occurs in the fibrinopeptides which are cut off from fibrinogen during blood clotting and then discarded. The transferrins gather, transport, and deliver iron atoms. Their mutation rate is expected to be about that of the globins, which do exhibit marked differences in subunit interaction between species. The extent of these differences, if reflected also in the transferrins, should be sufficient to resolve the controversy over the subunit nature of the protein.

References

1. F. C. Greene and R. E. Feeney, Biochemistry, 7, 1366 (1968).
2. R. E. Feeney and S. K. Komatsu, Struct. Bonding, 1, 149 (1966).
3. P. Aisen, A. Liebman, and H. A. Reich, J. Biol. Chem., 241, 1666 (1966).
4. G. A. Jamieson, J. Biol. Chem., 240, 2914 (1965).
5. J.-O. Jeppson, Acta Chem. Scand., 21, 1686 (1967).
6. J. Williams, Biochem. J., 82, 355 (1962).

7. K. G. Mann, W. W. Fish, A. C. Cox, and C. Tanford, Biochemistry, 9, 1348 (1970).

8. J. N. Tsunoda, K. Y. Yasunobu, and H. R. Whitely, J. Biol. Chem., 243, 6262 (1968).

9. B. Weinstein, Biochem. Biophys. Res. Comm., 35, 109 (1969).

10. E. S. Lennox and M. Cohn, Ann. Rev. Biochem., 36, 365 (1967).

11. M. W. Rechler and C. B. Bruni, J. Biol. Chem., 246, 1806 (1971).

12. E. R. Stadtman in "The Enzymes," Vol. I, P. D. Boyer (ed.), Academic Press, 1970, p. 398.

13. G. N. Cohen, "The Regulation of Cell Metabolism," Holt, Rinehart, and Winston, Inc., 1968, c. 9.

14. R. E. Dickerson and I. Geiss, "The Structure and Action of Proteins," Harper and Row, 1969, c. 3.

15. J. L. Phillips and P. Azari, Biochemistry, 10, 1160 (1971).

16. J. Frelinger, Department of Biology, California Institute of Technology, personal communication.

17. R. O. Webster and B. Pollara, Comp. Biochem. Physiol., 30, 509 (1969).

18. G. A. Jamieson, M. Jett, and S. L. DeBernardo, J. Biol. Chem., 246, 3686 (1971).

PROPOSITION II

The use of "street" drugs of unknown composition is widespread. To make information about the constituents of these drugs available prior to use, it is proposed that analytical methods suitable for use by the chemically unsophisticated be developed for the determination of the two potentially lethal constituents STP and strychnine; that an analytical service, using the sensitive and precise GLC methods recently developed, be initiated to identify the constituents of drug samples submitted for analysis by members of the Caltech community.

In the universal search for altered mental states, contemporary society in the United States has endorsed caffeine, nicotine, and alcohol as its culturally permissive drugs.[1] Supposedly available only on prescription are the sedative/muscle relaxant barbiturates, the stimulant/appetite suppressant amphetamines, and the various opium derivatives, e.g., morphine. Drugs that are legally proscribed include cannabis, hashish, and LSD. The ready availability and wide usage of both prescriptive and proscriptive drugs is a fact of contemporary life.

A survey[2] among students at Caltech in March 1967 indicated that at least 13.7% had used marijuana one or more times, and that 5.5% had used LSD one or more times. There is no reason to believe that these figures have decreased. Consequently, the occurrence of a number of "bad" trips remains a feature of student life.

Careful quality control procedures are employed in the production of caffeine, nicotine, and alcohol. No such precautions can be expected for drugs made available through illegal channels, especially "street drugs". Most buyers of these drugs are young, many of college age.

They face a real risk of physical damage from drug constituents that occur in all combinations from innocuous chalk dust to rat poison. The structures of the drugs referred to in this proposition are shown in Figure 1.

Two common constituents of street drugs can result in inadvertant injury or death. 2,5-dimethoxy-4-methylamphetamine (STP) is being used increasingly in drugs sold as LSD or mescaline. An individual under the influence of STP is quite likely to enter a state of physiological shock if treated for a "bad" trip with either of the commonly employed anti-hallucinatory and anti-confusion agents, $\alpha\alpha$-diphenyl-4-piperidenemethanol (azacyclonol, frenquel), and 2-chloro-10-(3-dimethylaminopropyl)-phenothiazine (chlorpromazine, thorazine). Several deaths were attributed to this reaction when STP first appeared in street drugs. Strychnine, a common rat poison, is extremely toxic to humans. The minimum lethal dose[3] orally in rats is 5 mg/kg, corresponding to 350 mg for the standard 70 kg man. Strychnine also stimulates the circulatory and central nervous systems, and so finds its way into street drugs. Its effective dose as a hallucinatory stimulant is dangerously close to the lethal dose, and this has apparently led to several deaths.

Because of its importance in toxicology, several simple colorimetric tests[4-7] are known for strychnine. Understandably, no critical assessment of possible interference from street drug constituents has appeared.

Gas-liquid chromatographic (GLC) procedures for the analysis of amphetamines and barbiturates have been developed for medical[8,14] and forensic[9] purposes, although their use is not widespread. A recent study[9] reports the relative retention times of 42 derivatives of mescaline, amphetamines, and related compounds. The homologous internal reference used was n-propyl amphetamine, which is not commercially available, for use or abuse. Volatility was decreased by using acetamide derivatives. A sensitivity of 0.02 μg/ml was achieved. This was sufficient to determine from a 2.5 ml blood sample therapeutic use (0.04 μg/ml, 2 hours after ingestion of 25 mg of amphetamine) as well as cases of abuse (0.15-0.55 μg/ml blood; 1-200 μg/ml urine). The sensitivity and separation characteristics of GLC make it the preferred method[10] of detection over thin layer chromatography and colorimetric methods.[13]

These analytical procedures are commonly applied to physiological samples obtained after drug ingestion. To meet the real need for information about the constituents of a random street drug sample prior to ingestion, it is proposed that the following program be initiated.

(1) The two most obviously dangerous constituents are strychnine and STP. Simple analytical methods, not requiring sophisticated instrumental techniques should be developed to allow chemically non-sophisticated users to identify these compounds. Some of the colorimetric tests for strychnine include: oxidation by dichromate in sulphuric acid (80%), producing a blue-violet solution (the Otto reaction for lactams)[6]; addition of nitric acid to give a yellowish

coloration[4]; addition of ammonium vanadate in sulphuric acid to produce a deep blue color that changes into red[7]; other procedures[5] involving extractions have been reported. These strychnine tests should be reinvestigated to evaluate their reliability in the presence of street drug constituents. The marked structural dissimilarity between strychnine and these constituents suggests little interference, yet the well-known reactivity of a methoxy substituted phenyl ring will probably complicate any test involving oxidation.

A possible methodology for equally simple tests to distinguish STP from mescaline and other amphetamines can be described. Unlike the other amphetamines listed, the phenyl ring of STP is substituted. The methoxy substituents can be identified qualitatively by Zeisel's test[11] for alkoxyl groups. Hydriodic acid cleaves the methoxy group on warming, releasing volatile methyl iodide, which reacts with a mercuric nitrate moistened filter paper. The mercuric iodide formed creates a light orange or vermilion color. Both STP and mescaline would give positive Zeisel's tests, and be converted to the polyphenols shown below.

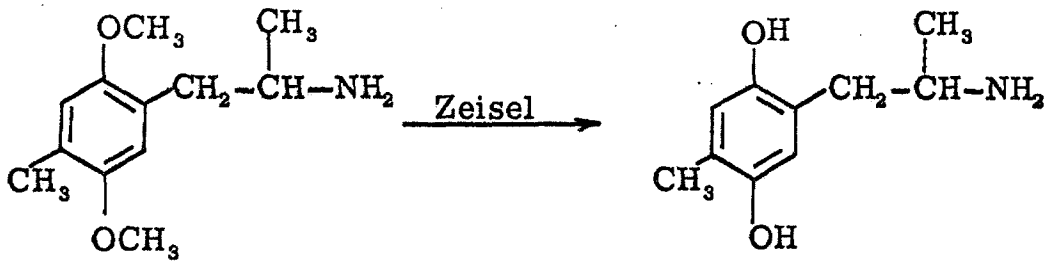

STP

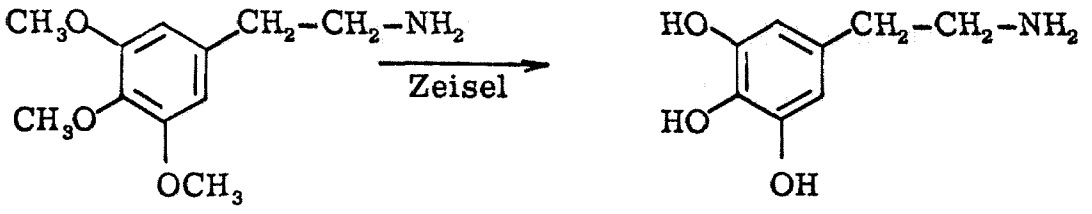

mescaline

Both these phenols are ortho- or para-diphenols and are very sensitive to oxidation. The triphenol may be so reactive as to scavenge oxygen from the atmosphere, giving a quinone. The stereochemistry of the -OH groups in the triphenol only is suitable for chelation to transition metal ions. Complex formation with simple hydrated iron(III) ions would inevitably lead to oxidation of the ligand. Complex formation can drastically alter the redox potential of the iron(II)-iron(III) couple. The 1:1 complexes of iron(III) with the quadridentate ligand nitrilotriacetate (NTA) and the pentadentate ligand N'-(2-hydroxyethyl)ethylenediamine-NNN'-triacetate (HEDTA) may be stable to reduction by the phenolic ligand and preferentially form a 1:1 adduct with either phenol that would exhibit an intense charge transfer band in the visible region. Such a band is responsible for the bright red color of the 1:1 iron(III): thiocyanate complex.

(2) In a wider sense individuals should have the opportunity to find out what is present in a mixture of drugs, many of whose combinations are dangerous, if not toxic. Their decisions to ingest such a mixture will then not be made out of ignorance of the constituents and their possible damaging side effects. Such information is available

to users of nicotine, caffeine, and alcohol. A service should be initiated to analyze these drug mixtures using the instrumental facilities available. The rapid and reliable GLC methods discussed above have been developed for fast batch analysis, and the time required to perform the analyses for the Caltech student community could not involve more than two to three hours per week. Samples for analysis would be submitted anonymously, with a code number supplied by the owner, and the analytical results with code numbers posted on a general noticeboard. An attempt is being made[12] by students and health officials to establish such a service at the State University of New York, Stony Brook.

The many social and legal obstacles to the implementation of the second proposal are hopefully not insurmountable. As a student health service, this analytical service would be invaluable. Since the phenomenon of street drug usage is not likely to disappear, it seems sensible to minimize the health hazards it poses.

References

1. L. E. Hollister, Chemical Psychoses, C. C. Thomas, 1968, p. 143.
2. K. Eells, psychologist, "A survey of student practices and attitudes with respect to marijuana and LSD," Caltech, 1967.
3. The Merck Index, P. G. Stecher, ed., Merck and Co., 1968, p. 989.
4. The Pharmacopeia of the U.S.A., ed. 17, 1969.
5. W. Wisniewski and A. Pietura, Acta Pol. Pharm., 27, 279, 567 (1970). Chemical Abstracts listing 91216s, 115932a (1971).
6. H. L. Holmes in The Alkaloids, Vol. 1, R. H. F. Manske and H. L. Holmes (eds.), Academic Press, 1950, p. 375.

7. T. A. Henry, The Plant Alkaloids, P. Blakiston's Son and Co., Ltd., Philadelphia, 1939, p. 506.

8. H. E. Sine, M. J. McKenna, T. A. Rejent, and M. H. Murray, Clin. Chem., 16, 587 (1970).

9. P. Lebish, B. S. Finkle, and J. W. Brackett, Jr., Clin. Chem., 16, 195 (1970).

10. R. C. Baselt and L. J. Casarett, J. Chromatogr., 57, 139 (1971).

11. R. L. Shriner, R. C. Fuson, and D. Y. Curtin, The Systematic Identification of Organic Compounds, John Wiley, 1964, p. 130.

12. Anonymous, Playboy, 18 (8), 45 (1971).

13. C. S. Frings, C. Queen, and L. B. Foster, Abstract No. 24 from 23rd National Meeting A. A. C. C., Clin.Chem., 17 (7),(1971).

14. J. MacGee, Clin. Chem., 17, 587 (1971).

Figure 1

Strychnine:

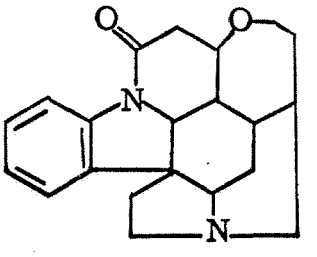

Amphetamines:

(derivatives of phenethylamine)

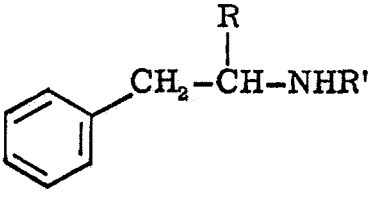

	Isomer	R	R'	ring subst.
amphetamine, benzedrine	D,L	CH_3	H	none
dextroamphetamine, dexedrine	D	CH_3	H	none
metamphetamine, methedrine	D,L	CH_3	CH_3	none
STP	L	CH_3	H	2,5-dimethoxy-4-methyl
mescaline	--	H	H	3,4,5-trimethoxy

Barbiturates:

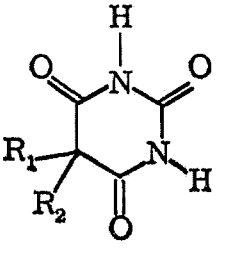

Figure 1 (Continued)

	R_1	R_2
barbital	$CH_3 \cdot CH_2-$	$CH_3 \cdot CH_2-$
amobarbital	$CH_3 \cdot CH_2-$	$(CH_3)_2CH \cdot CH_2 \cdot CH_2-$
pentobarbital	$CH_3 \cdot CH_2-$	$CH_3 \cdot CH_2 \cdot CH_2 \cdot CH(CH_3)-$
secobarbital (seconal)	$CH_2=CH \cdot CH_2-$	$CH_3 \cdot CH_2 \cdot CH_2 \cdot CH(CH_3)-$

"Downers":

chlorpromazine

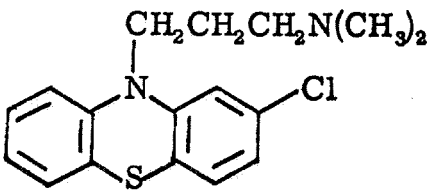

azacyclonol

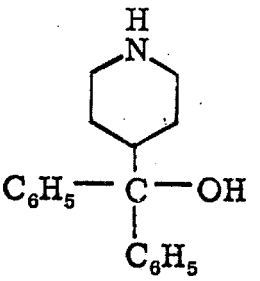

PROPOSITION III

The possible role of glycoproteins in tissue calcification can be investigated through a detailed physical chemical study of the interaction between sialic acid and calcium(II) ions. It is proposed that the interaction be investigated using the calcium(II) isomorphs europium(II) and (III). Suitable techniques for this study include Mössbauer and ^{1}H n. m. r. spectroscopy. The competition for binding to the isomorphs among ions that bind calcium(II) in vivo would be investigated.

Glycoproteins[1] are conjugated proteins with one or more heterosaccharides as covalently bound prosthetic groups. They occur in a variety of species from platyhelminths to vertebrates as the dominant components of the important mucous secretions. The biological significance and wide distribution of the glycoproteins are apparent from the following examples that have been studied[2]: α_1-acid glycoprotein of serum; hen albumin; sub-maxillary gland glycoproteins, typical of components of mucous secretions; milk caseins; fetuin, the α-globulin from foetal calf serum; transferrin, with genetic polymorphism resulting in large part from heterosaccharide variations; urinary glycoproteins that can neutralize the infectivity of swine influenza in chick embryos; enzymes as ribonuclease B and serum cholinesterase; the all-important immunoglobulins; blood group specific substances dependent on the heterosaccharide sequence for specificity; glycoprotein components of bone and connective tissue.

The most characteristic carbohydrate component of glycoproteins is sialic acid, the general name for N-acylated and N-acylated, O-acetylated neuramic acid. Open chain and ring structures for neuramic

acid are shown in Figure 1. Most of the glycoproteins listed above contain significant amounts of sialic acid. When present in a heterosaccharide chain sialic acid commonly occupies the terminal position. It is a strong acid, $pK_a \sim 2$, and under physiological conditions interacts strongly with ions in the environment. The function of glycoproteins and their constituent sialic acid in bone and connective tissue will be of concern in this proposition.

The X-ray pattern of the mineral phase of bone and teeth is that of the mineral apatite.[3,13] Ideally, apatite is $Ca_{10}(PO_4)_6(OH)_2$ but the biological apatite deposits are characterized by poor crystallinity, crystal sizes of colloidal dimension, and variable composition. Other ions that have been found in these deposits include magnesium, sodium, pyrophosphate, carbonate, fluoride, citrate, and organic components probably from the surrounding matrix. Studies and theories of tissue calcification have been many over the years yet to quote a recent review,[3] "no theory of biological calcification is at present available that can provide a satisfactory biochemical and biophysical explanation of this phenomenon at the molecular level."

Calcification has been variously suggested[3] to result from the spontaneous precipitation of calcium phosphate--the action of a phosphatase on organic esters built up during the glycolysis that accompanies calcification--the combined action of a specific ATPase producing matrix bound pyrophosphate and a pyrophosphatase to subsequently split the pyrophosphate. Evidence for each of these proposals is incomplete, and results apparently in conflict with each have been reported. Crystal

nucleation by matrix components has also been intensively studied. The existence of a biological catalyst or "local factor" to bind Ca^{2+} and PO_4^{3-} and release apatite has been proposed. There is however good evidence from electron microscope studies for the role of matrix biopolymers in nucleation catalysis. Apatite crystallization has been observed in the 640 Å interband region of collagen, with the c-axes of the crystallites alligned almost parallel to the collagen fiber axis. The role of mucopolysaccharides and glycoproteins in the calcification of connective tissue has been a matter of controversy[4] for some time. The following recent evidence strongly suggests an important role for these biopolymers.

A purified protein-polysaccharide fraction from hyaline cartilage has been shown[5] to prevent the precipitation of apatite even in supersaturated solutions. Hydrolysis by proteolytic or hyaluronidase action abolished this inhibitory effect. Electron microscopy showed mucopolysaccharide containing vesicles in the extracellular matrix. They accumulate apatite and have no morphological relation to collagen fibres. A homogeneous cation-binding glycoprotein has been isolated recently[6,7] from bone powder. Of the 40% carbohydrate, 16% is due to sialic acid as N-acylneuramic acid.

The cellular and extracellular matrix components of the calcifying tissues in enamel, cartilage and bond vary. Obviously more than one mechanism of calcification might operate in different tissues. There is good evidence that glycoproteins play some role as nucleation catalysts. They could act as ion binders to build up local conditions of high supersaturation that would lead to mineralization. Sialic acid occurs

as an anion at the end of carbohydrate chains and interacts with the surrounding environment. It is expected to be one of the major carbohydrates that bind Ca^{++}.

There is at present no experimental information on the nature and extent of the interaction between calcium(II) and sialic acid. Unfortunately, the calcium(II) ion is inert to most spectroscopic techniques. It provides only a small perturbation to properties of the sialic acid that are amenable to spectroscopic investigation, e.g., ^{1}H n.m.r. ^{43}Ca n.m.r. is possible but inconvenient and a strict isomorphous replacement for calcium(II) is needed. The criteria for choosing this isomorph are that it closely resemble calcium(II) in ionic radius, stereochemistry, and steric requirements. Charge similarity is of less importance than ionic size. Europium(II) has been reported[8] to partly mimic the biological activity of muscle stimulation that is associated with calcium(II). The compatibility of Eu(II) and Ca(II) in terms of the above criteria can be seen from the data listed in Table I.[8]

Table I

Property	Europium(II)	Calcium(II)
ion size (Å)	1.12	0.99
main coord. no.	8	8
log K for EDTA*	9.6	10.6
log K for pic†	2.8	2.5

* EDTA is ethylenediamine tetra-acetate.

† pic is picolinate.

Europium(III) also mimics the ionic radius (0.95 Å) and main coordination number (8) of calcium(II). Other possible probes for calcium(II) might come from the series of lanthanides, although the one closest in ionic radius is promethium (0.98 Å) a fleeting fission product of uranium.

There are several favorable consequences of the use of europium as a probe for calcium. Europium is a Mössbauer nucleus. ^{151}Eu has a nuclear spin of 5/2 and a natural abundance of 47.8%. The isomer shifts of europium(II) and (III) are very different and appear to be sensitive,[9] at least in the case of europium(II), to the nature of the compound. Europium(II) has an absorption band at 400 nm that has some sensitivity to the chelating groups.[8] Both valencies are paramagnetic and are expected to greatly shift the ^{1}H n.m.r. resonances of molecules that are bound to them. Tris(dipivalomethanato) europium(III)[10] and its dipyridine adduct[11] have been shown to cause remarkably large shifts in the ^{1}H n.m.r. spectrum of coordinated molecules. Shifts of tens of p.p.m. have been reported, sufficient to reduce a spectrum with substantial regions of overlap to one of first order. Use of the shift reagent and spin decoupling has led to the complete spectral analysis for cis-4-terbutylcyclohexanol, the steroid androstan-2-ol and the triterpene friedelan-3-ol.[12]

The possible role of glycoproteins in tissue calcification deserves clarification through a detailed physical chemical study of the interaction between sialic acid and calcium(II) ions. It is proposed that this interaction be investigated using the calcium(II) isomorphs europium(II) and (III). Mössbauer and ^{1}H n.m.r. spectroscopy are suitable for study

of the nature and extent of the binding between the isomorphs and sialic acid. The nucleation catalysis aspect of glycoprotein activity can be studied by competition studies between sialic acid, phosphate, and carbonate for the calcium(II) isomorphs. ^{1}H n. m. r. resonances of sialic acid are sensitive to europium binding, and these resonances would reflect any displacement of sialic acid by competing ions. These studies might well be extended to include other carbohydrate disaccharides and other metal ions that compete with calcium(II) ions in tissue mineralization.

References

1. A. Gottschalk and E. R. Bruce Graham in, "The Proteins," IV, H. Neurath, ed., Academic Press, 1966, p. 96.
2. A. Gottschalk, ed., "Glycoproteins," Elsevier, 1966, pp 297-569.
3. B. N. Bachra, Intern. Rev. Conn. Tissue Res., 5, 165 (1970).
4. B. N. Bachra in "Biological Mineralization," I. Zipkin, ed., Wiley, 1971.
5. M. Schubert and M. Pras, Clin. Orthop. Related Res., 60, 235 (1968). Discussed in reference 3.
6. G. M. Herring, Nature, 201, 709 (1964).
7. A. T. de B. Andrews, G. M. Herring, and P. W. Kent, Biochem. J., 111, 621 (1969).
8. R. J. P. Williams, Quart. Rev., 24, 331 (1970).
9. O. Berkooz, J. Phys. Chem. Solids, 30, 1763 (1969).
10. J. K. M. Sanders and D. H. Williams, Chem. Commun., 422 (1970).
11. C. C. Hinckley, J. Amer. Chem. Soc., 91, 5160 (1969).

12. P. V. DeMarco, T. K. Elzey, R. B. Lewis, and E. Wenkert, J. Amer. Chem. Soc., 92, 5734, 5737 (1970).

13. E. D. Eanes and A. S. Posner in "Biological Calcification," H. Schraer (ed.), Appleton-Century-Crofts, 1970, p. 1.

Figure 1

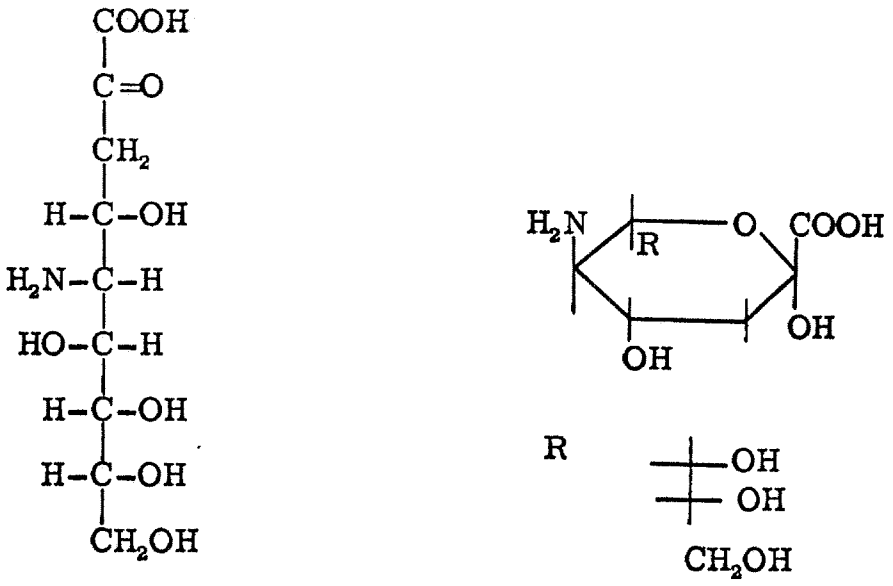

neuramic acid

PROPOSITION IV

Knowledge of the solution conformational behavior of the anti-inflammatory drug indomethacin, whose crystal structure has recently been determined, is important in the study of this drug's action. It is proposed that this behavior be studied through the temperature dependence of the ^1H n. m. r. spectrum; that the importance of the peptide torsion observed in the solid state be determined through a proposed chemical modification and through the determination of the crystal structure of two other anti-inflammatory drugs structurally related to indomethacin.

One of the most potent of the many and varied drugs used[1] to combat inflammation is indomethacin, 1-(p-chlorobenzoyl)-5-methoxy-2-methylindole-3-acetic acid. A two dimensional representation of the molecule and the numbering used in the following discussion is shown in Figure 1. It has recently been reported[2-4] that during the complex and largely unknown biochemical processes that occur during inflammation indomethacin acts as a potent inhibitor of the production of local hormones called prostaglandins. These hormones are released locally by tissues as part of the defensive responses to infection or trauma. Their presence in other tissues is inflammatory. Indomethacin apparently acts as an anti-defensive drug,[5] preventing the uncontrolled distribution of these hormones by inhibiting their synthesis. In this respect indomethacin is 20 times more potent than aspirin.

The molecular details of the synthesis of prostaglandins and the inhibition of that synthesis by indomethacin are largely unknown. It has been suggested[6] that indomethacin may inhibit enzymes and affect cellular membranes. Such mechanistic considerations on a molecular level depend strongly on detailed information about the molecular structure

yet only very recently has the crystal structure of indomethacin been reported.[7] The structure does have several unusual features which can be best seen in the stereo view of the molecular configuration shown in Figure 2.

The geometry of the linkage between the p-chlorophenyl group and the indole ring is subject to two steric influences. In the first instance the methyl substituent at C(2) of the indole ring is only 2.85 Å from the carbonyl oxygen, preventing the carbonyl group from being coplanar with the indole ring. The torsion angle O(1)-C(10)-N(1)-C(2) is 25.5°. As a result the C(10)-N(1) bond loses some double bond character in being lengthened from a normal amide length of 1.32 Å to 1.416 Å. The N(1) is moved 0.06 Å out of the plane of its three adjacent carbon atoms. The second steric constraint involves H(8) of the indole ring and H(16) of the benzene ring. The planes are tilted away from each other with a torsion angle C(12)-C(11)-C(10)-O(1) of 39.3°. The major intermolecular interactions observed in the crystal packing are the formation of molecular dimers through the carboxylic acid residues and the overlapping of the indole ring with the acetic acid group of another molecule. It was suggested[7] that these unusual "orientations of the benzene ring, the carbonyl group, and the indole ring under reaction conditions might play an important role in the chemistry of indomethacin."

These reaction conditions occur of course in the solution, not the solid phase. The crystal structure results show the molecule in one low energy configuration with some intermolecular influences operating.

Their influence on which configuration the molecule takes up in the solid phase is unknown. The study of space-filling molecular models shows that the molecule has available several different conformations resulting from rotation about the bonds linking the two rings, N(1)-C(10) and C(10)-C(11). These rotations involve the two steric influences mentioned earlier. N(1)-C(10) rotation brings the indole methyl and carbonyl oxygen into proximity while C(10)-C(11) rotation causes the indole H(8) and benzene H(16) to interact sterically.

Rapid rotation about these bonds and the resultant time averaged ^{1}H n. m. r. spectrum is hindered by appreciable energy barriers. For N(1)-C(10) rotation the potential energy maxima occur with close steric interaction of the O(1)-indole methyl and the O(1)-indole H(8) pairs. The maxima for C(10)-C(11) rotation correspond to the contact of H(16) and H(12) of the benzene with H(8) of the indole. Both rotations could operate simultaneously. The height of these barriers is probably less than 20 kcal/mole. These interactions as seen viewing along the indole ring are shown in Figure 3 together with qualitative potential energy profiles.

The relative amount of each low energy conformation present in solution depends on the height of the energy barriers between them and on the temperature. A careful analysis of the ^{1}H n. m. r. spectrum and its temperature dependence is the most promising method of study of the preferred solution conformations of indomethacin. Two of the resonances that are expected to be most sensitive to rotational changes are the indole

methyl and H(8) peaks. Both can be expected to be unambiguously determined in a stable conformation since the methyl is the only C-bonded methyl in the molecule, and H(8) is partly shielded by its position over the benzene ring. The temperature dependence of the methyl resonance will monitor the N(1)-C(10) rotation while that of H(8) will monitor the C(10)-C(11) rotation.

Since the knowledge of the conformational behavior of indomethacin in solution is important in the study of this drug's action, it is proposed that this behavior be studied through the temperature dependence of the ^{1}H n. m. r. spectrum.

The effects of this unusual twisting about the peptide bond on the pharmacological activity could be separated from those resulting from the relative non-planar orientations of the aromatic rings by ring closure between indole H(8) and benzene H(16). A possible methodology for the reaction using chemical activation of the peptide followed by photochemically induced ring closure and dehydrogenation is shown[8] in Figure 4. The structures of two other anti-inflammatory drugs, phenylbutazone and aminopyrine, are shown and compared to the peptide part of indomethacin in Figure 5. These two pyrazolones bear some structural similarities, as well as obvious differences, to indomethacin around their amide type linkage. Their preferred configuration in the solid state as shown by X-ray structure determinations might shed some further light on the importance of the unusual torsion observed in indomethacin.

References

1. M. W. Whitehouse, Progr. Drug. Res., 8, 321 (1965).
2. J. R. Vane, Nature New Biology, 231, 232 (1971).
3. J. B. Smith and A. L. Willis, Nature New Biology, 231, 235 (1971).
4. S. H. Ferreira, S. Moncada, and J. R. Vane, Nature New Biology, 231, 237 (1971).
5. H. O. J. Collier, Nature, 232, 17 (1971).
6. T. Y. Shen, private communication to the authors of ref. 7.
7. T. J. Kistenmacher and R. E. Marsh, submitted for publication, June 1971.
8. Suggested by R. G. Bergman, Caltech, 1971.

Figure 1

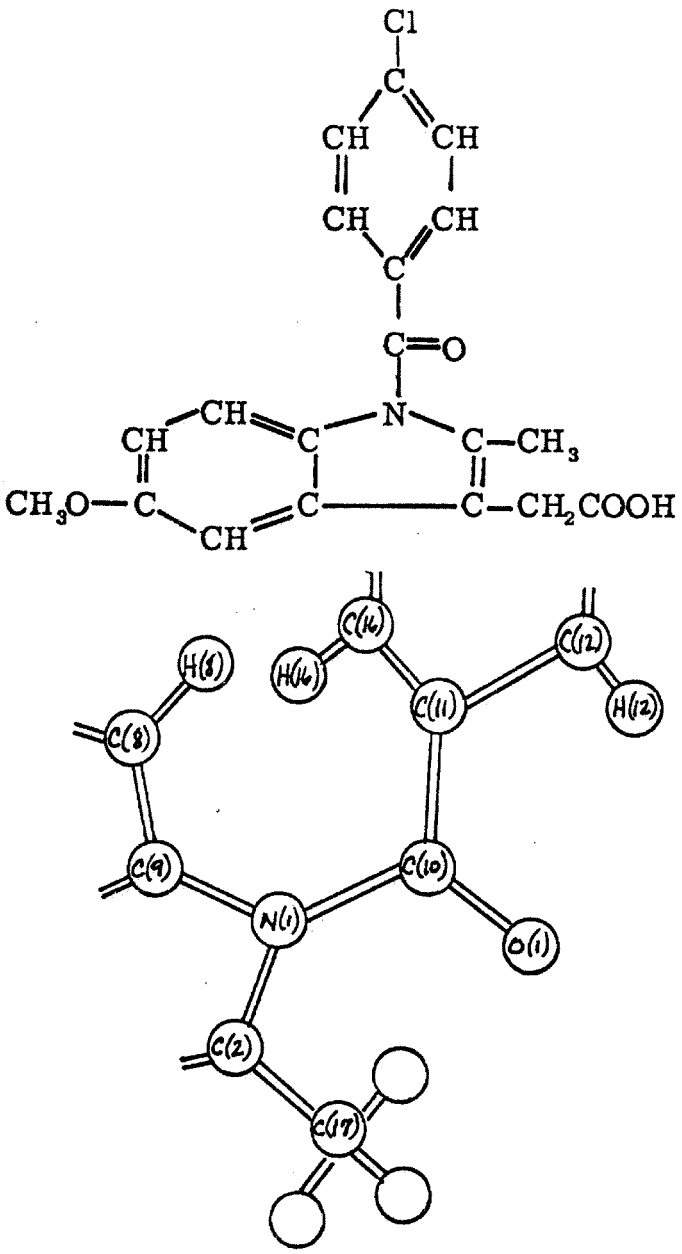
Cl
C
CH
CH
CH
CH
C
C=O
N
CH
CH
C
C—CH3
CH3O—C
C
C—CH2COOH
CH
C(14)
H(14)
C(12)
H(12)
C(11)
H(8)
C(8)
C(9)
C(10)
N(1)
O(1)
C(2)
C(17)

Figure 2

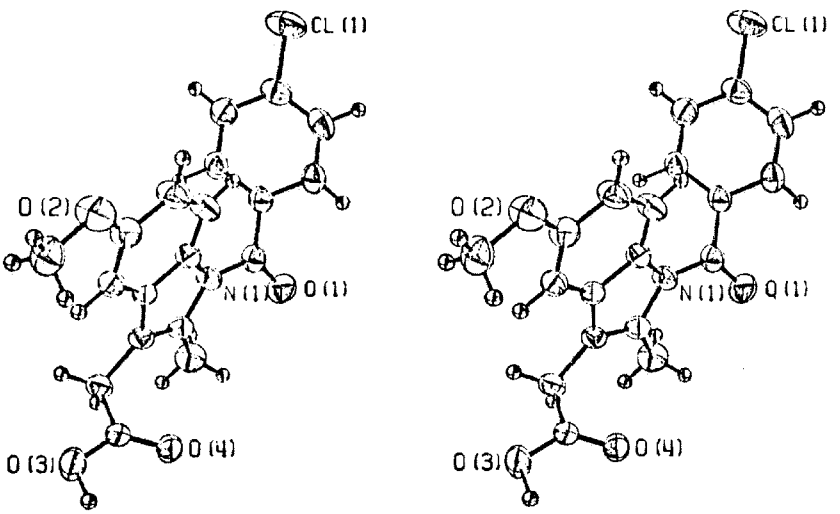

Figure 3

N(1)-C(10) rotation:

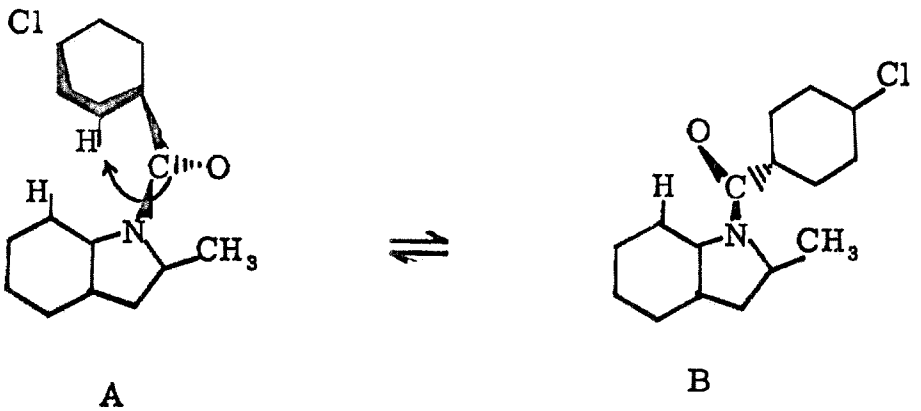

A B

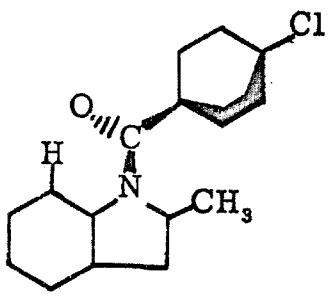

C

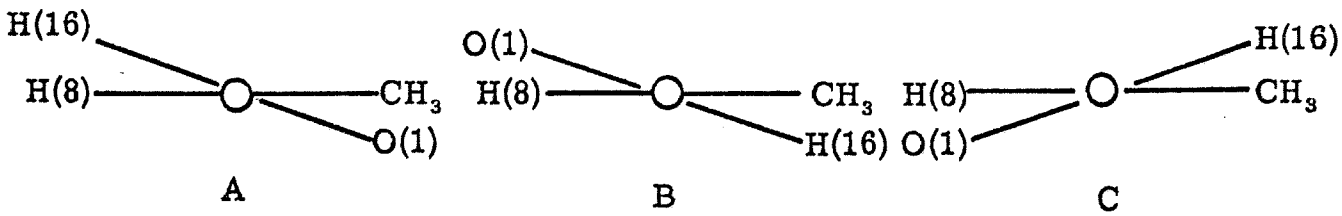

A B C

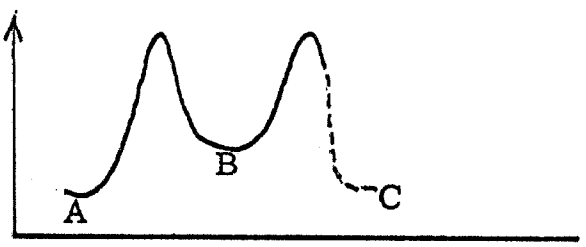

Figure 3 (Continued)

C(10)-C(11) rotation:

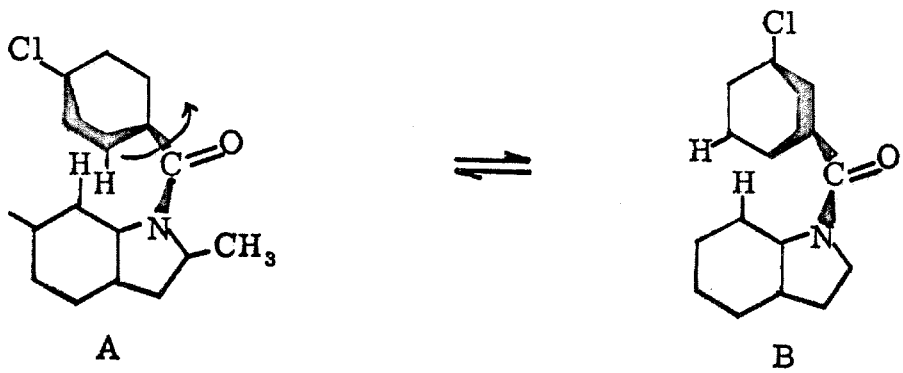

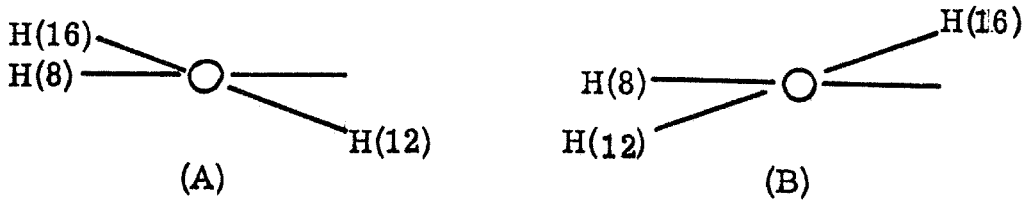

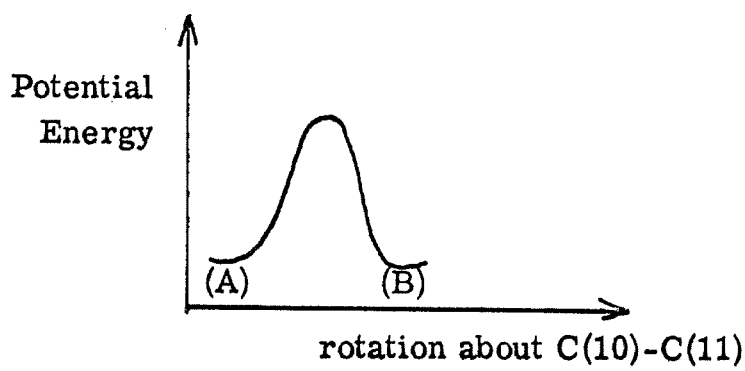

Figure 4

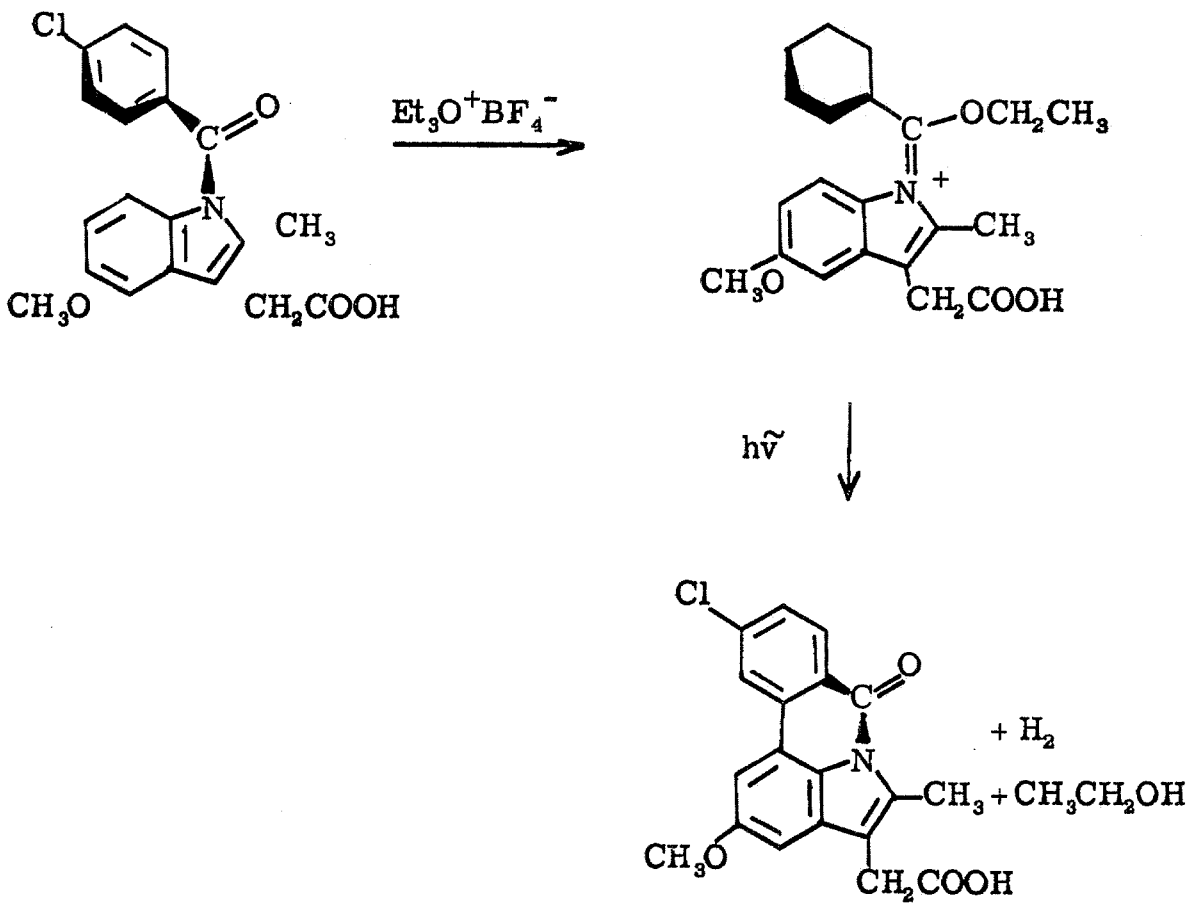
Cl
O
N
CH3
CH3O
CH2COOH
Et3O+BF4-
OCH2CH3
N+
CH3
CH3O
CH2COOH
hν̃
Cl
O
N
+ H2
CH3 + CH3CH2OH
CH3O
CH2COOH

Figure 5

phenylbutazone

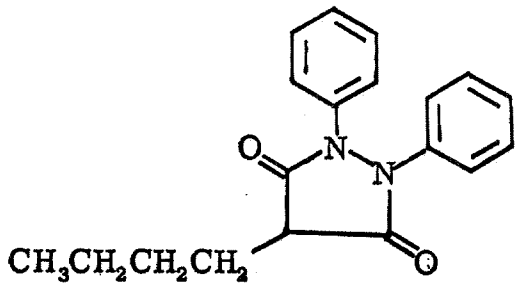

aminopyrine

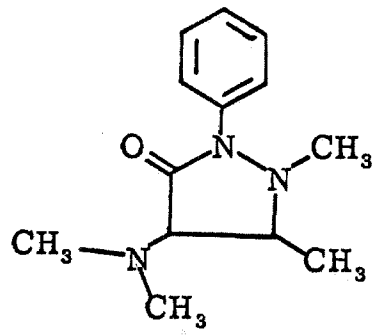

A structural comparison -

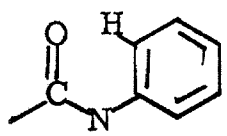

<u>cf</u>

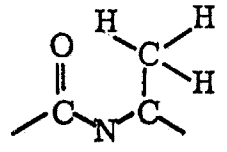

phenylbutazone
aminopyrine

Indomethacin

PROPOSITION V

Chronic manganese poisoning produces some of the neurological symptoms of Parkinson's disease and can be treated in a similar way, by the administration of ℓ-dopa, a metabolic precursor of the missing neurotransmitter dopamine. It is proposed that the strength and nature of the bonding interactions between manganese and the ligands ℓ-dopa and dopamine be investigated.

One of the most spectacular clinical applications of a chemical agent in the treatment of a diseased state has been the recently developed[1,5] treatment of Parkinson's disease with ℓ-dopa, 3-(3,4-dihydroxyphenyl)-ℓ-alanine. Parkinson's disease is known to be a degenerative process characterized by a lessening of voluntary movement with increasing tremors and muscle rigidity. A lack of a biogenic amine neurotransmitter dopamine, 4-(2-aminoethyl)pyrocatechol, was implicated as the metabolic irregularity but administered dopamine was bound or inactivated at the periphery of the brain and never reached the target tissue in the corpus striatum. The therapy was modified by the replacement of dopamine by its inactive precursor ℓ-dopa which can penetrate the blood-brain barrier. The subsequent intracerebral synthesis of dopamine from ℓ-dopa resulted in an almost complete reversal of the disease syndrome. The structural formulae for ℓ-dopa and dopamine are shown in Figure 1.

Chronic manganese poisoning has been recognized as an industrial hazard for manganese miners that leads to substantial disablement. The impact of flooding the brain with manganese is to produce neurological symptoms resembling those of Parkinson's disease.

However the connection between the therapuetic effects of ℓ-dopa and the metabolic processes in the brain effected by manganese remains largely unknown.

Manganese poisoning apparently causes some permanent brain damage that persists after the introduction of excessive amounts of manganese has ceased. The nature of this permanent damage in the brain and the part played in it by manganese is unknown. Healthy working miners maintain a high tissue concentration coupled to a rapid turnover rate. In the ex-miners suffering from poisoning this rate has returned to normal and the high tissue load of manganese has cleared; excessive manganese is assumed to be still present in the brain, but even such elementary information as its state of ionization has not been reported.

It has been suggested that brain manganese is tightly bound by the catecholamines. It is also possible that manganese binds to and inactivates an enzyme in the catabolic production of the amines.[3] Formation of a very stable complex between ℓ-dopa and manganese would in effect make the neurotransmitter dopamine unavailable for use.

There is little information available on the bonding interactions between manganese and catecholamines. It is proposed that these be investigated in the particular instances of ℓ-dopa and dopamine. Both compounds are likely to act as bidentate ligands. Study of molecular models shows that only ℓ-dopa can adopt a configuration suitable for binding two manganese ions. Dimer formation is possible in either of the two conformations shown in Figure 2. Formation constants for the complexes could be established by pH titrations which, together with

solution susceptibility studies would detect any dimer formation. Any isolated solids could be compared by solid state infrared and electron spin resonance methods. The d^5 manganese system exhibits only spin forbidden bands of low intensity ($\epsilon < 0.1$) in the visible and near-infrared spectral region and these would probably be hidden under charge transfer bands in the metal complexes.

The bidentate ligand acetylacetone forms a 3:1 ligand:metal complex with manganese(II) that is trimeric and readily oxidized in air[4] to manganese(III).

The ease of oxidation and polymer formation may well differ between manganese(II) complexes formed with ℓ-dopa and dopamine. A detailed study of these complexes is a necessity before further speculation and investigation on the neurological role of manganese is possible.

References

1. G. Bryson, Clin. Chem., 17, 5 (1971).

2. I. Mena, J. Court, S. Fuenzalida, P. S. Papavasiliou, and G. C. Cotzias, New Eng. J. Med., 282, 5 (1970).

3. P. S. Papvisiliou, S. T. Miller, and G. C. Cotzias, Nature, 220, 74 (1968).

4. F. A. Cotton and G. Wilkinson, "Advanced Inorganic Chemistry," John Wiley, 1966, p. 838.

5. G. C. Cotzias and A. C. Foradorium, "The Biological Basis of Medicine," I, E. E. and N. Bittar (eds.), Academic Press, 1968, p. 105.

Figure 1

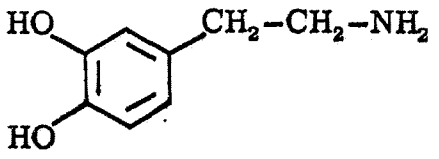

dopamine

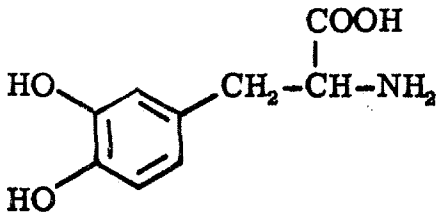

ℓ-dopa

Figure 2